



저작자표시-비영리-변경금지 2.0 대한민국

이용자는 아래의 조건을 따르는 경우에 한하여 자유롭게

- 이 저작물을 복제, 배포, 전송, 전시, 공연 및 방송할 수 있습니다.

다음과 같은 조건을 따라야 합니다:



저작자표시. 귀하는 원저작자를 표시하여야 합니다.



비영리. 귀하는 이 저작물을 영리 목적으로 이용할 수 없습니다.



변경금지. 귀하는 이 저작물을 개작, 변형 또는 가공할 수 없습니다.

- 귀하는, 이 저작물의 재이용이나 배포의 경우, 이 저작물에 적용된 이용허락조건을 명확하게 나타내어야 합니다.
- 저작권자로부터 별도의 허가를 받으면 이러한 조건들은 적용되지 않습니다.

저작권법에 따른 이용자의 권리는 위의 내용에 의하여 영향을 받지 않습니다.

이것은 [이용허락규약\(Legal Code\)](#)을 이해하기 쉽게 요약한 것입니다.

[Disclaimer](#)

공학박사학위논문

서비스 로봇 주행 플랫폼을 위한
2-자유도 변형 바퀴 메커니즘

2-DOF Transformable Wheel Mechanism
for Service Robot Mobile Platforms

2019 년 8 월

서울대학교 대학원

기계항공공학부

김 영 수

서비스 로봇 주행 플랫폼을 위한 2-자유도 변형 바퀴 메커니즘

2-DOF Transformable Wheel Mechanism
for Service Robot Mobile Platforms

지도교수 김 종 원

이 논문을 공학박사 학위논문으로 제출함

2019 년 4 월

서울대학교 대학원

기계항공공학부

김 영 수

김영수의 공학박사 학위논문을 인준함

2019 년 6 월

위 원 장: _____ 박 희 재 _____

부위원장: _____ 김 종 원 _____

위 원: _____ 김 윤 영 _____

위 원: _____ 차 석 원 _____

위 원: _____ 김 화 수 _____

Abstract

This thesis presents a new 2-degree of freedom (DOF) transformable wheel mechanism for service robot mobile platforms. On flat grounds, conventional wheel is a simple and effective structure for the mobile platforms. However, it is difficult for the mobile platforms with conventional wheels to overcome obstacles in human living environment due to high required friction and large fluctuations on main body while overcoming obstacles. By 2-DOF transformation, the wheel can effectively reduce friction dependency as the transformed wheel maintain contact only with a bottom surfaces of various obstacles. Also, bottom surface contact condition allows the platform to climb various obstacles regardless of the existence of vertical surfaces of obstacles. In addition, fluctuation of a main body while overcoming various obstacles is also reduced by the effect of the curved shaped transformed wheel. Consequently, the platform with 2-DOF transformable wheel can overcome various obstacles in human environment at high speed up to 40 m/min which is average walking speed of adult human.

The concept and required functions of 2-DOF transformable wheel was defined and a preliminary simulation and experiments were performed to verify performance of transformed wheel shape. 36 Types of 2- DOF transformable were explored by type synthesis of 2-bar serial and 5-bar parallel mechanisms. By excluding mechanisms that do not satisfy kinematic requirements, and by applying mechanisms synchronizing 3 lobes, five different types of design alternative mechanisms were created. Through the step overcoming simulation, kinematic characteristics analysis and evaluation of design alternatives was performed in terms of range of

transformation, interference, and singularity. 5-bar mechanism with two P joint at base (PRRRP) was selected as an optimal mechanism. To achieve both control simplicity and design simplicity, a pair of RRPP 4-bar mechanism was synthesized to the selected PRRRP mechanism to ensure independencies between wheel rotation DOF and transformation DOFs. The design variables were selected to satisfy the required transform range through kinematic analysis, and power transmission parts were designed based on static analysis. Selected mechanism based mobile platform “STEP” was designed and fabricated. The size and the weight of the platform is 1150 mm x 250 mm x 420 mm and 18 kg respectively. CompactRio was used as the main controller, and was controlled by the PC's labview wirelessly. The performance of the 2 DOF wheel based mobile platform was verified by experiments on step obstacles of various heights (70 mm, 110 mm) and stair obstacles of various sizes (300 mm x 100 mm, 320 mm x 140 mm, 300 mm x 160 mm). In addition, field tests had been performed on actual stairs in our living environment. As a result, the platform could overcome various obstacles at high speed up to 40 m/min.

The transformable wheel based mobile platform ‘STEP’ that is proposed in this study can be used as a mobile platform of service robots so that the service robots could expand their applications by increasing their range of activity.

Keyword: Service robot, Mobile platform, 2-DOF Transformable wheel, Mechanism, Stair climbing, Kinematics

Student Number: 2013-20652

Table of Contents

Abstract	ii
Contents	iv
List of Figures	v
List of Tables.....	viii
1. Introduction	1
1.1. Mobile platform for service robots	1
1.2. Limitations of wheeled mobile platforms.....	1
1.3. Previous researches.....	4
1.3.1. Wheel linkage mechanisms	4
1.3.2. Transformable wheel mechanisms	6
1.4. Performance indices for mobile platforms	9
1.4.1. Required friction coefficient	9
1.4.2. Trajectory smoothness	10
1.5. Research objectives	12
2. The Concept Transformable Wheel.....	13
2.1. The Concept of 2-DOF transformable wheel	13
2.1.1. Definition of transformable wheel	13
2.1.2. Objective obstacles in human environment	15
2.1.3. Necessity of 2-DOF transformation.....	17
2.2. Obstacle overcoming process of transformable wheel	18
2.3. Preliminary experiments with curved wheel	19
2.3.1. Trajectory analysis.....	19
2.3.2. Required friction coefficient	23
2.3.3. Preliminary experiments results	26
3. Type Synthesis of 2-DOF Transform Mechanism	29
3.1. Requirements of transform mechanisms	29
3.2. Exploration of 2-dof mechanisms	33
3.2.1. Systematic process of developing design alternative mechanisms	33
3.2.2. Exploration of 2-dof mechanisms.....	34
3.2.3. Exclusion of alternatives with passive prismatic joints	37
3.2.4. Design alternatives by combining synchronization mechanism	39

3.3. Characteristic analysis of alternative mechanisms....	40
3.4. Step overcoming simulation and evaluation	47
3.4.1. Simulation conditions	47
3.4.2. Inverse kinematics of alternatives	48
3.4.3. Simulation results	48
3.4.4. Analysis and evaluations	51
3.5. 5-bar 3R2P mechanism.....	55
4. Design of the STEP Platform	56
4.1. Concept design of the STEP platform	56
4.1.1. Issues of actuator location	56
4.1.2. Final concept of the mobile platform STEP	57
4.2. Design of the STEP platform.....	60
4.2.1. Description of mechanical parts	61
4.2.2. Kinematics based parameter selection	66
4.2.3. Static analysis	69
4.3. Fabricated STEP Platform.....	75
4.4. Design modifications	80
4.4.1. Link supporting ball roller	80
4.4.2. Clearance of a screw axis	81
4.4.3. Gap between motor-boxes.....	82
4.4.4. Timing belt deviation.....	83
5. Experiments	84
5.1. Experimental setup	84
5.1.1. Testbench : various sizes of stairs and steps	84
5.1.2. Active supporter	86
5.1.3. Initial condition.....	87
5.1.4. Guide to constrain pitch motion & trajectory	87
5.2. Transformation tests.....	89
5.3. Tests on flat surfaces	90
5.4. Stair overcoming experiments	91
5.5. Step overcoming experiments.....	98
5.6. Size varying stairs overcoming experiments.....	100
5.7. Field tests	102
6. Conclusion	104
Bibliography	106
Abstract in Korean	108

List of Figures

1.1. Conventional service robot mobile platforms.....	1
1.2. Limitations of Existing Service Robot Driving Platform.....	3
1.3. Limitations of the wheel structure.....	3
1.4. Rocker–bogie based mechanisms	5
1.5. Step climbing process of rocker bogie mechanism	5
1.6. Wheel transformer(SNU)	6
1.7. Morphing wheel (DARPA)	7
1.8. Variable–diameter wheels for lunar rover.....	8
1.9. Deformable wheel for Segway platform (Hyundai)	9
1.10. Required friction coefficient (a) comparison of required friction coefficient for various wheel–linkage mechanisms (b) definition of required friction coefficient (c) various wheel–linkage mechanisms.....	10
1.11. Influence of fluctuation on main body	11
1.12. Smooth movement reference line	11
2.1. Parameters and various shapes of 2–dof morphing wheel...	13
2.2. Concept of transformable wheel based mobile platform	14
2.3. Various obstacles in human living environment.....	16
2.4. Objective sizes of obstacles.....	16
2.5. Stair overcoming process for transformed wheel shape.....	17
2.6. The process of overcoming the step obstacle of the transformable wheel.....	18
2.7. Stair climbing simulation results of curved shaped wheel.	21
2.8. Stair climbing trajectories of robots.....	22
2.9. Static modeling of robot with curved shape wheel.....	23
2.10. Required friction coefficient of a robot with curved shape wheel.....	25
2.11. Fabricated prototype for preliminary experiment	26
2.12. Stair climbing experiment of curved shaped wheel.....	28
3.1. Necessary morphed shape of wheel for an obstacle sizes	30
3.2. Target obstacle and required range of transformation	32
3.3. Systematic process of developing design alternative mechanisms.	33
3.4. Synchronized motion of all lobes.	34
3.5. Kinematic structure of 5–bar parallel mechanism.	34
3.6. 36 design alternative mechanisms.....	36
3.7. Linkage software simulation of RPRPR 5bar mechanism.....	38
3.8. Linkage software simulation result of RPRPR 5bar mechanism.	38
3.9. Remained alternative mechanisms.....	39
3.10. 5–types of 2–dof morphing design alternatives.....	39

3.11. Structure and operation of design Alternative #1.	40
3.12. Analysis of transform range and characteristic.....	41
3.13. The coupling property of design alternative #1.....	42
3.14. Structure and operation of design Alternative #2.....	43
3.15. Structure and operation of design alternative #3	44
3.16. Structure and operation of design alternative #4	44
3.17. Structure and operation of design alternative #5	45
3.18. Step overcoming simulation conditions	47
3.19. Required $r1-\theta1$ transform trajectory for step overcoming	47
3.20. Configuration of the 5-bar 5R mechanism	48
3.21. The process of obtaining the configuration of a mechanism satisfying $r1-t1$ with inverse kinematics.....	48
3.22. Step overcoming simulation results (1/2) for 5 design alternative mechanisms.....	49
3.23. Step overcoming simulation results (2/2) for 5 design alternative mechanisms.....	50
3.24. Analysis of design alternative #2 5R mechanism	51
3.25. Singularity and interference of simulation results of design alternative #2.....	52
3.26. New design parameters of design alternative #2	53
3.27. Simulation results with new design parameters	53
3.28. Configuration of design alternative 4	54
3.29. Configuration of selected design alternative 5 mechanism..	55
4.1. Issues of actuator location	56
4.2. the only DOF that is independent of wheel rotation	57
4.3. Components of design alternative #5	57
4.4. Modified design alternative #5.....	58
4.5. Conceptual design of mobile platform based on modified design alternative mechanism #5	58
4.6. 2-DOF transformation motion of modified design alternative #5.....	59
4.7. Detail design of a new mobile platform STEP	60
4.8. Structure of the motor-box part of STEP platform.....	62
4.9. Cross-sectional view of motor box	63
4.10. Designed Transformable wheel part	64
4.11. The transformed motion of the wheel mechanism	65
4.12. Kinematic parameters of the mechanism	66
4.13. Step overcoming simulation of selected design parameters	68
4.14. Selected design parameter based 3d cad design.....	68
4.15. Static modeling of STEP wheel mechanism.....	69
4.16. Step obstacle overcoming simulation	70
4.17. Static analysis results	72

4.18. Analysis of the results of static analysis 1	72
4.19. Analysis of the results of static analysis 2	73
4.20. Fabricated parts of the STEP platform	75
4.21. Fabricated wheel parts assembly of the STEP platform.....	76
4.22. Fabricated motorbox parts assembly of the STEP platform	77
4.23. The STEP platform	78
4.24. Electric parts of the STEP platform.....	78
4.25. Link supporting parts description.....	80
4.26. Modification on screw axis contacting parts.....	81
4.27. Modification on motor–box parts	82
4.28. Timing belt deviation.....	83
5.1. Tap hole position in testbench.....	84
5.2. Various stair sizes for experiments	85
5.3. Active supporter	86
5.3. Block for Initial condition setting.....	87
5.5. Guide structure to constrain pitch motion & trajectory	88
5.6. Transformation test results	89
5.7. Tests on flat surfaces	90
5.8. Experiments on stairs 300 x 100, 5 m/min.....	94
5.9. Experiments on stairs 300 x 100, 20m/min.....	95
5.10. Experiments on stairs 300 x 160, 20m/min	96
5.11. Experiments on stairs 320 x 140, 20m/min	97
5.12. Objective step obstacle and concept of overcoming the obstacle.....	98
5.13. Step overcoming test	99
5.14. Size varying stairs	100
5.15. Experiments on size varying stairs	101
5.16. Field test on step obstacle : 120 mm	102
5.17. Field test on stair obstacle.....	103
6.1. Application of STEP mobile platform	104

List of Tables

Table 3.1. Requirements of morphing wheel mechanism	30
Table 3.2 Qualitative evaluation based on requirements of morphing wheel mechanism	46
Table 4.1 Specifications of the STEP platform.....	79
Table 5.1 Lookup table of transformation for various stair climbing	92
Table 5.2 Lookup table of transformation for various stair descending	93

Chapter 1. Introduction

1.1. Mobile Platform for Service Robots

Wheel is an effective structure for robots traveling on flat ground due to its simple structure, control, high efficiency and smooth motion on the ground even at high speed. Among various attempts to commercialize service robots, service robots that have been released recently are mostly based on wheel structures, such as Starship robot (Fig. 1.1 (a), Starship Technologies), Ava (Fig. 1.1 (b), iRobot).

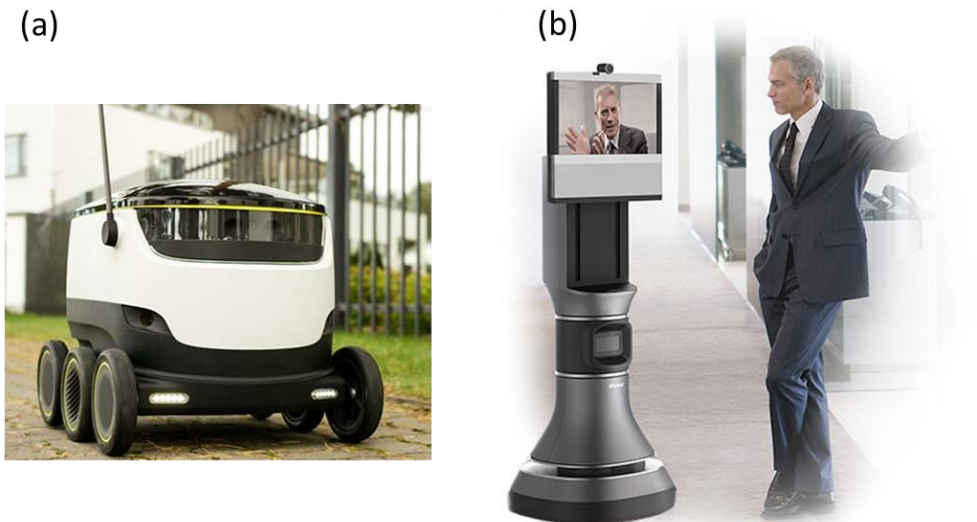


Figure 1.1 Conventional service robot mobile platforms (a) Starship robot (Starship Technologies) (b) Ava robot (iRobot)

1.2. Limitations of Wheeled Mobile Platforms

While wheels are effective on flat floors, it is difficult for mobile robots with conventional wheels to overcome obstacles in indoor environment. As can be seen in Fig. 1.2, the delivery robot cannot climb the stairs and a person must come down the stairs to receive



Figure 1.2. Limitations of Existing Service Robot Driving Platform
- A person must come down the stairs and get goods

the goods. The telepresence robot ava also cannot overcome obstacles. Service robot's mobile platform should be able to reliably overcome various obstacles in the human living environment in order to perform various operations assisting human.

There are two main reasons why the wheel structure itself cannot overcome obstacles well. The first is a way to overcome obstacles that depend on frictional forces. As can be seen in Fig. 1.3 (a), the force that lifts the robot's payload(W) is the traction of the front wheel(T_1), which is created by traction of the rear wheel(T_2). For the wheel structure to overcome obstacles, proper load distribution of front and rear wheels and high coefficient of friction are required. Since the wheel structure is highly relying on frictional forces in overcoming obstacles, a larger coefficient of friction is required to overcome high obstacles. In other words, if the actual frictional force of the wheel is smaller than the required frictional force, slip occurs and the obstacle cannot be overcome. To maintain friction, it is important to maintain consistent contact condition between every wheel of the robot with floor surfaces. The wheel structure thus has difficulty overcoming obstacles without vertical surfaces (Fig. 1.3. (b)) such as stairs without riser or obstacles with uneven vertical surfaces because of insufficient friction forces.

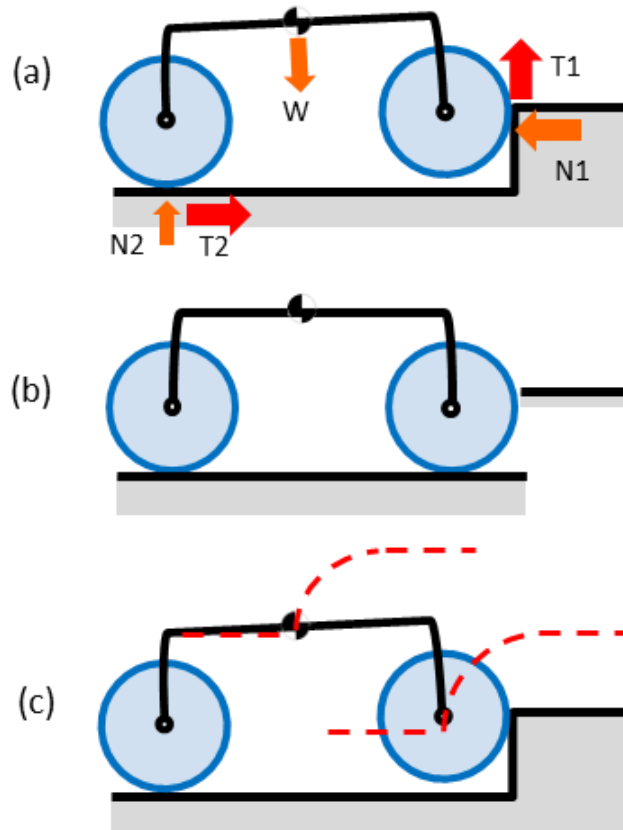


Figure 1.3. Limitations of the wheel structure (a) The large friction force of the rear wheel is needed to overcome obstacles. (b) When vertical surfaces are not present, they cannot be overcome. (c) The fluctuation of the main body is large.

Second reason is fluctuations (Fig. 1.3 (c)). Even if obstacles can be overcome with a large coefficient of friction, due to the fluctuation of the wheels, it is difficult for the platform to maintain stability and proper contact condition. The platform needs to move very slowly while overcoming obstacles, because dynamic effects caused by the fluctuation of the wheel while overcoming obstacles disturb maintaining good contact condition so that the robot easily loses contacts and fails to overcome obstacles.

These limitations of the wheel structure result in a large restriction on the range of activity of the robot in an indoor environment. In order for service robots to perform various tasks effectively, the robots should be able to overcome step and stair obstacles in the indoor environment which has a height up to 180 mm with a low required friction coefficient.

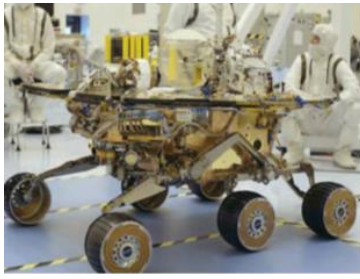
1.3. Previous Researches

The previous studies to improve the limitations of the wheel structure are divided into two categories. First is the study of the linkage mechanisms that links the wheels and second is the transform mechanisms that transform the wheels themselves.

1.3.1. Wheel Linkage Mechanisms

There have been many studies to improve the obstacles overcoming ability of the wheel structure while maintaining the advantages of it. Rocker-bogie [1] is the most popular example of wheel-linkage structure which was applied in the structure of the mars rover [2]. For Rocker-bogie mechanism based robot, it is possible to overcome obstacles twice as high as the wheel radius by distributing the load on the six wheels, lowering the required coefficient of friction. In addition, the linkage mechanism reduces fluctuations of the main body. Rocker-bogie mechanism greatly improves the obstacle overcoming ability of the wheel. CRAB [3], RCL-E [4], Shrimp [5] and ORL-F [6] are wheel-linkage mechanisms that improve obstacle overcoming ability of Rocker-bogie mechanism by modifying Rocker-bogie mechanism.

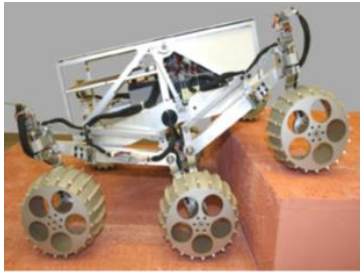
However, due to the inherent limitations of the wheel structure relying on friction, the robot should maintain slow speed while overcoming obstacles to maintain good contact condition and it is sensitive to surface condition of obstacles as well, especially of vertical surfaces. In addition, since the link mechanism increases the number of parts to be moved relative to each other, to avoid unexpected dynamic effects of linkages, the robot should maintain slow speed. And it is necessary to maintain a good contact state at all times, and therefore, it is impossible to make a fast travel. Since the rotation amount of six wheels is different, precise velocity control is required for every wheel.



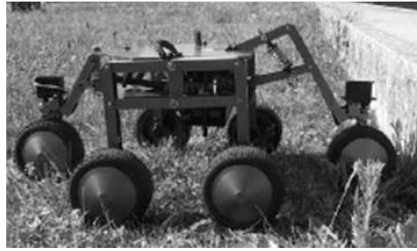
a) Mars Rover [1]



b) CRAB [3]



c) RCL-E [4]



d) Shrimp [5]

Figure 1.4. Rocker-bogie based mechanisms a)~d)



a)



b)



c)



d)



e)



f)

Figure 1.5. Step climbing process of the rocker bogie mechanism

1.3.2. Transformable Wheel Mechanisms

There has been another approach of studies to overcome limitations of wheel structure by transforming the shape of the wheels. The Wheel Transformer [7] overcomes obstacles of 150 mm which are twice the diameter of the wheel, through transformation of the wheel shape. It is remarkable to note that the transformation is done passively by one degree of freedom pin–slot slide mechanism. However, friction between the wheel and the vertical surface is necessary for the transformation and obstacle overcoming process. Moreover, stability of body decreases due to the fluctuations in the process of overcoming obstacle.

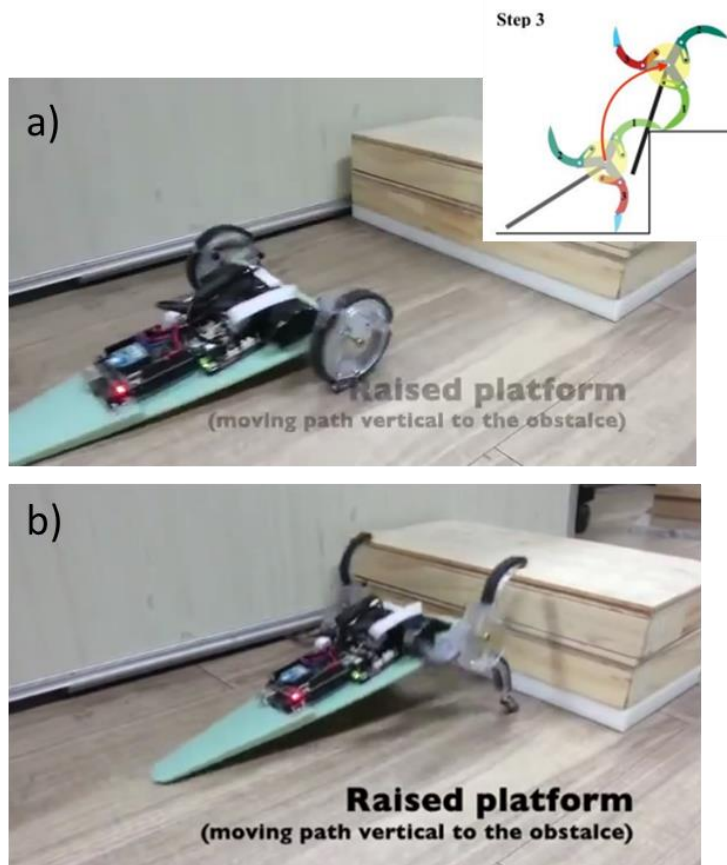


Figure 1.6. Wheel transformer(SNU)

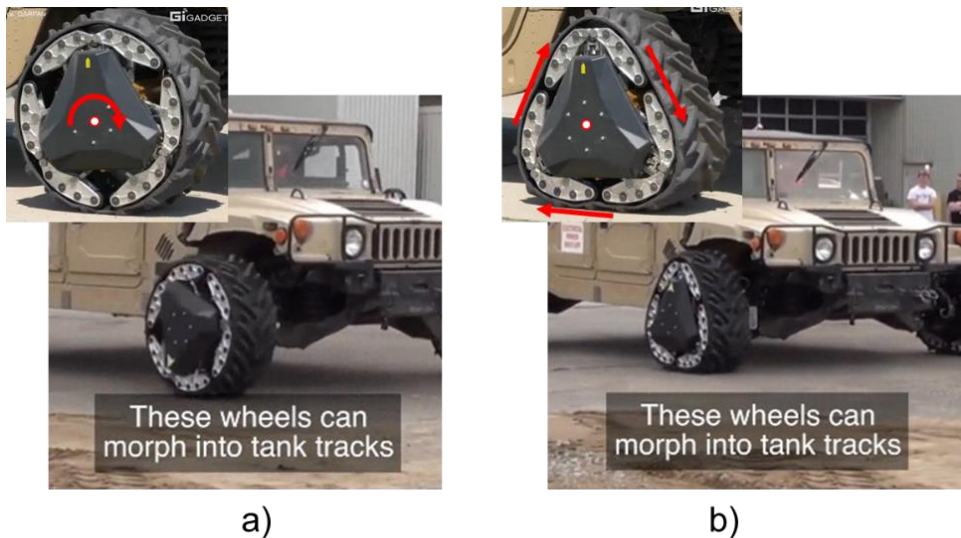


Figure 1.7. Morphing wheel (DARPA) (a) Wheel mode (b) Track mode

The morphing wheel [8] is a mechanism that can change the mode of wheels and infinite orbit using the planetary gear mechanism. (Fig. 1.7) Although it was a remarkable study that improved driving performance by changing the mode of wheels and tracks on uneven terrains, it is not suitable to be used as a service robot mobile platform because of the limitations of track structure when driving on flat ground.

The wheel [9] of Fig 1.8 (a) is also a transformable wheel, which is a mechanism that changes the size of the wheel through a transformation of one degree of freedom. By increasing the size of the wheel, it is possible to effectively overcome large obstacles, and the soft terrain of the moon can also be driven effectively. However, when the wheel is raised only in size, the stability of the main body is threatened because of the heavy vibration on the main body when the obstacle is overcome. Therefore, it is not suitable to be used as a service robot mobile platform.

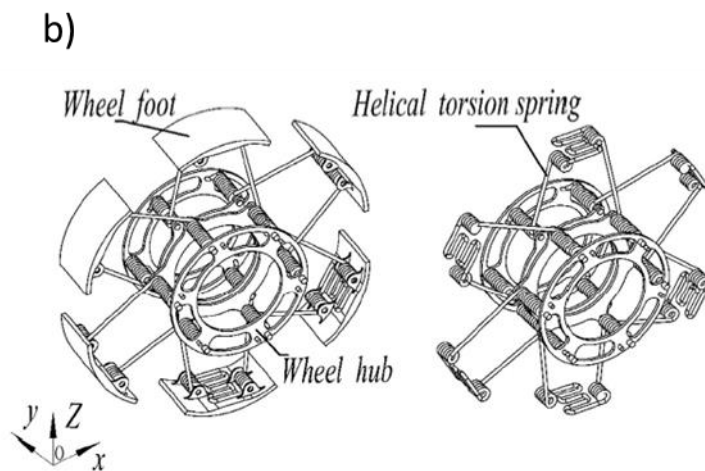
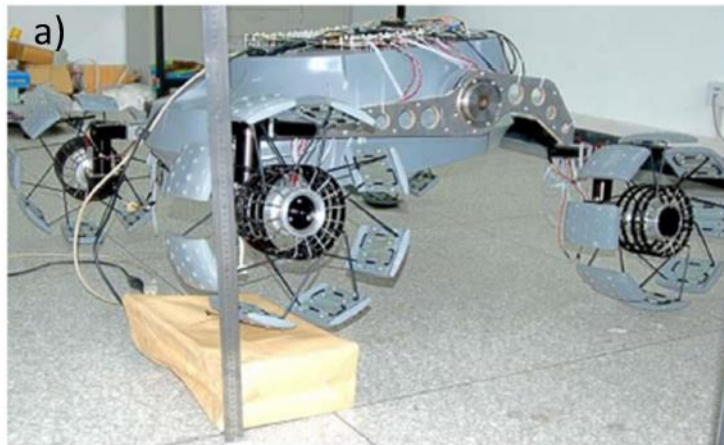


Figure 1.8. Variable-diameter wheels for lunar rover

The NAMU wheel [10] developed by Hyundai (Fig 1.9) has overcome obstacles by using deformable rubber wheels instead of using an active actuator. It is a good way to overcome the limitation of the wheel structure because it is able to move smoothly with only rotation driving like a wheel without recognizing an obstacle. However, the size of the wheel must be large to overcome various obstacles in indoor environments. Moreover, the wheel maintains deformed state not only on the obstacles but also on floors so the deformation interferes with the steering of the flat road as shown in Figure 1.9 (b). The effect is similar as that of the track structure. Therefore, it is not suitable to be used as a service robot mobile platform.

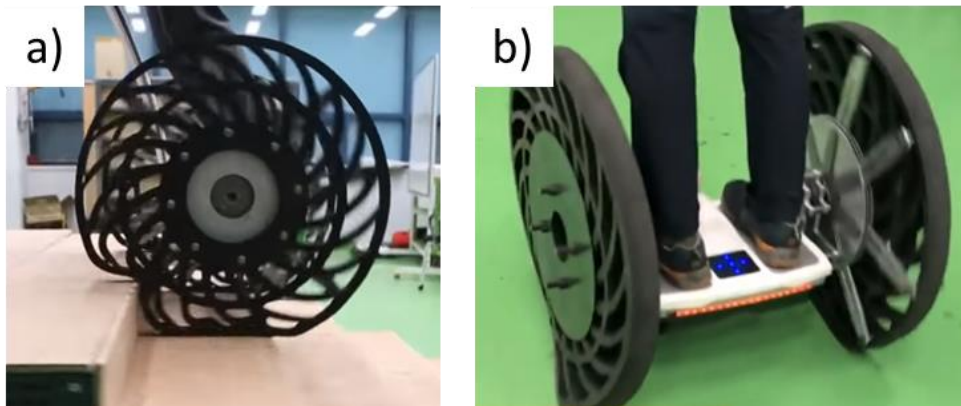


Figure 1.9. Deformable wheel for Segway platform (Hyundai)

1.4. Performance Indices for Mobile Platform

1.4.1. Required Friction Coefficient

One of the standard indices for evaluating the performance of a mobile robot is a necessary friction coefficient value [11]. This is defined as the maximum value of the friction coefficient value required to raise the step of the wheel diameter height. A smaller value means that it is possible to overcome obstacles even for slippery friction surfaces, which means that a relatively higher obstacle can be overcome for the same coefficient of friction value. The Rocker-bogie mechanism is a typical example of overcoming obstacles by reducing the required friction coefficient by distributing the load through the link structure. As shown in Fig 1.10(a), Wheel-linkage robots reduced the required friction coefficient effectively by using linkage structures compared to 4WD structure.

However, the limit of the obstacle-overcoming method that highly depends on friction has not been overcome, and the value of the necessary friction coefficient has to be reduced and the friction dependent overcoming process has to be simplified in order to be applied to service robots.

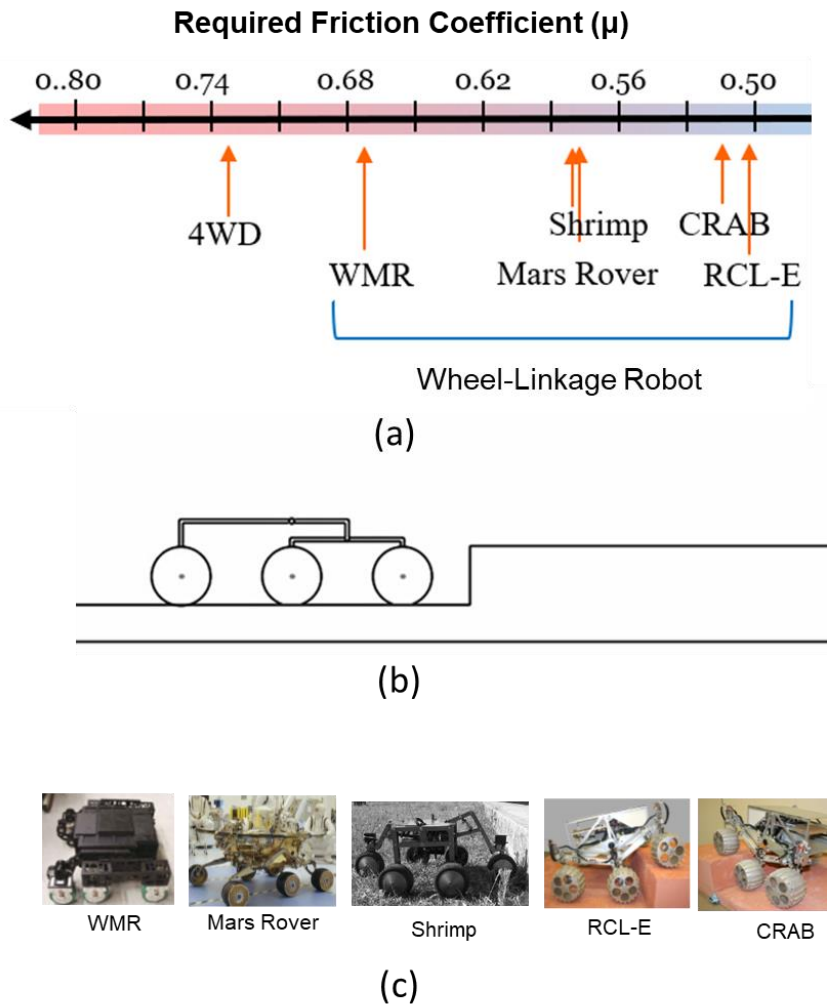


Figure 1.10. Required friction coefficient (a) comparison of required friction coefficient for various wheel-linkage mechanisms (b) definition of required friction coefficient (c) various wheel-linkage mechanisms

1.4.2. Trajectory Smoothness

For stable obstacle driving, it is necessary to minimize the shaking of the main body. In particular, service robots that perform various tasks to interact with human beings and assist human beings within the radius of human life are narrow and center of gravity is high. As shown in Figure 1.11, the higher the height of the center of gravity, the greater effects on the stability even for small shakes. Therefore, it is important for the service robot mobile platform to make the body shake smaller.

The simplest criterion that can be considered intuitively in the process of overcoming obstacles is the smooth passage of straight lines, regardless of the types of obstacles. Therefore, in this study, we study a mobile platform that not only minimize the dependence on the frictional force but also maximize the closeness of the center of gravity trajectory to the straight line.

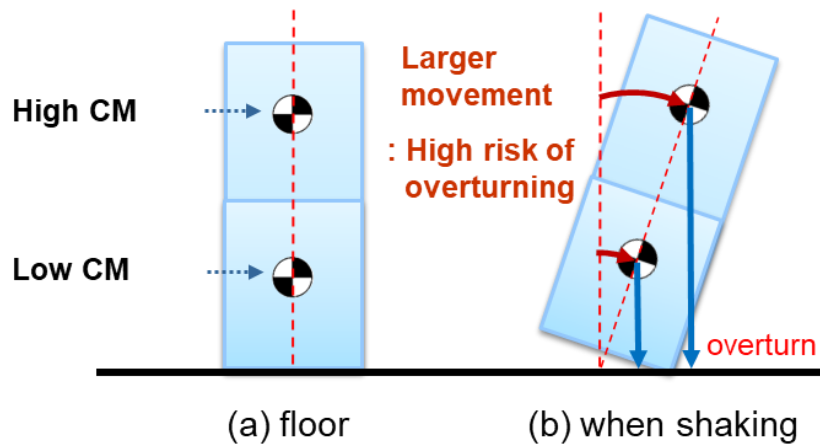


Figure 1.11. Influence of fluctuation on main body

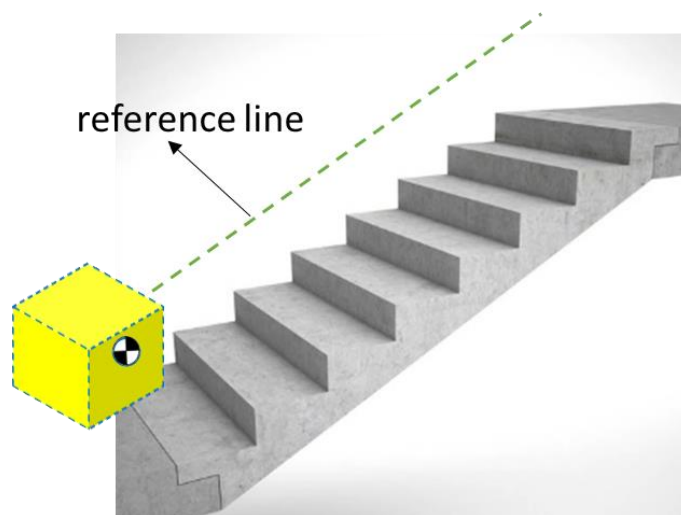


Figure 1.12. smooth movement reference line

1.5. Research Objectives

In this research, we proposed 2-dof transformable wheel concept that can move on both flat grounds and various obstacles in indoor environments with low required friction. Since only the contact between the wheel and the ground is required, the required coefficient of friction of the contact points can be minimized and even obstacles without a vertical surface can be overcome in the same way. And through the continuous two-degrees-of-freedom transformation of the three lobes, almost every types of obstacles existing in the human living environment can be overcome with smooth trajectory of center of gravity of the main body.

In this paper, based on the concept of the 2-DOF transformable wheel and kinematic requirements such as interferences and singularities in required transforming range, the 5-bar PRRRP mechanism is selected as an optimal base mechanism for wheel transformation. In addition, to ensure independencies of wheel rotation and transformation DOFs while minimizing design complexity, a pair of RRPP 4-bar mechanism is synthesized to each base wheel mechanism so that 2-linear motions on wheel axis transform the wheel independent of rotation of the wheel. The design variables are selected to satisfy the required transform range through kinematic analysis, and motors and power transmission parts are selected based on static analysis. The power transmission for the rotation and transformation of the wheels was made with a timing belt-pulley. The selected mechanism based platform "STEP" is designed and fabricated for verifications. The performance of the 2 DOF wheel based mobile platform is verified by experiments on step obstacles and various sizes of stair obstacles including 300 mm x 100 mm, 320 mm x 140 mm, 300 mm x 160 mm. In addition, experiments were performed on size varying stair and real stairs in our living environment

Chapter 2. The Concept of Transformable Wheel

2.1. The Concept of 2-DOF Transformable Wheel

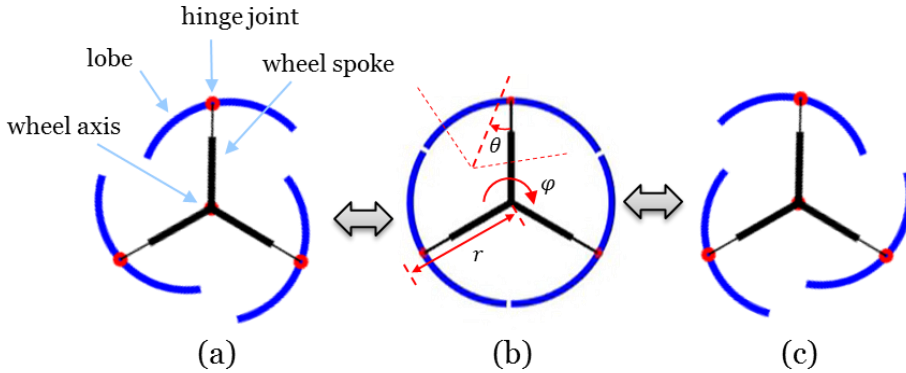


Figure 2.1. Parameters and various shapes of 2-dof transformable wheel (b) full circle wheel shape which is the most efficient configuration on floor (a), (c) bi-directional transforming shape of the wheel

2.1.1. Definition of Transformable Wheel

Proposed transformable wheel is composed of plural number of wheel lobes (blue arc parts on figure 2.1 (a)) which are segments of full circle wheel. The wheel forms a full circle shape as figure 2.1 (b) so that the robot can move smoothly and efficiently on flat ground. For various obstacles, the wheel shape is transformed into the optimal shape by 2-dof motion of the lobes which is defined by θ and ϕ . As shown in figure 2.2, low-step obstacles can be smoothly passed over ((a) to (d)) with continuous transformation of wheel shape, and regularly repeated stair obstacles can also be overcome smoothly ((e) to (h)) with a transformed shape wheel optimal for the stairs.

The position and posture of wheel segments is defined by 2-degrees of freedom (r , θ) and three wheel segments are synchronized mechanically so that the 2 degree of freedom wheel motion could be achieved with only 2 actuators. On figure 2.1 (b), ' r ' is defined as a length of a straight line which connects the

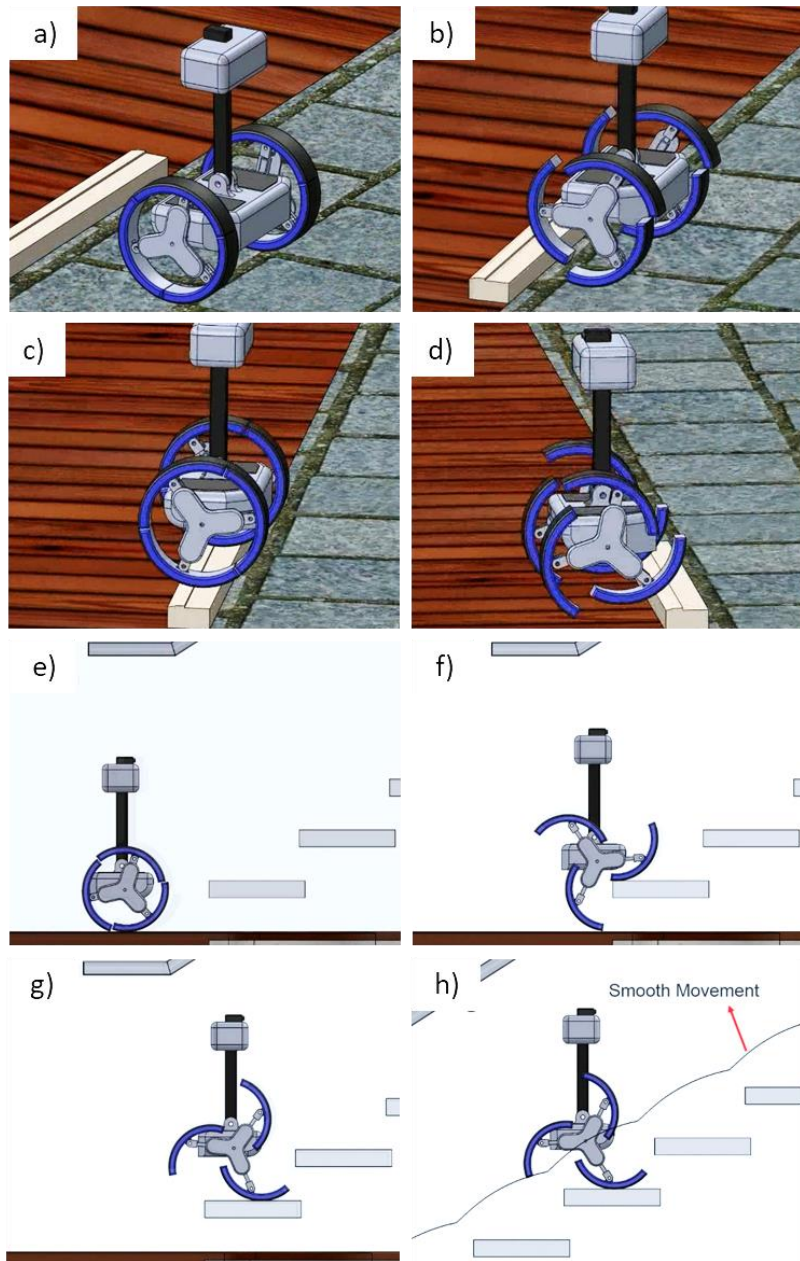


Figure 2.2. Concept of transformable wheel based mobile platform

center of rotation of the wheel and the center of the spoke. That is, 'r' corresponds to the length of the black cylindrical wheel spoke of the figure. Lobes rotate about the hinge marked with a red dot, and 'theta' means the angle of rotation. 'theta' is defined as an angle between the straight line which connects the center of circle of the wheel segment and the arc center of the segment with the straight

line which connects the center of rotation of the wheel and the center of the spoke. More intuitively, 'r' refers to the radius of transformed wheel, and 'theta' refers to the angle of transformed wheel. Wheel spoke and hinge joint has 1-dof respectively and they can be replaced by various two degree of freedom mechanisms. The goal of this paper is to find the optimal 2 DOF mechanism to replace it.

In this study, the number of lobes and wheel diameter are selected as 3 and 250 mm respectively. Larger wheel is obviously more advantageous to overcome high obstacles, but it is inefficient because the overall size of the robot increases. One of a key advantages of the transformable wheel proposed in this study is that it can overcome various size of obstacles up to 200 mm while maintaining small wheel size which is similar to the wheel size of a general indoor robot. The length of the lobes is determined based on the length of the shortest tread of the stair obstacle, 260 mm, and the size of the wheel is set to 250 mm using 3 lobes.

2.1.2. Objective Obstacles in Human Environment

There are various artificial obstacles in the human living environment. There are a variety of step obstacles in the room, such as a)~b) in figure 2.3. There are also staircase obstacles of various sizes in every building which has plural number of layers. In the human living environment obstacles are common in that they consist of horizontal and vertical surfaces and can be classified into step and stair obstacles.

There are criteria that define the size of stairways and step obstacles. According to the Building Code [12], the target obstacle of the service robot mobile platform can be defined as figure 2.4. Service robots should be able to overcome various step obstacles ranging from 0 to 100 mm in height and stair obstacles ranging from 260 to 340 mm in width and 100 to 180 in height in order to assist humans and perform various tasks efficiently.



Figure 2.3. Various obstacles in human living environment

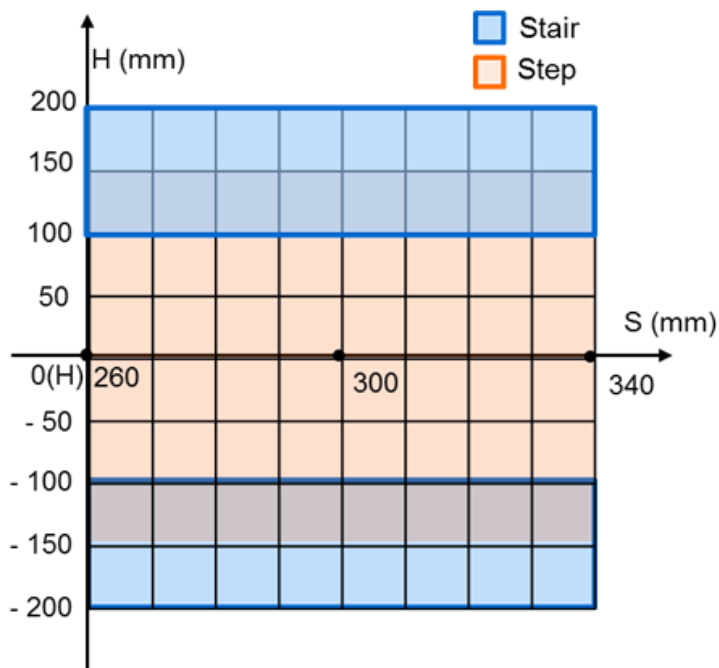


Figure 2.4 Objective sizes of obstacles

2.1.3. Necessity of 2-DOF Transformation

As in 2.1.2., The various obstacles defined are given in width and height. The transformed wheel serves to move the contact of the wheel from the floor to the floor of the obstacle. Considering the stair obstacles, the wheel rotates 120 degrees every time you move one step. (Fig.2.5) Assuming a non-slip tangent contact between the wheel and the floor, the horizontal and vertical travel of the center of rotation is kinematically defined as the wheel rolls as follows.

$$l = r_2 \left(\theta_2 - \frac{\sqrt{3}}{2} \right) + r_1 (\sin \theta_1 - \sin(\theta_1 - \theta_2)), \quad (2.1)$$

$$h = \frac{3}{2} r_2 + r_1 (-\cos \theta_1 + \cos(\theta_1 - \theta_2)). \quad (2.2)$$

Then, we can easily find out that 2 degrees of freedom are required to always have solutions for various obstacle sizes S (tread length) and H (height).

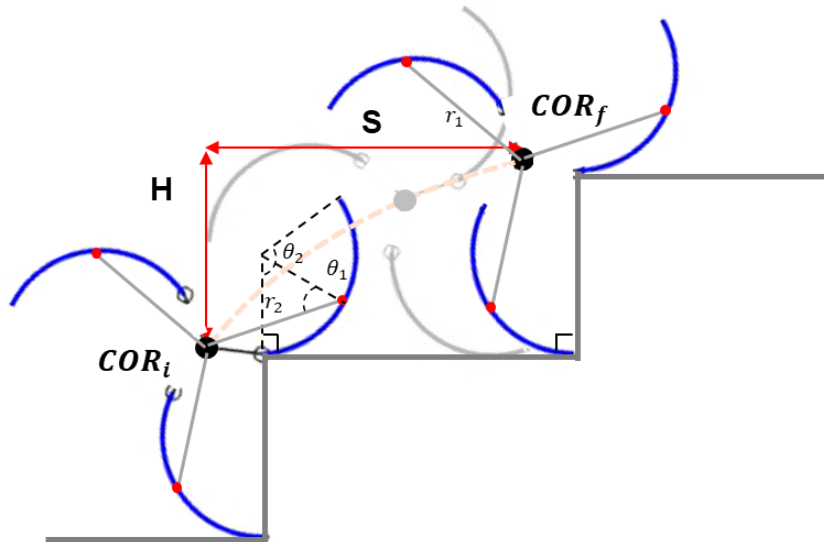


Figure 2.5. Stair overcoming process for transformed wheel shape

2.2. Obstacle Overcoming Process of Transformable Wheel

Figure 2.6 shows the process of the transformable wheel passing over a step obstacle. We assume tangent contact condition of the lobe with the floor and a non-slip condition. For a given size of obstacle, the wheel transforms to an optimal shape that smooths the trajectory of the wheel axis while overcoming the obstacle. In Figure 2.6, the area marked with a red bar on the bottom is the area of rolling of single lobe which is the length(l) of the single lobe. And the yellow area indicates the distance β until the next lobe touches, in other words, the air gap that does not be touched by any lobe. The pre-

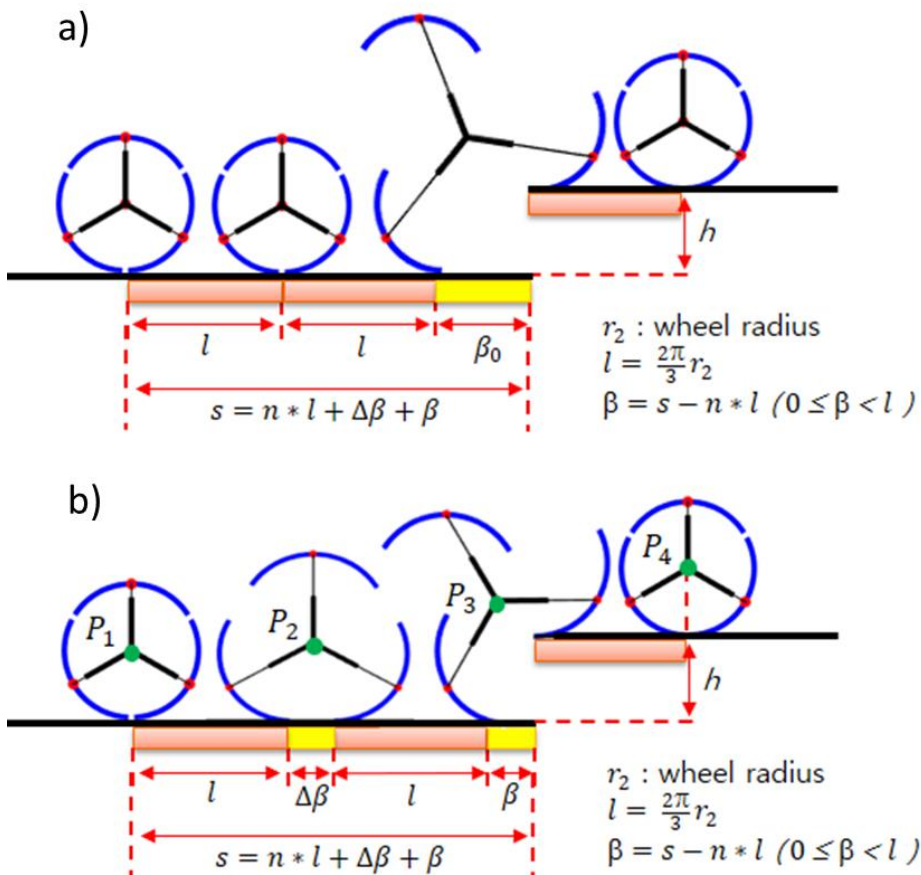


Figure 2.6. The process of overcoming the step obstacle of the transformable wheel (a) When the wheel starts far from the step, it must be transformed largely. (b) If the wheel comes close to the step through the pre-transform, the transformation can be reduced.

transform at state 2 distributes the air gap length into optimal β value to make the trajectory smoother and assure the corner contact at 3 correctly. In addition, the transformed wheels can be transformed into mirror symmetric shape as in 3 and 5, so that both climbing and descending of steps can be performed bi-directional.

Target obstacles can be classified into stairs and steps. The stair can be smoothly and steadily driven by the rotation driving only by transforming to the stair size, but the step obstacle can obtain the smooth trajectory only by climbing through the continuous transformation. The first column and the last column of the stairs can be thought of as the same process as step climbing.

If we analyze the process of the transverse wheel passing over the step obstacle, assuming that there is no slip, the state of the wheels must pass 4 exact points P1~P4 as shown in Fig. 2.6 (b). If the initial phase difference between the wheel and the step obstacle is large, the size of the wheel to be transformed is large as shown in Fig. 2.6 (a). Here, as shown in Fig. 2.6 (b), the required transform size can be minimized through a pre-transform process.

The pre-transform process can also be used to align the left and right wheels when they are out of phase.

2.3. Preliminary Experiments with curved wheel

2.3.1. Trajectory analysis

To perform stable stair-climbing, the kinematic parameters should be selected carefully. In this paper, the design parameters are selected based on perfect step climbing with no slippage, and step-climbing is sequentially repeated to enable the robot to climb the stairs. Based on this assumption, the kinematic parameters can be simply determined using a system of algebraic equations

Figure 2.5 shows the kinematic configuration of stair-climbing. There are four independent parameters, r_1 (radius of the center circle), r_2 (radius of the curved spoke), θ_1 (angle between the

radius of the center circle and the spoke), and θ_2 (angle of the curved spoke piece). Here, θ_2 is designed to be 120° , so as to make a tri-wheel mechanism. If the movement of CoR is moved from the initial position (CoRi) to the final position (CoRf) in an ideal way, the length l and height h can be derived using the following algebraic equations:

$$l = r_2 \left(\theta_2 - \frac{\sqrt{3}}{2} \right) + r_1 (\sin \theta_1 - \sin(\theta_1 - \theta_2)), \quad (2.1)$$

$$h = \frac{3}{2} r_2 + r_1 (-\cos \theta_1 + \cos(\theta_1 - \theta_2)). \quad (2.2)$$

From these relations, r_1 , r_2 , and θ_2 can be defined for given stair dimensions l and h . Note that r_2 should satisfy the inequality constraint to make the rolling length less than the length of a stair:

$$\frac{2}{3} \pi r_2 < l. \quad (2.3)$$

To determine the kinematic parameters, we designed r_2 to be 124 mm, so as to satisfy (2.3) for the same stepping length when $l = 260$ mm. Based on r_2 , r_1 and θ_1 are determined to be 86 mm and 50° , respectively, from (2.1) and (2.2). l and h were selected as 300 160, which is the most common step size existing in human living environment.

The linearity characteristics of the selected design variables are analyzed by simulation. We selected three different mechanisms, i.e., Rocker-bogie [1], Rocker-Pillar[13] and RHyMo [14], which are specifically designed for stair-climbing. Figure 2.7 shows the results of the simulation. The red line is a straight line parallel to the slope of the stairs and curves show the center of the mass trajectory of each mechanism. Rocker-bogie mechanism shows a backward movement of the center of mass during stair climbing, which is undesired motion in terms of stability. Rocker-pillar is a mechanism proposed to increase traversability during stair climbing by using the front active track. Rocker-pillar eliminated backward

motion but has large fluctuations due to the rear Rocker mechanism.

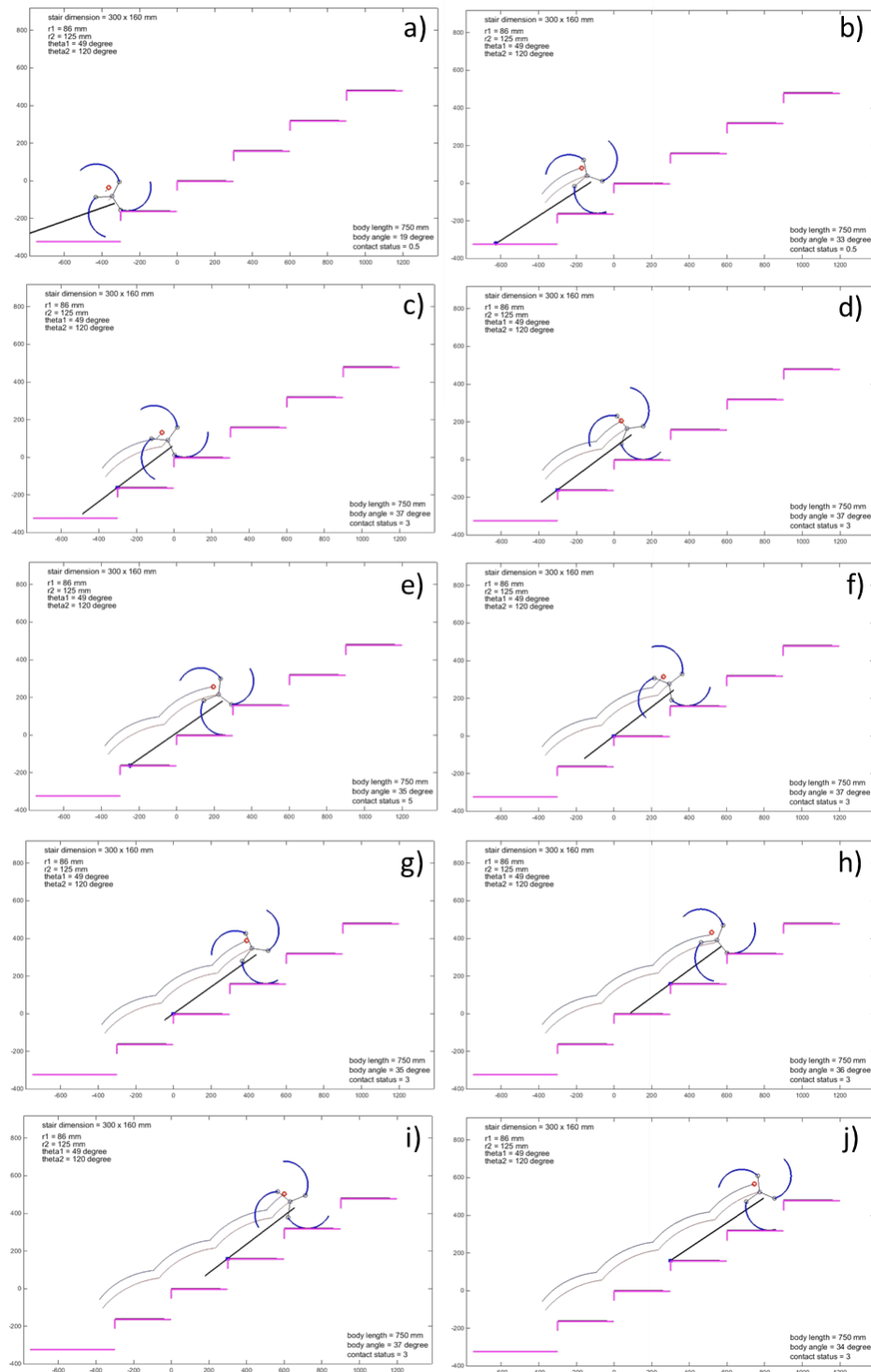


Figure 2.7. Stair climbing simulation results of curved shaped wheel

By applying the inverse four-bar linkage mechanism, RHyMo effectively minimizes fluctuations of center of mass and shows smooth trajectory which is close to the straight line.

The linearity of the CoR line was defined as the average and maximum value of the deviation of the vertical displacement with respect to the linear trajectory. The maximum values of the proposed curved-spoke tri-wheel, rocker-bogie, rocker-pillar and RHyMo were 24.1, 28.4, 33.9 and 26.2, respectively, and the maximum values were 37.8, 70.4, 78.4 and 51.1, respectively. The proposed curved-spoke tri-wheel robot showed the smallest average value and the maximum value. In particular, the maximum value shows a significant difference. The maximum instantaneous value is important for the stability of the robot in overcoming the stairs, which is a meaningful result.

As a result, the proposed curved-spoke wheel mechanism shows the best linearity of CoR line, as compared to other mechanisms. Based on the simulation results, we expect stable stair-climbing for this design.

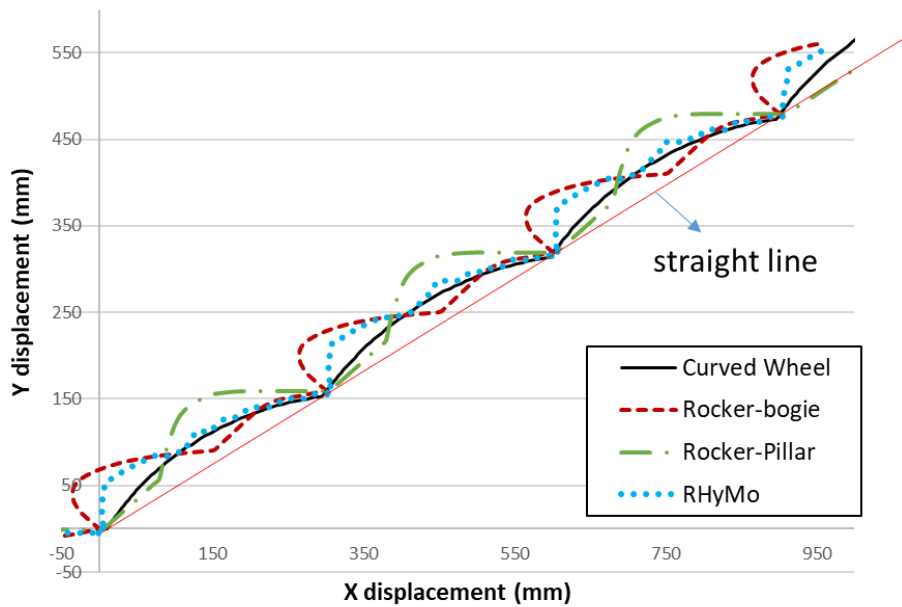


Figure 2.8. Stair climbing trajectories of robots

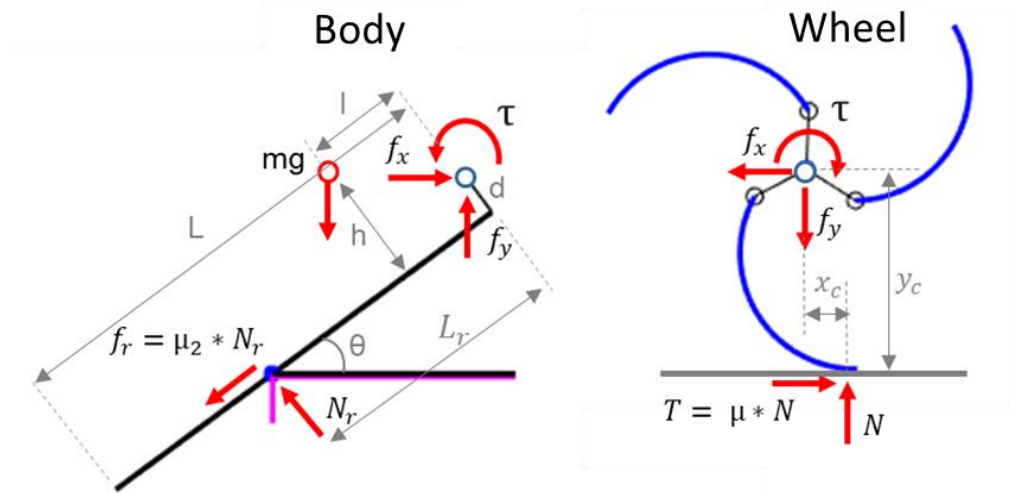


Figure 2.9. Static modeling of robot with curved shape wheel

2.3.2. Required Friction Coefficient

The friction between the wheel and the stair is particularly important for performing stable stair-climbing. It is important to reduce the maximum required friction coefficient because it is directly connected with the ability to overcome obstacles. If the

actual friction coefficient value is smaller than the required friction coefficient value, slip occurs and the obstacle cannot be overcome. To maximize the stair climbing ability, while minimizing the required coefficient of friction structurally, wheel materials with sufficiently high friction coefficient should be used to fabricate the wheels. The minimum required friction coefficient is widely used to evaluate the stability of stair-climbing [11].

Static analysis is performed based on the free-body diagram shown in Fig. 2.8. The force and moment equilibrium equations for the main body ((2.4)-(2.6)) and tri-wheel mechanism ((2.7)-(2.9)) are as follows:

$$\Sigma F_x = -\mu_2 N_r \cos \theta - N_r \sin \theta + f_x = 0, \quad (2.4)$$

$$\Sigma F_y = -mg - \mu_2 N_r \sin \theta + N_r \cos \theta + f_y = 0, \quad (2.5)$$

$$\Sigma M_{CoR} = mg(h_b - d_b) \sin \theta + mgl_{bf} \cos \theta - N_r l_r - \mu_2 N_r d_b + \tau = 0, \quad (2.6)$$

$$\Sigma F_x = \mu_1 N_w - f_x = 0, \quad (2.7)$$

$$\Sigma F_y = -N_w + f_y = 0, \quad (2.8)$$

$$\Sigma M_{CoR} = -N_w x_c - \mu_1 N_w y_c + \tau = 0. \quad (2.9)$$

where N_r , N_w , f_x , f_y , and τ are unknown forces, and μ_1 and μ_2 are undefined parameters, which are expected to be geometrical parameters. Because μ_2 should be minimized for better step-climbing, we set μ_2 to 0.1 for the robot. Then, the six unknown parameters can be determined using (2.4) - (2.9).

The simulated minimum required μ_1 value is shown in Fig. 2.8. We used the same kinematic parameters as in Section 3; the other values of (2.4) - (2.9) are set as follows: (l_{bf} , L , d_b , h_b) = (50, 600, 30, 80) mm. As shown in Fig. 2.8, the required value of μ_1 is increased when the contact point is changed from the floor to the edge and is decreased when the contact point is changed from the edge to the floor, which indicates that the edge contact is insufficient, in terms of required friction coefficient. The value of required friction coefficient is changed as the CoR and center of gravity (CoG) become mismatched, as shown in Fig. 2.9 (wherein a red line indicates the CoG, which has a horizontal offset of 50 mm from the CoR). To design a high-performance robot, the CoG should be coincident with the CoR so as to guarantee a low required friction coefficient.

The maximum required friction coefficient of the proposed curved-spoke-based tri-wheel robot is compared to other robotic solutions. The length of the robot and the size of the wheel is set 600 mm and 250 mm respectively. The value of the maximum required friction coefficient when the rocker-bogie mechanism overcomes the stairs is as high as 2.1 [15].

The robots of the wheel-link structure depend on the frictional force of the wheel in the process of overcoming obstacles, so the value of the required friction coefficient is high. The RHyMo

mechanism has an inverse four-bar mechanism that distributes the load evenly across the wheel, effectively reducing the required friction coefficient when overcoming obstacles to 0.44 [14].

The results show that the proposed robot required relatively little friction coefficient to perform stair-climbing. The maximum required friction coefficient is 0.22. It is half the value compared to the RHyMo mechanism. This is possible because the proposed robot maintains only bottom and edge contact in the obstacle overcoming process. By eliminating contact with the vertical plane, it is possible to avoid the situation where the load of the robot should be supported by the frictional forces. In the next section, we describe the verification of the effectiveness of the proposed design using experiments.

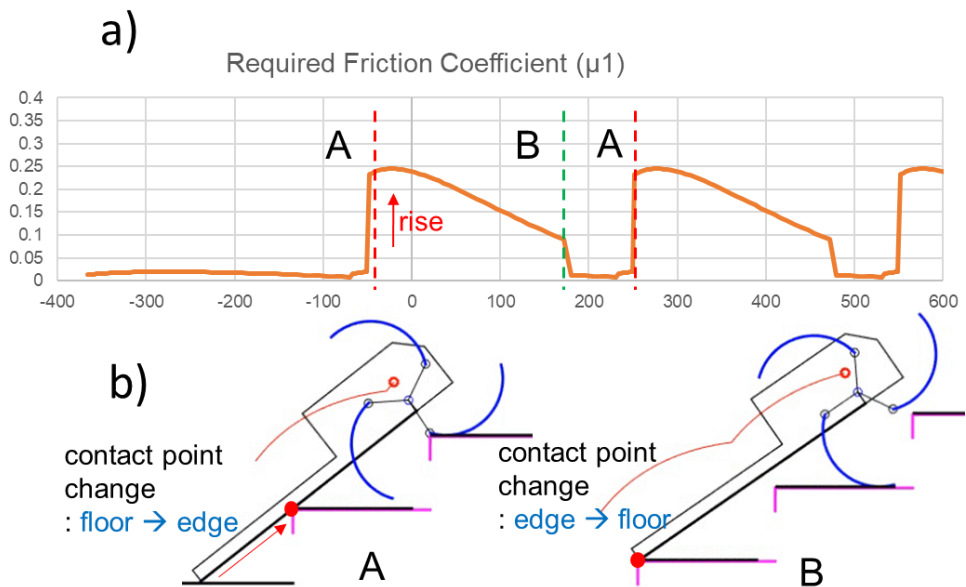


Figure 2.10. Required friction coefficient of a robot with curved shape wheel

2.3.3. Preliminary Experiment Results

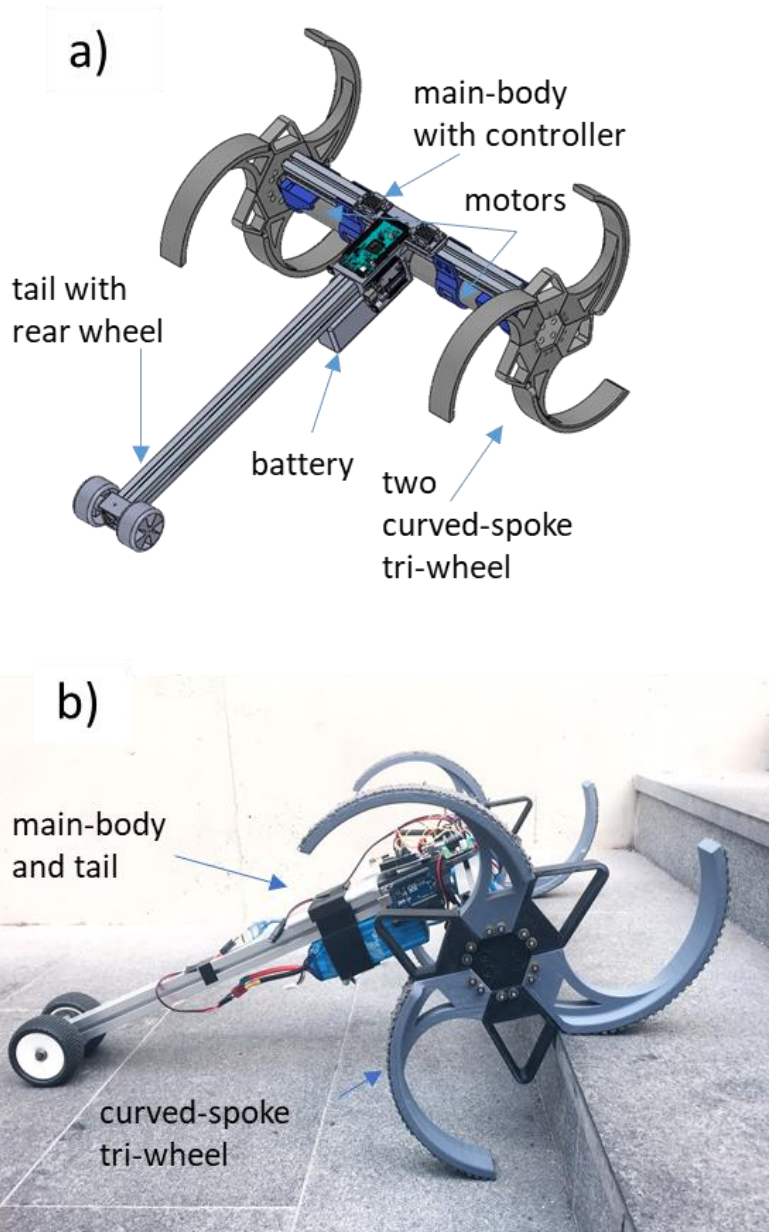


Figure 2.11. Fabricated prototype for preliminary experiment

The prototype was assembled as shown in Fig. 2.10. The fabricated dimension of the curved-spoke wheel mechanism was based on the results of the analysis ($r_1 = 86 \text{ mm}$, $r_2 = 124 \text{ mm}$, $\theta_1 = 50^\circ$). The size of the prototype is $500 \text{ (width)} \times 600 \text{ (length)} \text{ mm}^2$ and the weight is 6 kg . Two DC-g geared motors (52GM, 1:53 gear ratio, 48.6 W) are used with a battery. Arduino Uno is used for the controller with a DC-motor driver. The main body and tail are made of aluminum. The curved spoke with a stopper mechanism is made using a 3D printer and ABS material.

The prototype was tested on two stairs of different sizes, $300 \times 160 \text{ mm}^2$ and $300 \times 100 \text{ mm}^2$, as shown in Fig. 2.11 (a-h) and (i-p), respectively. Please refer to the detailed diagram of step-climbing in the Multimedia supplement. The speed is varied from 5 m/min to 40 m/min , which is a higher speed than that of typical human stair-climbing. The results showed that the robot can stably climb the stairs at high speed via repeated motion. As shown in Fig. 2.11 (a-b), the stopper mechanism causes the initial condition for each new step to be the same; the curved spoke is used to walk on the stairs stably. The mechanism works well on different sizes of stairs. Without the stopper mechanism, the slip length is changed, as shown in Fig. 2.11(c-d), which shows the stepping posture for first and second steps without the stopper. As the length of the stopper mechanism increases, the range of applicable step sizes increases. Therefore, the stopper mechanism of an appropriate size suitable for the environment in which the robot is used may be selected.

As shown in Fig. 2.11 (a-d), field test was also performed on stairs with dimensions of $300 \times 160 \text{ mm}^2$ with size deviations of 10 mm to check the practicality of the mechanism. For stairs in real life, not only size deviations but low friction condition also exists compared to experimental environment. It also went up well despite the stairs with the nose as shown in Fig. 2.11(i). Wheel linkage mechanism robot is unable to overcome stairs with nose or stairs without riser, but our proposed curved wheel robot can overcome various types of stairs even when the friction coefficient is low.

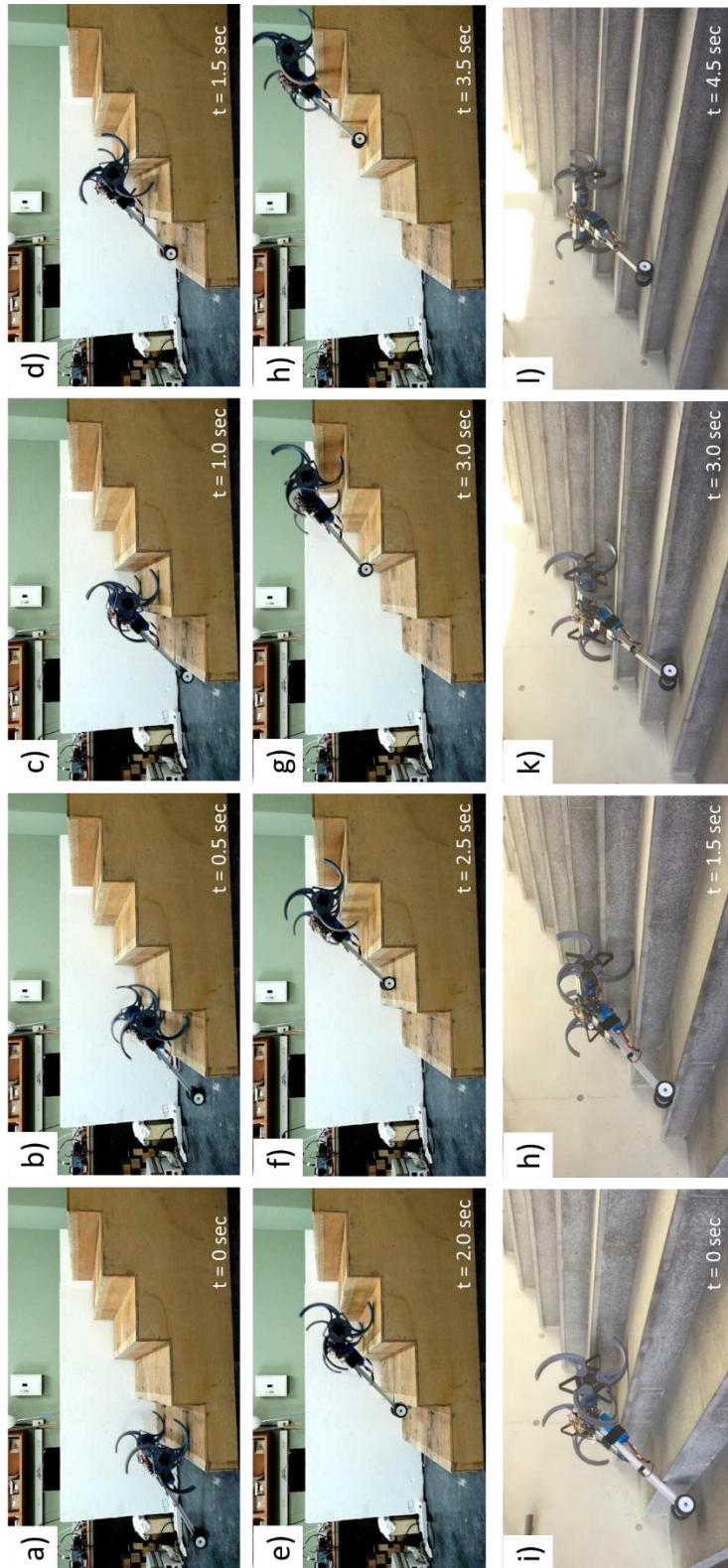


Figure 2.12. Stair climbing experiment of curved shaped wheel

Chapter 3. Type Synthesis of 2-DOF Transform Mechanism

In order to find the optimum 2-DOF transformation mechanism, the key requirements such as the required transformation range of the transformation mechanism are defined, and the mechanism is searched through a systematic type synthesis method and selected through the evaluation based on the requirements.

3.1. Requirements of Transform Mechanisms

The key requirements that the transformation mechanism must satisfy are defined. Table 3.1 shows requirements for a transformable wheel mechanism which are associated with its kinematic structure.

R1 is a constraint on wheel size. The larger the wheel size is, the better it is to overcome obstacles. However, in this study, we aimed to develop transformable wheel mechanism that can overcome various obstacles even with a wheel size of 250 mm which is similar to the wheel size of a general indoor robot. We also assumed a wheel with three lobes, which is a value determined so that the length of one lobe is less than the minimum step width (260 mm).

R2 to R3 are requirements related to the kinematic structure of the transformable wheel mechanism.

R1-R6 are the basic requirements that wheel transform mechanisms must satisfy, which are success/fail requirements, and R7-R11 are the qualitative requirements. In particular, R1 to R4 are the most fundamental requirements to be considered from the step of creating mechanism structures, which are shown in Figure 3.1. As discussed in Section 2.1.3, the transformation mechanism requires two degrees of freedom (R2). In addition, all lobes must be moved together (R3) to simplify the structure by minimizing the number of actuators for the mechanism. In order to perform the function of the rolling wheel, interference with the outside should not occur (R4).

Table 3.1. Requirements of transformable wheel mechanism

Requirement	Description
R1	Diameter of the wheel is 250 mm
R2	Transform mechanism has two degrees of freedom
R3	Motions of every lobes are synchronized by the mechanism
R4	All parts of the mechanism must be located inside the wheel
R5	The wheel morphs into various shapes for various obstacles
R6	No interference with external environment and wheel itself
R7	Required torque should be small
R8	Structurally sufficient stiffness must be ensured
R9	The error for transformation should be small.
R10	The simpler the structure, the better
R11	Ease of fabrication
R12	Avoid singularity

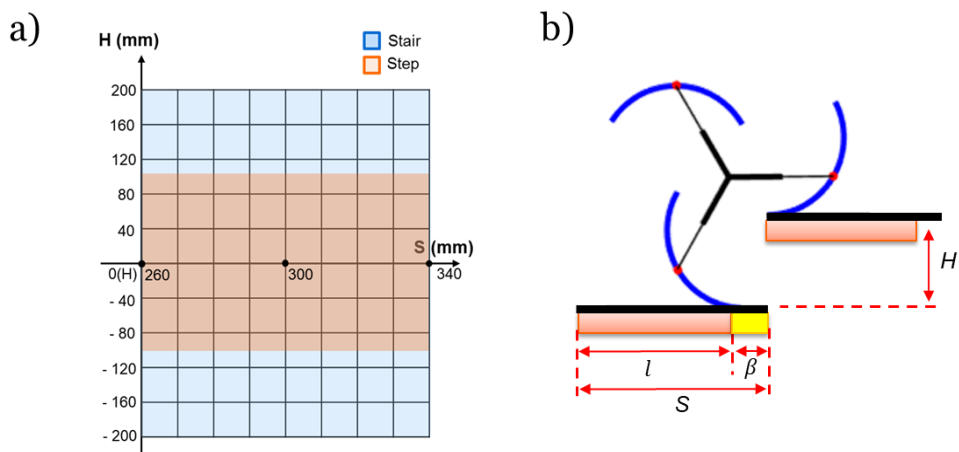


Figure 3.1. Necessary morphed shape of wheel for an obstacle sizes

To derive various shape of morphed wheel in requirement 5, it is necessary to define the range of obstacles to be overcome. Various obstacles in the human living environment are defined as shown in Fig. 3.2 (a). Most obstacles in the human living environment consist of a combination of vertical and horizontal surfaces, and can be largely classified as stairs and step obstacles. According to the Building Code [12], the width of the public stairway should be at least 260 mm, and the height should be less than 200 mm. Various step obstacles are defined as 0 ~ 100 mm height.

Given initial posture and position of the wheel, distance from the obstacle and the height of the obstacle, we can derive a unique shape of the wheel that the wheel must be transformed into. This is because the wheel determines the posture at the transition point at which the contact point of the lobe moves as shown 2,3,5 and 6 in Fig 3.2 (b). The shape of the wheel is determined according to the following kinematic equations.

$$S = R * \theta_2 - R \sin\left(\frac{\theta_2}{2}\right) + r_1 \left(\cos\left(\theta_1 + \frac{\pi - \theta_2}{2}\right) + \cos\left(-\theta_1 + \frac{\pi - \theta_2}{2}\right) \right) - r_2 \cos\left(\frac{\theta_2}{2}\right)$$

(3.1)

$$H = -R \cos\left(\frac{\theta_2}{2}\right) + r_1 \left(\sin\left(\theta_1 + \frac{\pi - \theta_2}{2}\right) - \sin\left(-\theta_1 + \frac{\pi - \theta_2}{2}\right) \right) + r_2 \sin\left(\frac{\theta_2}{2}\right)$$

(3.2)

In particular, the size of the wheel to be transformed in a4 and a5 in Fig 3.2 is the most extreme cases, which is a necessary condition for a transformable wheel.

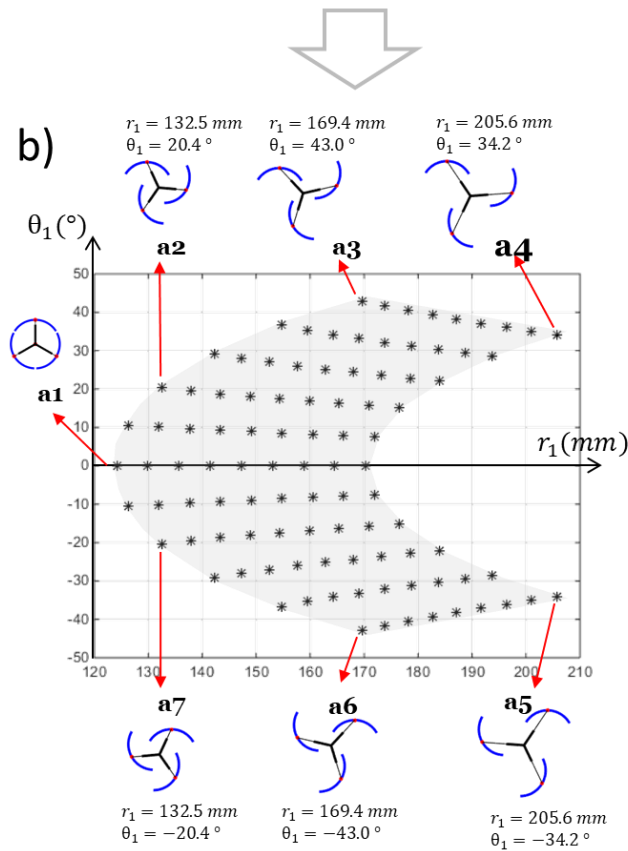
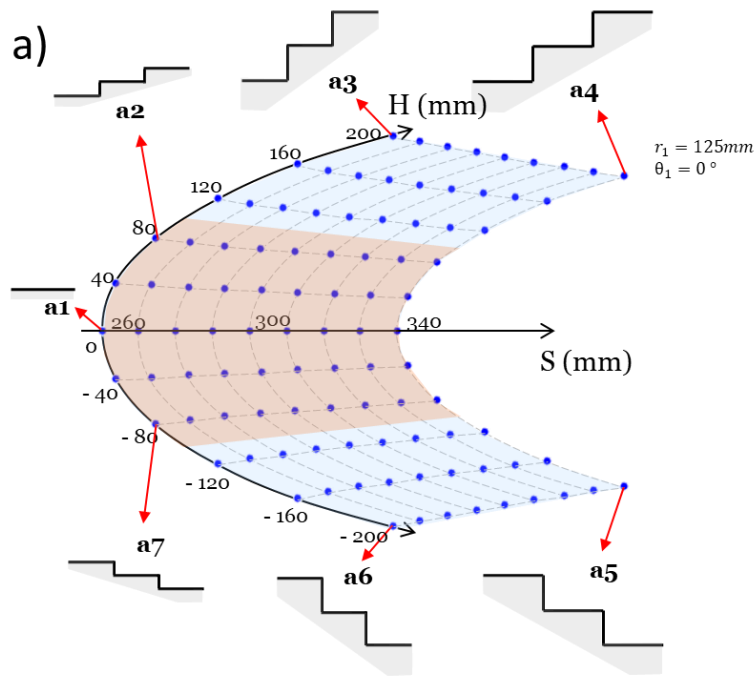


Figure 3.2. Target obstacle and required range of transformation (a) Target obstacle range (b) Required transform range and corresponding wheel variable and shape

3.2. Exploration of 2-dof mechanisms

3.2.1. Systematic process of developing design alternative mechanisms

In order to find the optimal mechanism for realizing the two degree of freedom motion of three lobes satisfying kinematic requirements, a systematic approach is required. It is difficult to find optimal mechanisms that meet defined functions, constraints, and requirements relying on intuition. Type synthesis is a method to search for optimal mechanism structure that performs predefined functions and is suitable to apply to this study. First, we explore a two degree-of-freedom kinematic structure that can transform one lobe relative to the base of the wheel (Fig.3.3). Among the mechanisms of 2 degrees of freedom, the simplest serial two – link structure and the parallel five – section link structure are explored. And among explored mechanisms, we exclude mechanisms that do not meet the requirements. Finally, we derive the final design mechanism by combining the appropriate mechanisms to drive the three lobes at the same time (Fig.3.4).

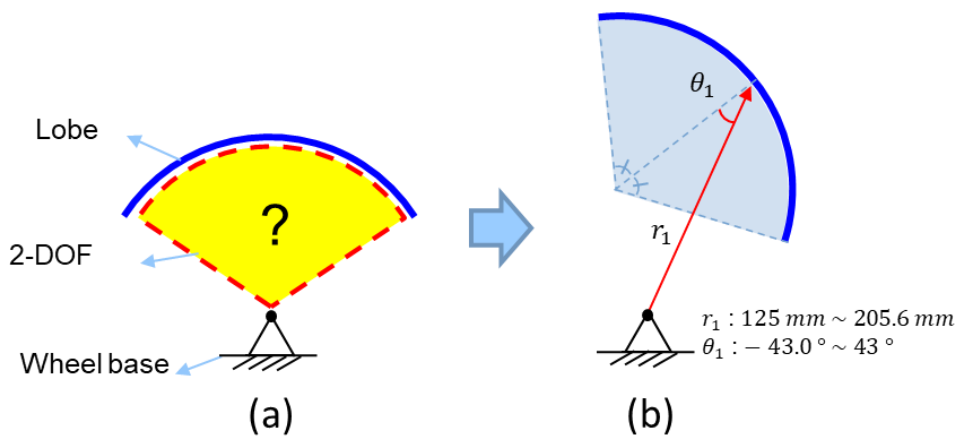


Figure 3.3. Systematic process of developing design alternative mechanisms
Basic requirements of the transformable wheel mechanism (a) 2-dof motion
of the wheel mechanism (b) synchronized motion of all lobes

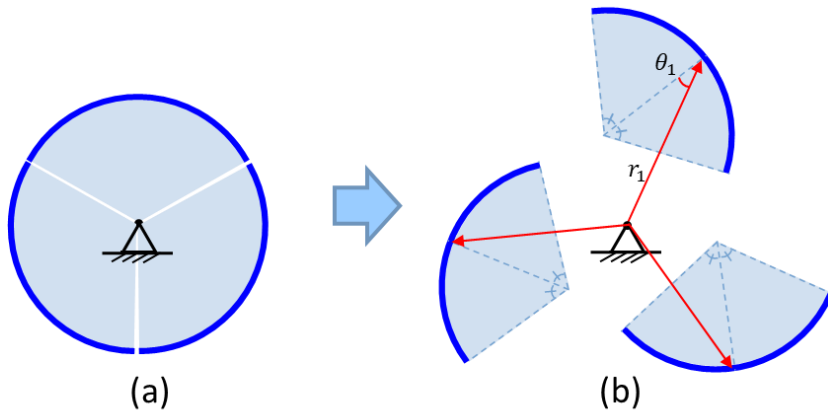


Figure 3.4 synchronized motion of all lobes

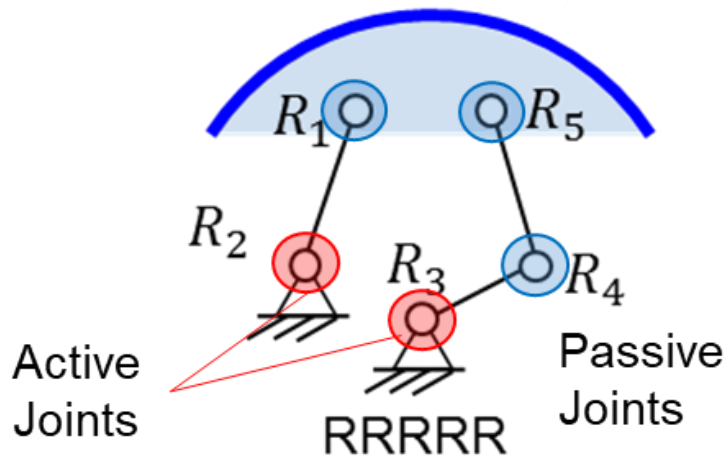


Figure 3.5. Kinematic structure of 5-bar parallel mechanism

3.2.2. Exploration of 2-dof mechanisms

According to the Gruebler' s equation, the two degrees of freedom mechanisms with the lowest number of links and joints are serial 2-dof mechanisms. Since there are only two joints, all joints must be actuated joints. As (1) – (4) in figure 3.6, there are four cases depending on the combination of revolute joint and prismatic joint.

Next, a simple two-degree-of-freedom mechanism that can be considered is a parallel mechanism consisting of five links and five joints. In this case, the two joints are actuated joints and the remaining three joints are passive joints (Fig.3.5). The actuated joint must be supported by base, hence two joints on the wheel base becomes the active joint. At this time, the active joint does not have to match the center of rotation of the wheel.

Figure 3.6. Consider, for example, the 5R structure of (5), a simple five-bar linkage structure where the two revolute joints in the base become the active joints and the remaining three revolute joints become the passive joints. The combination of revolute joint and prismatic joint creates a new combination of (6) – (36). As a result, there are a total 32 cases of kinematic structures according to the combination of the R and P joints. Mirror symmetric is considered as the same mechanism. As can be seen in Figure 3.6, total 36 cases of 2-DOF mechanisms are derived.

3.2.3. Exclusion of Alternatives with Passive Prismatic Joints

Among 36 mechanisms, firstly we need to exclude mechanisms that do not satisfy requirements of transformable wheel. In order to find the optimal mechanism effectively, first of all, qualitative evaluation should exclude the mechanisms that do not satisfy the requirements and reduce the scope of the alternative.

We have analyzed alternatives with passive prismatic joints among various design alternatives. RPRPR mechanisms is selected to be analyzed using linkage software (Fig. 3.7).

In order to realize the motion of the passive prismatic joint, a mechanical element is required for linear motion. In other words, a separate linear guide is required for the link to perform a linear motion, and the linear guide must have a stroke enough to satisfy the required range of deformation. However, it is difficult to satisfy the transformation range of the lobes as can be seen in Figure 3.8, which is the simulation result,

Moreover, according to a previous study on 2-dof planar parallel manipulators [16],

“prismatic joints must be active, because passive prismatic joints tend to have problems of friction and accuracy” .

Since the rotational motion of each actuator must be transformed into a passive linear motion as on figure 3.8, As a result, a force perpendicular to the direction of movement of the linear guide must exist, and resultantly, friction also becomes a big problem.

From these problems of mechanisms with passive p joints, the mechanism including the passive prismatic joint was excluded.

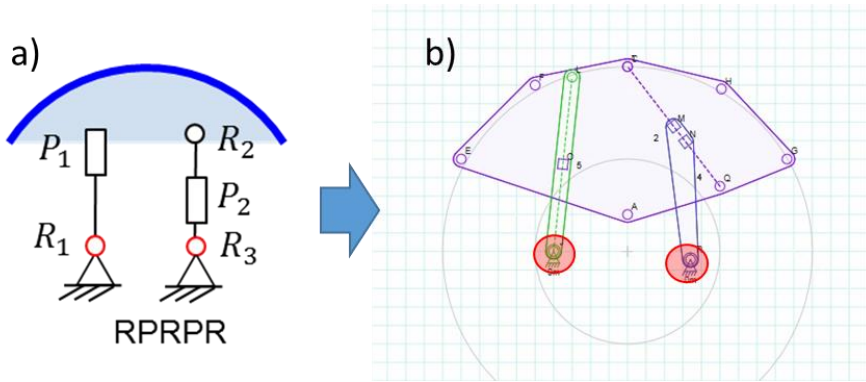


Figure 3.7 Linkage software simulation of RPRPR 5bar mechanism (a) kinematic structure of RPRPR mechanism (b) Linkage software modeling of RPRPR mechanism

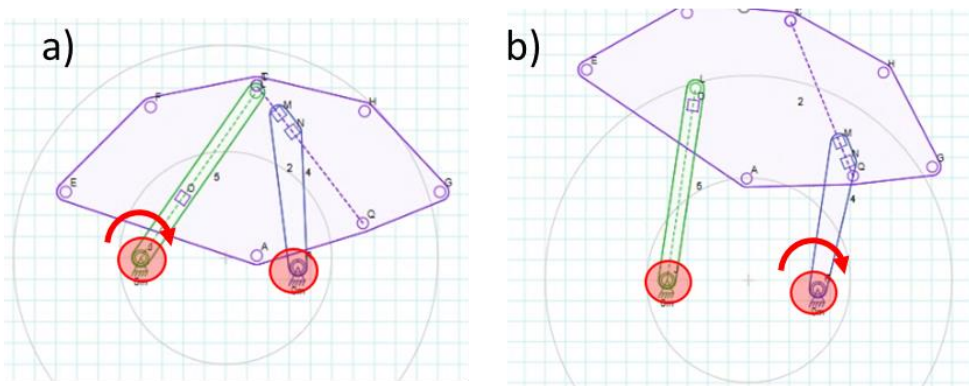


Figure 3.8 Linkage software simulation result of RPRPR 5bar mechanism

As a result, a total of four kinematic structures remain, as shown in Figure 3.9 below. In the case of the 5-bar link structure alternative, the number of the three cases according to whether the two joints of the base are revolute joints or prismatic joints are shown in (b) ~ (d).

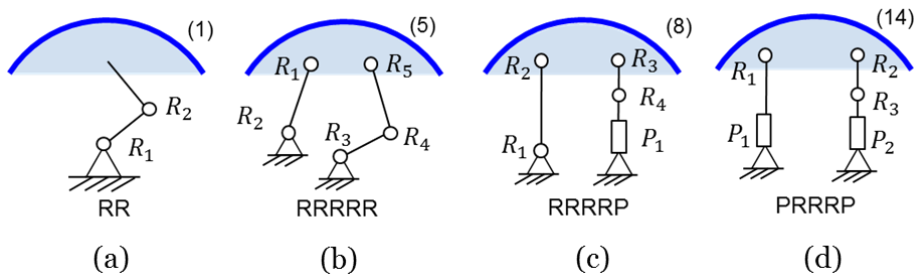


Figure 3.9. Remained alternative mechanisms

(a) 2R (b) 5R (c) 4R1P (d) 3R2P

3.2.4. Design alternatives by combining synchronization mechanism

Until 3.2.3, we searched for mechanisms of two degrees of freedom to move one lobe. This mechanism and the synchronization mechanism for moving the three lobes at the same time must be applied to complete the final two degrees of freedom transformation mechanism. Synchronization mechanisms includes gears, belts, ternary links, etc. A total of five variant wheel mechanism design alternatives were derived through appropriate combinations of 2-DOF mechanisms and synchronization mechanisms. Detailed operating principles of design alternatives are described in detail in Section 3.3.

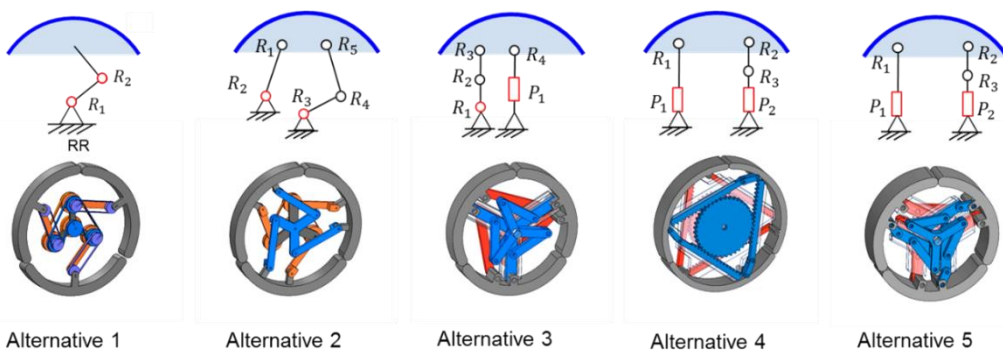


Figure 3.10. 5-types of 2-dof design alternatives

3.3. Characteristic analysis of alternative mechanisms

For the four kinematic structures derived in Section 3.3, we have derived five design alternative mechanisms of the transformable wheel by adding appropriate synchronizing mechanisms, as shown in Figure 3.10.

Design alternative # 1

The first design alternative is based on a serial 2-bar structure, in which the three lobes move synchronously through two pairs of belt-pulley mechanisms. Rotating the orange driving pulley 1 on the wheel's axis of rotation rotates the orange sub-pulleys and rotates the orange link on the sub-pulley. Figure 3.11 (c) shows the case when driving pulley 1 is rotated. Rotating the blue driving pulley 2 rotates the purple 1st sub-pulley and 2nd sub-pulleys which are attached to the end of the orange link, thereby rotating the lobe.

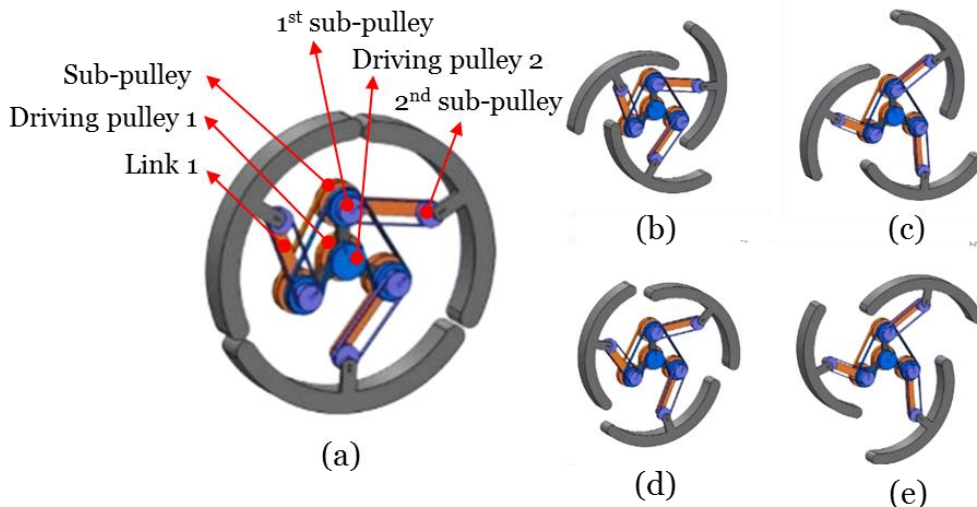


Figure 3.11. Structure and operation of Design Alternative #1. (a) Structure when in a circular wheel state (b) When the driving pulley 2 is rotated clockwise (c) When the driving pulley 1 is rotated counterclockwise (d), (e) When the driving pulley 1 is rotated counterclockwise and driving pulley 2 is rotated clockwise

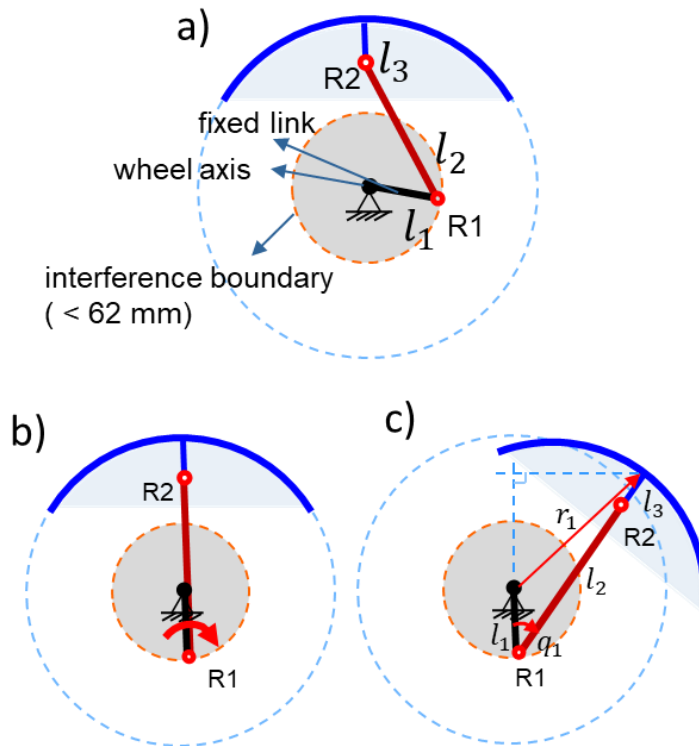


Figure 3.12. Analysis of transform range and characteristic of alternative 1 (2R) mechanism (a) Design variables (b) Configuration for maximum transformation of r_1 (c) One degree of freedom transformation from (b)

The 2-bar mechanism of Design Alternative # 1 can be simplified as shown in Figure 3.12 a) and R1, R2 are active joints. Figure 3.12 shows the configuration to satisfy the transform range of the wheel which must have a larger radius than the circular shape. That is, the sum of the distance from the rotation axis to the sub-pulley l_1 and the length of l_2 should be greater than the radius of the wheel. The maximum transformation amount in the r_1 direction corresponds to twice the length of l_1 . To avoid interference, the R1 joint must be within a 62 mm radius from the center of rotation, and the maximum length of l_1 is set to 62 mm. It can be seen that the maximum r_1 is 124 mm.

following equation (3.3) shows a nonlinear relationship between q_1 and r_1 .

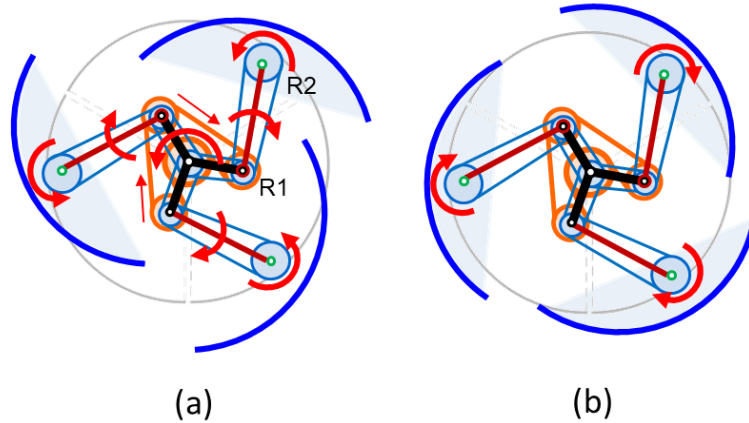


Figure 3.13. The coupling property of design alternative 1 (a) When R1 rotates only by the rotation of the orange belt, the R2 joint rotates by the revolution of the pulley located at R2. (b) When R2 rotates by the rotation of blue belt

$$r_1 = \sqrt{(l_2 + l_3)^2 - 2l_1(l_2 + l_3) \cos q_1 + l_1^2} \quad (3.3)$$

Another characteristic of alternative#1 is that each degree of freedom is coupled to each other. When R1 rotates only by the rotation of the orange belt, the R2 joint rotates by the revolution of the pulley located at R2.

Design Alternative # 2

Design alternative 2 is based on a parallel five-bar link, and all joints are composed of R joints. The three lobes are synchronized with a set of belt-pulley mechanisms (orange) and a ternary link (blue) rotating about the wheel axis (Fig.3.14 (a)). Transformed shapes according to the movements of the degrees of freedom can be seen from (b) to (d) in figure 3.14. All of joints are composed of R joints, and r_1 and θ_1 and the rotation of the wheels are both nonlinearly coupled with respect to two degrees of freedom of transformation.

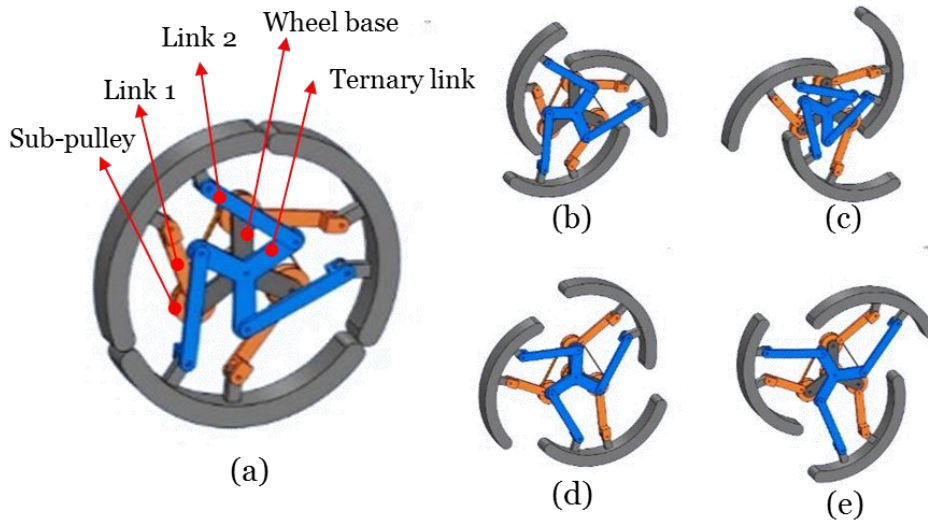


Figure 3.14. Structure and operation of Design Alternative #2. (a) Structure when in a circular wheel state (b) When the ternary link is rotated counterclockwise (c) When the driving pulley 1 is rotated counterclockwise (d), (e) When the driving pulley 1 is rotated counterclockwise and driving pulley 2 is rotated clockwise

Design Alternative # 3

Design alternative 3 is a 4R1P mechanism with one P-joint in the wheel base (Fig.3.15).

Design Alternative # 4

Design alternative 4 is a 3R2P mechanism with two P-joint in the wheel base (Fig.3.16). Two P-joints in the base drive the two-degree-of-freedom mechanism, all driven by a rack-pinion mechanism. If the driving lengths of the P joints are the same, only the deformation of the wheel in the radial direction (r_1) occurs and the rotation of the lobes (θ_1) occurs due to the difference of the P joint stroke difference.

The size of the pinion should be the same size as the circle tangent to the three racks. In order to avoid interference with the lobe, the length of the rack is also limited, and thus the stroke is limited.

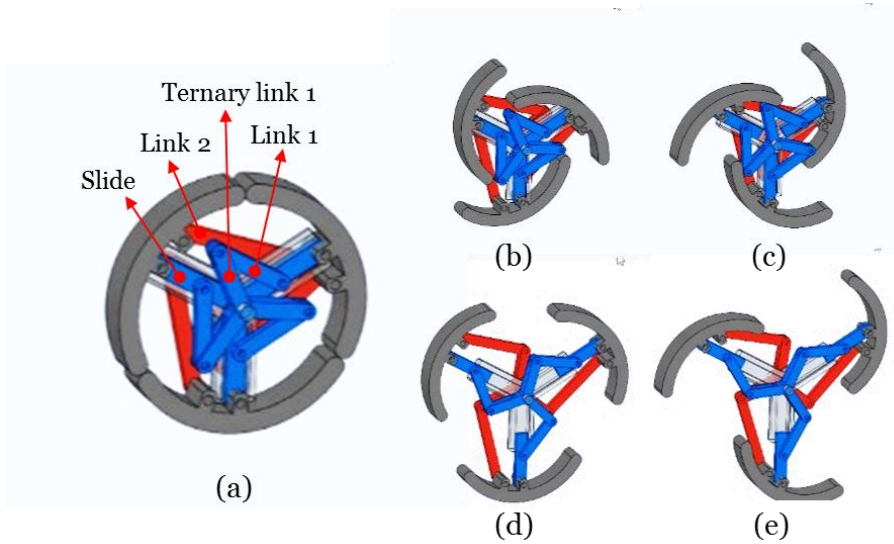


Figure 3.15. Structure and operation of Design Alternative #3. (a) Structure when in a circular wheel state (b) When the red ternary link is rotated counterclockwise (c) When the blue ternary link is rotated clockwise (d) When blue ternary link is rotated clockwise and red ternary link is rotated counterclockwise with same degree (e) When blue ternary link is rotated clockwise and red ternary link is rotated counterclockwise with angle difference

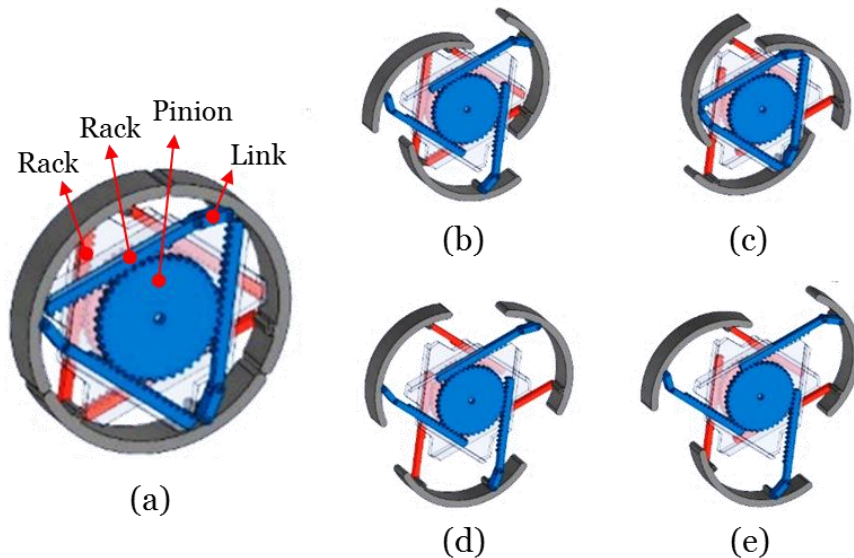


Figure 3.16. Structure and operation of Design Alternative #4. (a) Structure when in a circular wheel state (b) When blue pinion is rotated clockwise (c) When red pinion is rotated counterclockwise (d), (e) When blue pinion and red pinion 1 is rotated clockwise and counterclockwise respectively

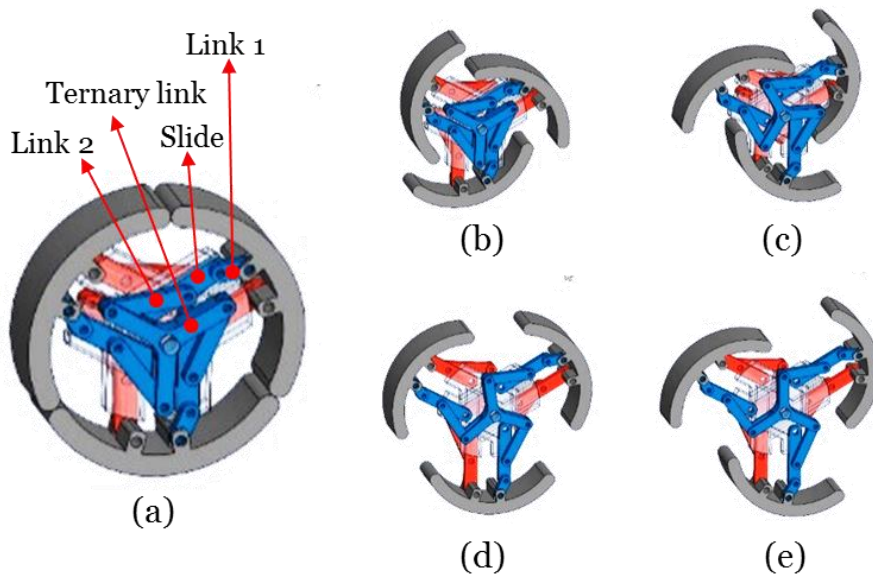


Figure 3.17. Structure and operation of Design Alternative #5. (a) Structure when in a circular wheel state (b) When the red ternary link is rotated counterclockwise (c) When the blue ternary link is rotated clockwise (d) When blue ternary link is rotated clockwise and red ternary link is rotated counterclockwise with same degree (e) When blue ternary link is rotated clockwise and red ternary link is rotated counterclockwise with angle difference



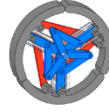
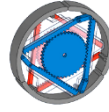
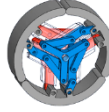
Design Alternative # 5

Design alternative 5 is a 3R2P mechanism with two P-joint in the wheel base (Fig.3.17).

Two P-joints in the base drive the two-degree-of-freedom mechanism, all driven by a rack-pinion mechanism. If the driving lengths of the P joints are the same, only the transformation of the wheel in the radial direction (r_1) occurs and the rotation of the lobes (θ_1) occurs due to the difference of the P joint stroke difference.

Design Alternative 5 is fundamentally the same mechanism as Design Alternative 4, but the mechanism of linking lobes is different. Design Alternative 4 The structure of Design Alternative 5 has a larger stroke because the prismatic slide is attached in the radial direction of the wheel, while the stroke is constrained by the rack-pinion structure.

Table 3.2 Qualitative evaluation based on requirements of morphing wheel mechanism

Requirements	#1	#2	#3	#4	#5
					
R5 The wheel morphs into various shapes for various obstacles	+	0	0	-	+
R6 No interference with external environment and wheel itself	-	0	-	-	+
R7 Required torque should be small	-	-	0	0	+
R8 Structurally sufficient stiffness must be ensured	-	-	0	0	+
R9 The error for transformation should be small.	-	0	0	-	0
R10 The simpler the structure, the better	-	0	-	-	0
R11 Ease of fabrication	-	-	0	-	-
R12 Avoid singularity	0	-	-	0	0

From the characteristics analysis and qualitative evaluation of the wheel, it is as shown in Table 3.2, and it can be seen that Design Alternative 5 is the best.

3.4. Step Overcoming Simulation and Evaluation

In order to compare the mechanism derived from 3.3, a kinematic-based obstacle overcoming simulation was performed.

3.4.1. Simulation Conditions

A harsh condition of 180 mm tall obstacle was assumed to climb and descend at a distance of 780 mm.

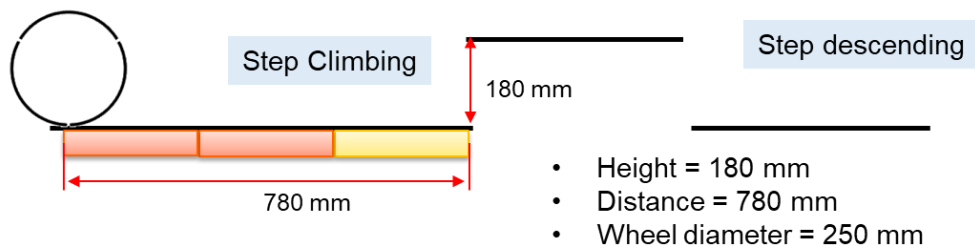


Figure 3.18. Step overcoming simulation conditions

At this time, the trajectory of $r1$ - θ_1 required when overcoming the step is shown in Figure 3.19. In the course of going beyond the step, we compare and evaluate whether interference occurs in the mechanism, satisfies the required transform amount, does not exceed the singularity.

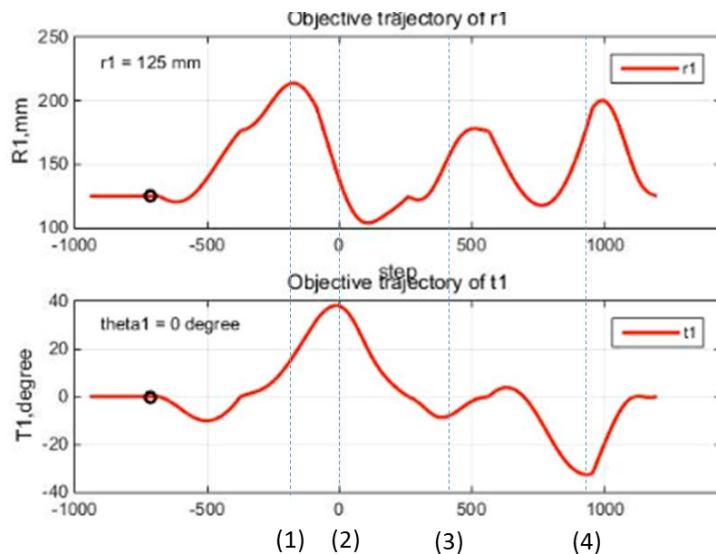


Figure 3.19. Required $r1$ - θ_1 transform trajectory for step overcoming

3.4.2. Inverse Kinematics of the Mechanisms

The process of deriving the solution of the inverse kinematics by geometric analysis based on the basic 5-bar 5R mechanism (Fig.3.20) is as follows. First, assume that the angle of r_1 is 0, and move the points R2 and R3 parallel to the y direction (r_1 direction) (Fig. 3.21 (b)). Then, R2, and R3 are rotated about the lobe center point by θ_1 angle and the equation to find the angle of r_1 is solved as shown in Fig. 3.21(c). The unknown at this point is the position of the R2 point, and is the intersection of a circle centered at COR and a radius of d and a circle centered at R1 and having a radius of l_1 (Fig. 3.21 (c)).

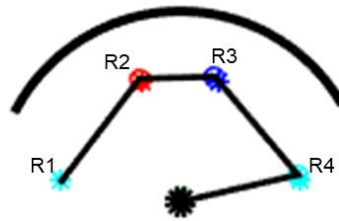


Figure 3.20 Configuration of the 5-bar 5R mechanism

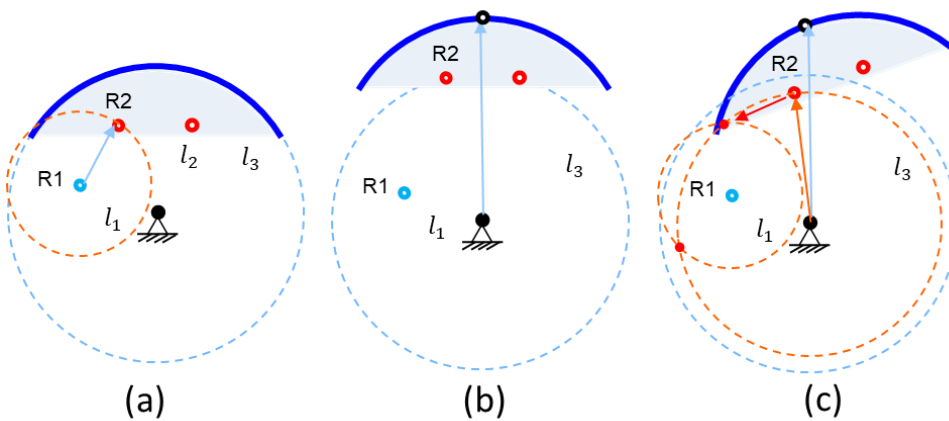


Figure 3.21 The process of obtaining the configuration of a mechanism satisfying r_1 - t_1 with inverse kinematics

3.4.3. Simulation Results



Figure 3.22. Step overcoming simulation results (1/2) for 5 design alternative mechanisms



Figure 3.23. Step overcoming simulation results (2/2) for 5 design alternative mechanisms

3.4.4. Analysis and Evaluations

Design Alternative 2

For the Design Alternative 2 mechanism, R1 and R4 joints must be within 60 mm of the center of rotation to avoid interference with the corners during step climb (Fig. 3.24 (a)). Fig. 3.25 (b) shows the interference condition of the mechanism and the step. In addition of the interference condition, in order to satisfy the required transformation range, $l_0 + l_1$ and $l_3 + l_4$ must be increased (Fig. 3.24 (c)). The configuration of the mechanism to satisfy all of these condition is as shown in Fig. 3.24 (d).

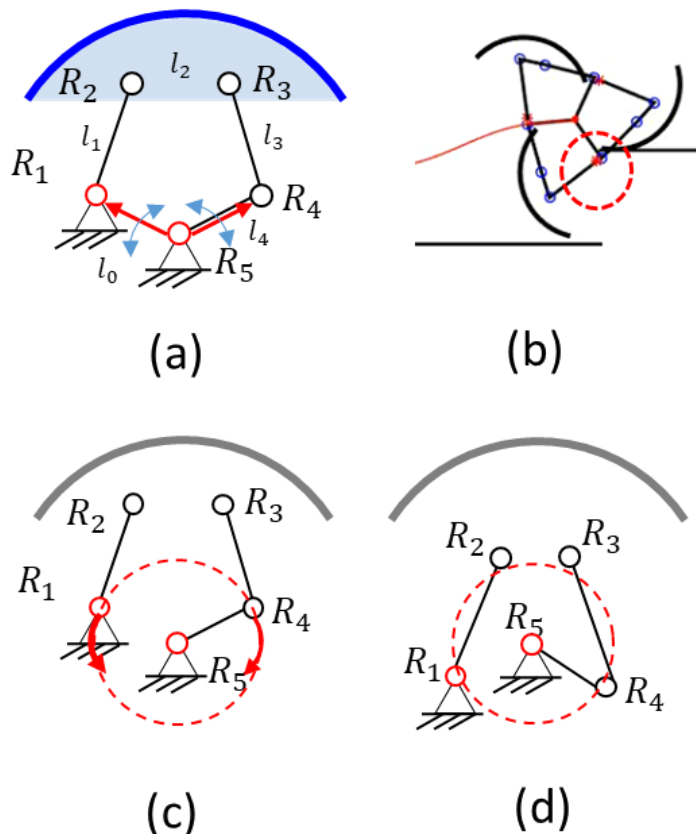


Figure 3.24. Analysis of design alternative #2 5R mechanism

Moreover, the singular point should be avoided because, first, the mechanism may not be extended anymore, and second, the actuator may be in a state where it cannot move to the desired configuration

by driving the actuator. the singularities that the mechanism can have are shown in Fig. 3.25, which shows that the singularities of COR-R1-R2 / COR-R4-R3 must be avoided. We defined the following conditions for avoiding singularities and found new satisfactory design variables.

1. $d(\text{COR-R2}) \leq d(\text{COR-R1}) + d(\text{R1-R2})$
2. $d(\text{COR-R2}) \geq d(\text{COR-R1}) - d(\text{R1-R2})$
3. $d(\text{COR-R2}) \geq d(\text{R1-R2}) - d(\text{COR-R1})$



$$|l_1 - l_2| \leq d(\text{COR-R2}) \leq l_1 + l_2$$

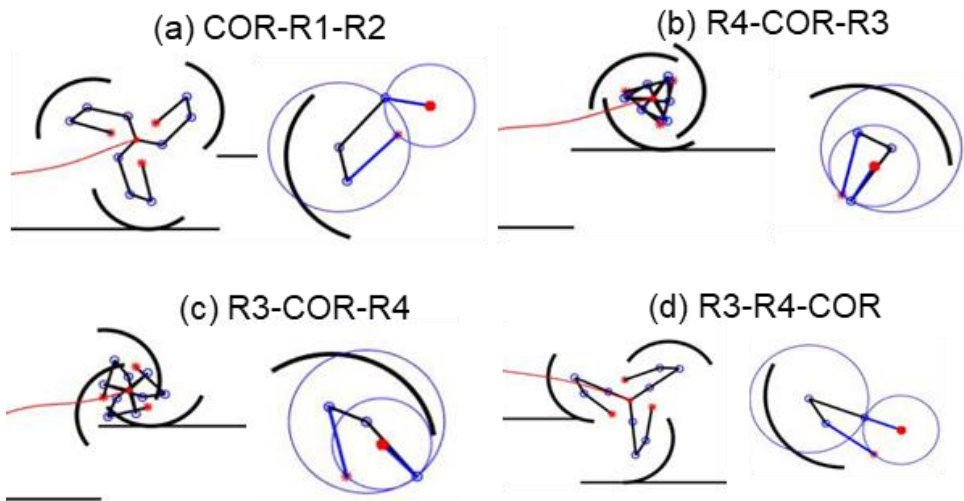


Figure 3.25. Singularity and interference of simulation results of design alternative #2

The new design parameters satisfying these conditions are as follows (Fig.3.26).

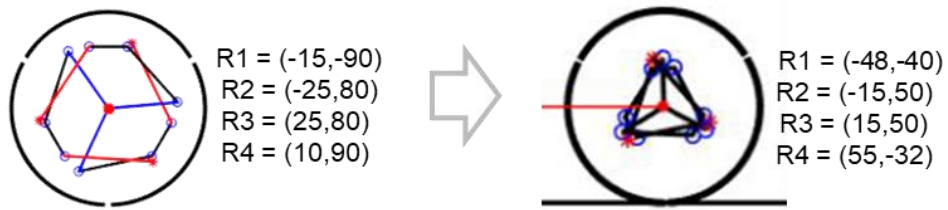


Figure 3.26. New design parameters of design alternative #2

It can be confirmed that the singularity of COR-R1-R2 / COR-R4-R3 does not occur but the R2-R3-R4 singularity occurs. Since the movement of the link cannot be defined by the driving of the actuator, the corresponding singular point must also be avoided. Moreover, the required rotational speed fluctuation of the design alternative 2 mechanism is large and there is a reverse rotation section, and as a result, and concluded that it is not suitable for transformable wheel mechanism.

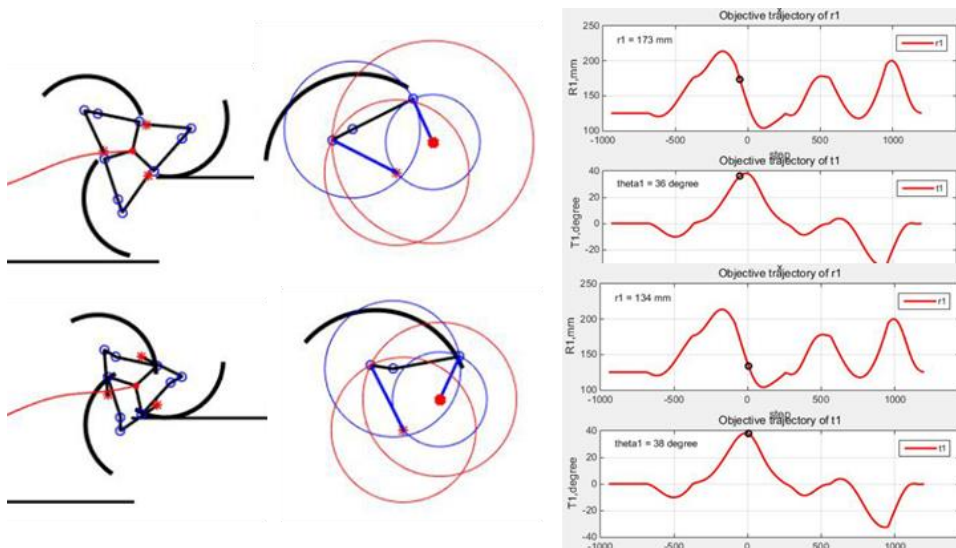


Figure 3.27. Simulation results of design alternative 2 with new design parameters: R2-R3-R4 singularity configuration

Design Alternative 4

Design Alternative 4 is based on the 5-bar mechanism with 2 P joints located at base, the two P-joints are mechanisms driven by the rack-pinion.

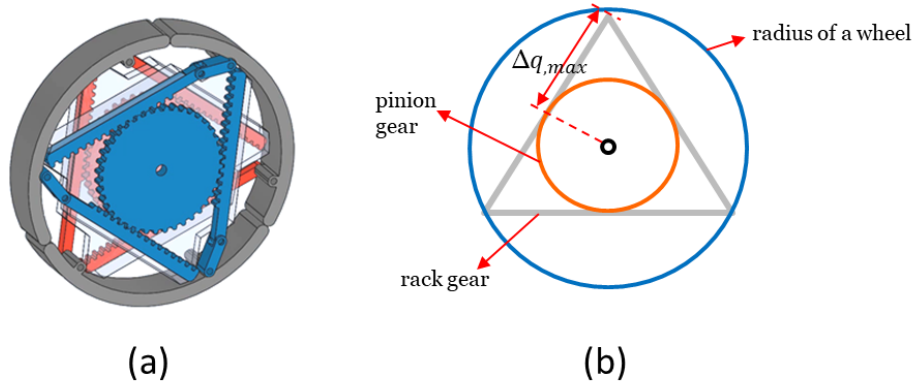


Figure 3.28. Configuration of design alternative 4

The geometric maximum delta q is determined as follows.

$$\Delta q = \frac{\sqrt{3}}{4} r_2$$

Assuming that the radius of the wheel is 125 mm, the maximum delta q is 54 mm. Required q1 q2 is 100 mm, but it is smaller than this and cannot be used as a transformation mechanism.

Although the rack-pinion structure was disadvantageous due to spatial constraints, the 3R2P mechanism with the largest number of P joints is advantageous because of its intuitive kinematics and simple structure easy to avoid interferences and singularities.

3.5. 5-bar 3R2P Mechanism

As a result, a 5-bar link structure with two P-joints at the base was selected as the most suitable mechanism for the modified wheel mechanism. The rotation angle θ_1 of the wheel changes according to the displacement difference of each active P joint, and when driven by the same displacement, the radius from the center of the spoke changes.

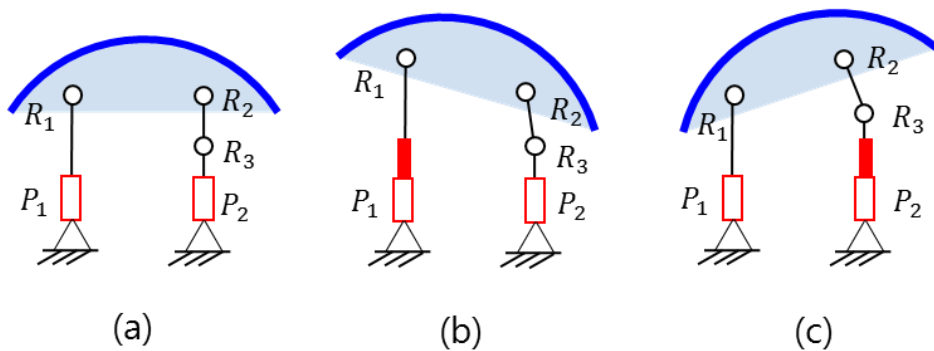


Figure 3.29. Configuration of selected design alternative 5 mechanism.
(a) Initial state (b) configuration when displacement of P1 joint exists (c)
configuration when displacement of P2 joint exists

Chapter 4. Design of the STEP platform

4.1. Concept design of the STEP platform

4.1.1. Issues of actuator location

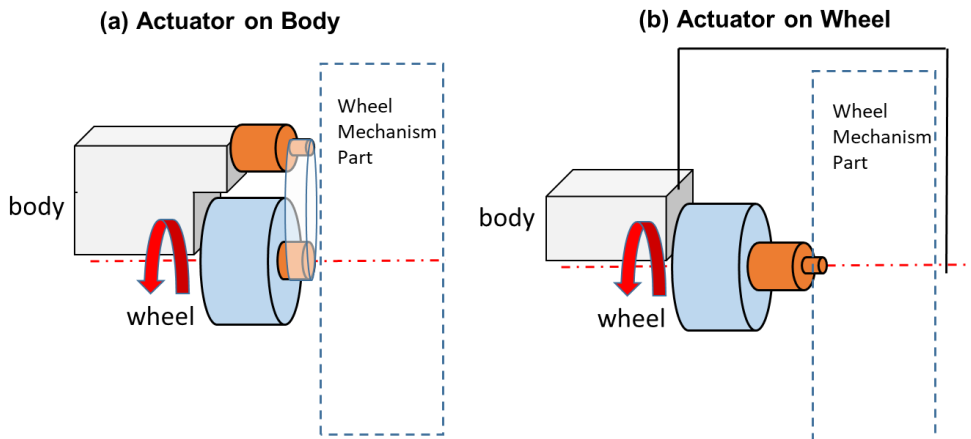


Figure 4.1. Issues of actuator location

In the process of implementing the mechanism, there is an issue of whether the actuator is located in the main body or the wheel. As shown in Fig.4.1 (a), when the actuator is placed in the body, the wheels can be designed lightly, but the structure for transmitting the driving force is required, thus complicating the overall design. Also, the degree of freedom of deformation is dependent on the rotation of the wheel, so that precise phase control of all the actuators is required when only the wheels are desired to be rotated or deformed.

Conversely, when the actuator is placed on the wheel, the above problems are eliminated, and the wheel can be deformed independently of the rotation. However, the mass of the wheel is increased, and a slip ring and a structure design are inevitably required to prevent the actuator from twisting the wire. Both of these issues are conflicts and both are important.

4.1.2. Final Concept of the mobile platform STEP

We explored ways to take all the advantages of the issue according to the location of the actuator, and whether there is a way to eliminate the disadvantages. Finding an independent degree of freedom for the wheel's rotation and using that degree of freedom in the deformation can make an independent transformation of the wheel's rotation while placing all the actuators in the body. As shown in Fig.4.2, we concluded that the degree of freedom is a linear motion on the axis of rotation of the wheel.

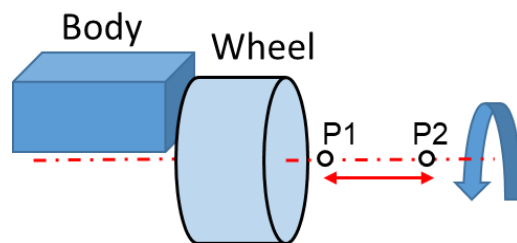


Figure 4.2. the only DOF that is independent of wheel rotation

Based on these conclusions, a new transform mechanism is derived by modifying the existing design alternatives mechanism # 5. In this case, the underlying 5-bar linkage modification mechanism uses the same 3R2P 5bar mechanism, and only the mechanism that synchronizes and modifies it is modified.

Modified Alternative Mechanism # 5 was derived by combining the 3R2P mechanism with a 4 bar (2R2P) mechanism including a P-joint in the wheel axis direction (Fig.4.4).

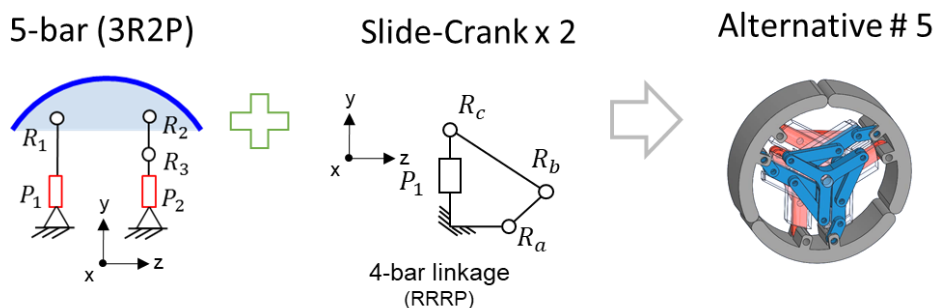


Figure 4.3. Components of design alternative #5

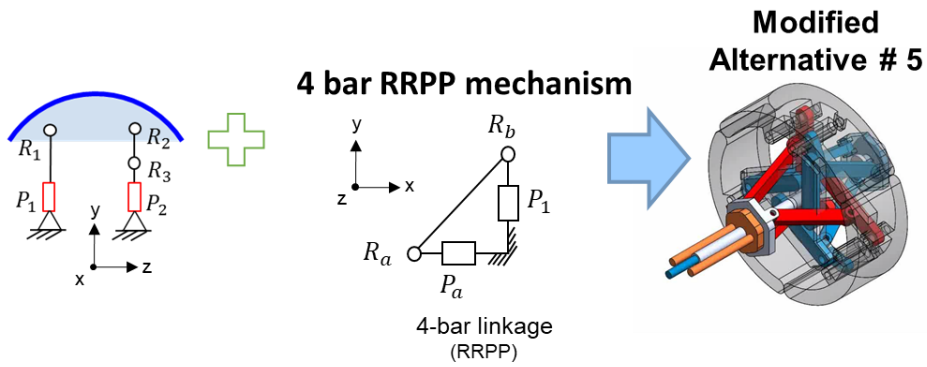


Figure 4.4. Modified design alternative #5

The conceptual design of platform STEP is shown in Fig.4.5. The platform consists of a body, two motor boxes containing three motors, and 2-DOF transformable wheels.

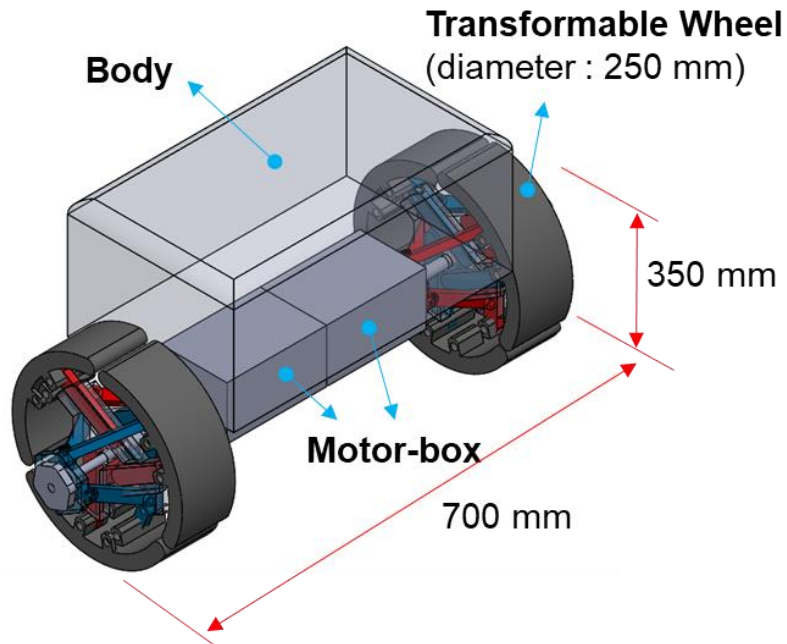


Figure 4.5. Conceptual design of mobile platform based on modified design alternative mechanism #5

The operation of the mechanism is as follows. The wheels are transformed through the orange and blue shaft provided in the motor box (Fig.4.6 (b) – (d)).

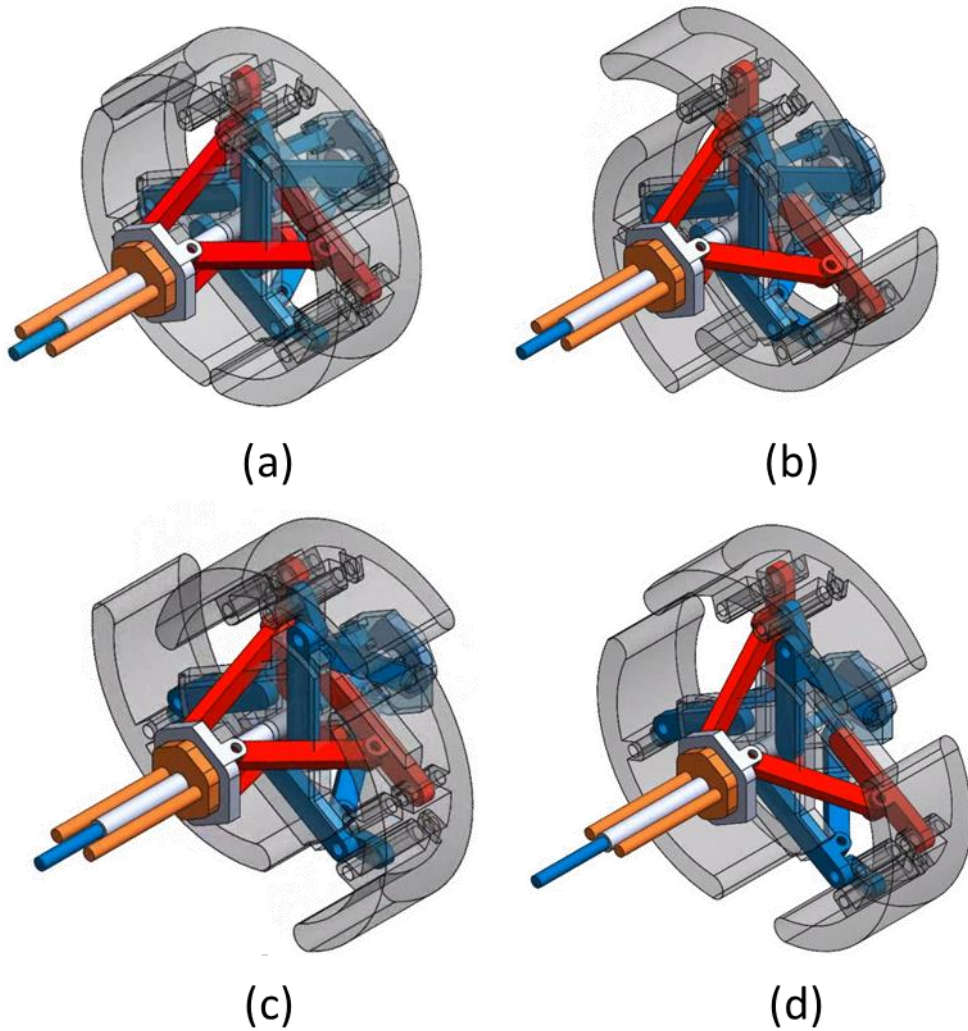


Figure 4.6. 2-DOF transformation motion of modified design alternative #5

4.2. Design of the STEP platform

The size of the designed STEP platform is 1150 mm x 250 mm x 420 mm. Power is transmitted from the motor box to the wheel mechanism via the timing belt–pulley structure.

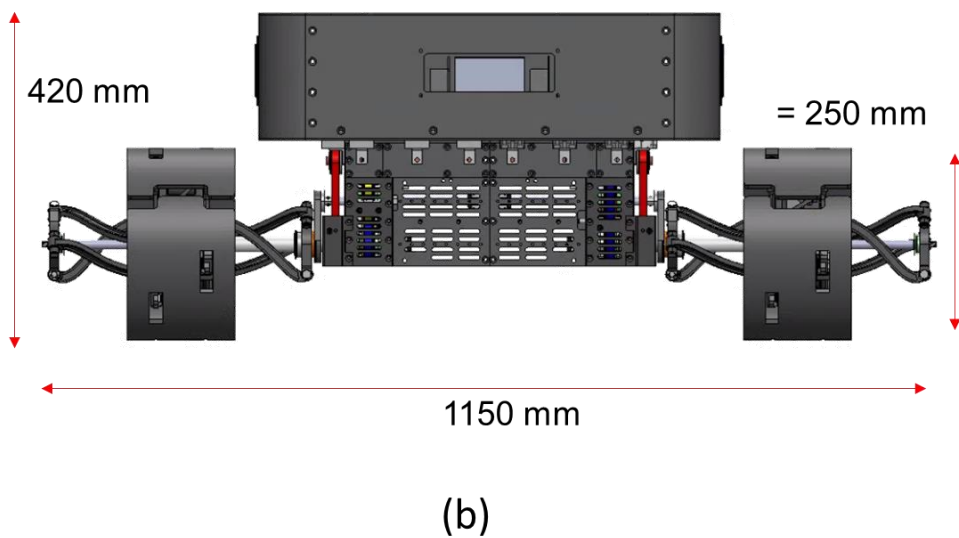
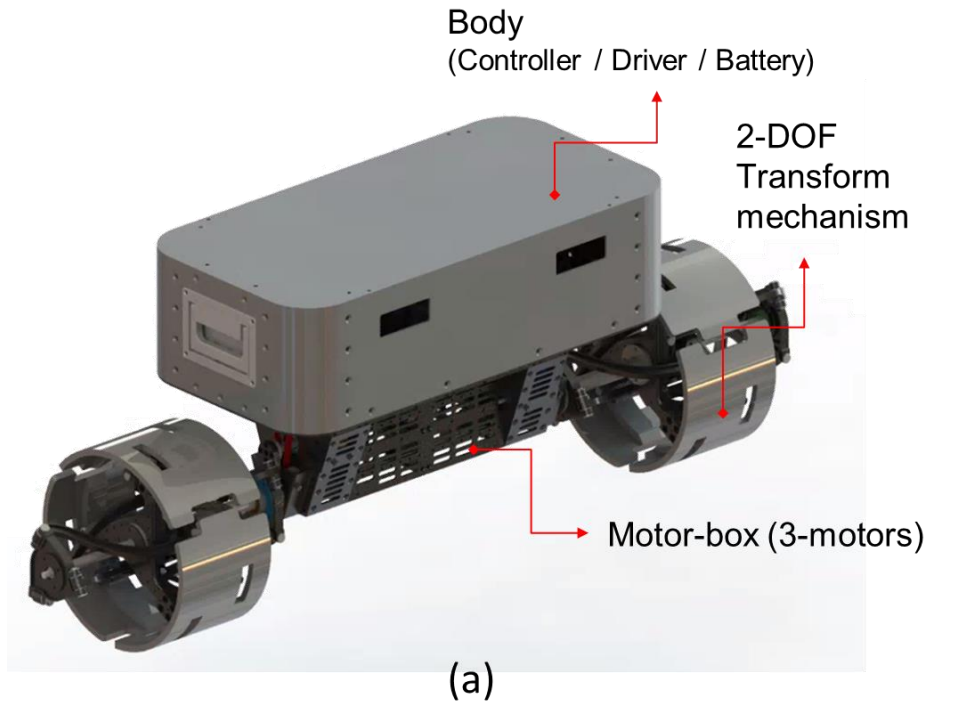


Figure 4.7. Detail design of a new mobile platform STEP (a) Isometric view of the STEP platform (b) front view of the STEP platform

4.2.1. Description of mechanical parts

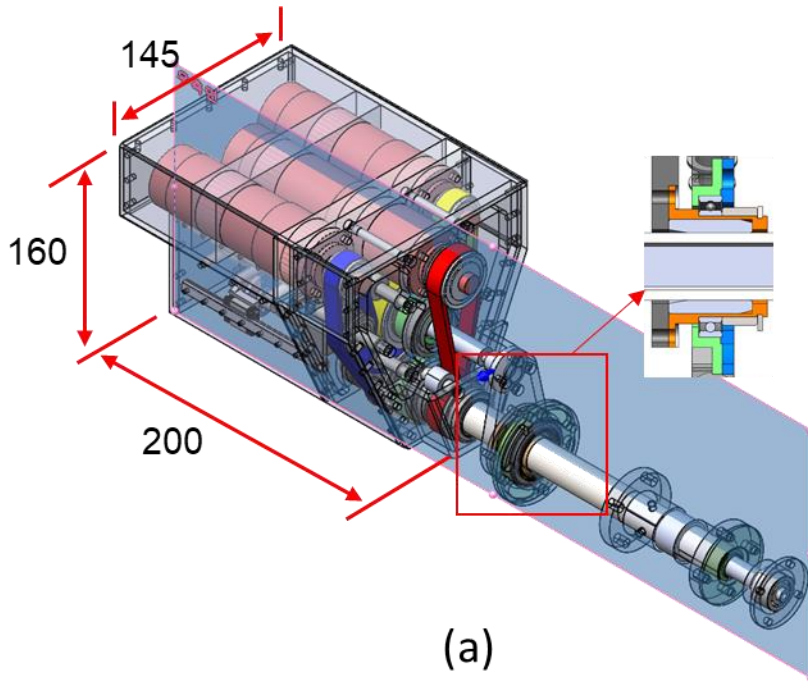
Motor–box

All three motors are located in the motor box, all of which are powered by a timing belt–pulley structure. The timing belt was selected because it had low noise and no backlash and high driving precision, and the arrangement of driver and drive shaft during design was free. As shown in Fig. 4.8. (b), in order to arrange the three pairs of timing belts in the space of the narrow motor box, interference was avoided through proper placement of the idler, and a tensioner was installed to adjust the tension.

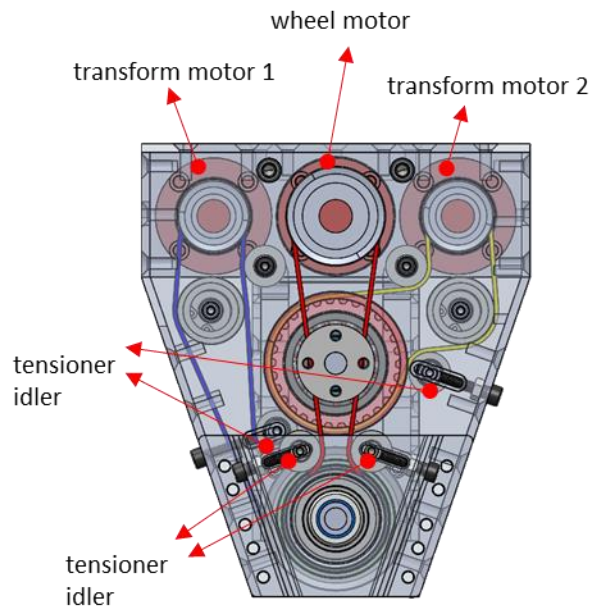
In the motor box, two linear motions and one rotation motions are created. At this time, as shown in Figure 4.8 (b), The driving of the transformation mechanism is carried out through a ball screw, in which the screw moves back and forth through the rotation of the nut restrained by the axial movement to perform the transformation operation of the wheel mechanism. The rotation of the screw is constrained through the LM guide inside the motor box (Figure 4.8 (b)).

The length standard of the timing belt standard is in 5 mm increments, and there are several sizes not in the middle. The belt is designed to be able to use the standard size of the belt through proper arrangement of the motor, drive shaft and idler. The following three belts are selected by calculating the belt length, 285 mm (yellow belt shown in Fig. 4.8 (a)), 325 mm (blue belt shown in Fig. 4.8 (a)), 360 mm (red belt shown in Fig. 4.8 (a)),

The two linear degrees of freedom provided in the motor box must be transmitted to the wheel mechanism. At this time, the transmitting link should be subjected to a relative linear motion with respect to the axis while relatively rotating on the wheel axis. In order to realize this, a bush is installed on the shaft and a bearing is installed thereon as shown in Fig 4.8 (a).



(a)



(b)

Figure 4.8. Structure of the motor-box part of STEP platform

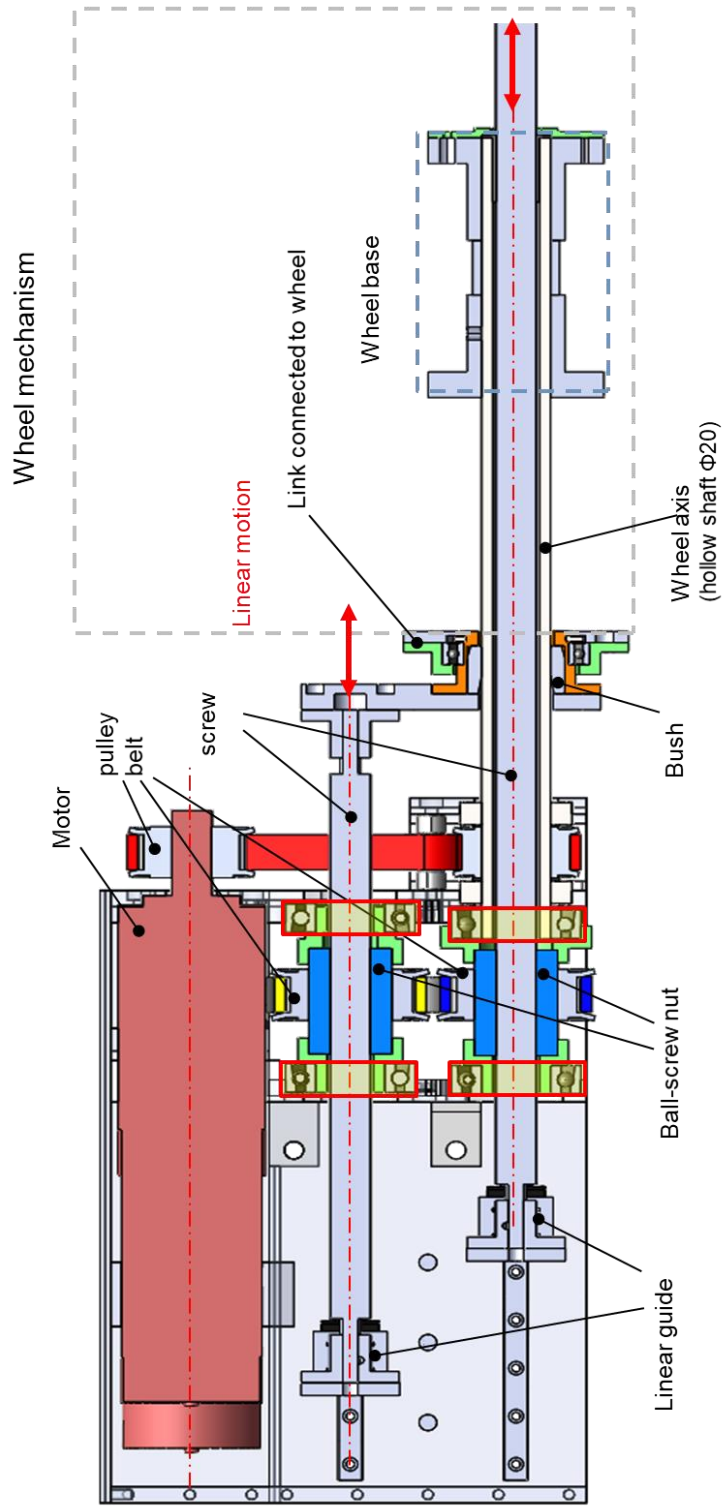


Figure 4.9 Cross-sectional view of motor box

Wheel Mechanism

The wheel mechanism consists of two wheel-hubs and links. To minimize the width of the wheel, both wheel-hubs are designed to cross each other. For the operation of the prismatic joints located at the base of the 5-bar 3R2P mechanism, six LM guides are installed in the wheel hub. The joints of the respective links are coupled to the bushes with pins. It is designed to avoid interference between links even if they are transformed.

The transformation mechanism consists of 5-bar 3R2P two-degree-of-freedom mechanisms related to the transformed shape of the wheel located on the wheel-hub and two 4-bar mechanisms on the wheel axle that actively move the prismatic joints of the wheel-hub 5-bar mechanism.

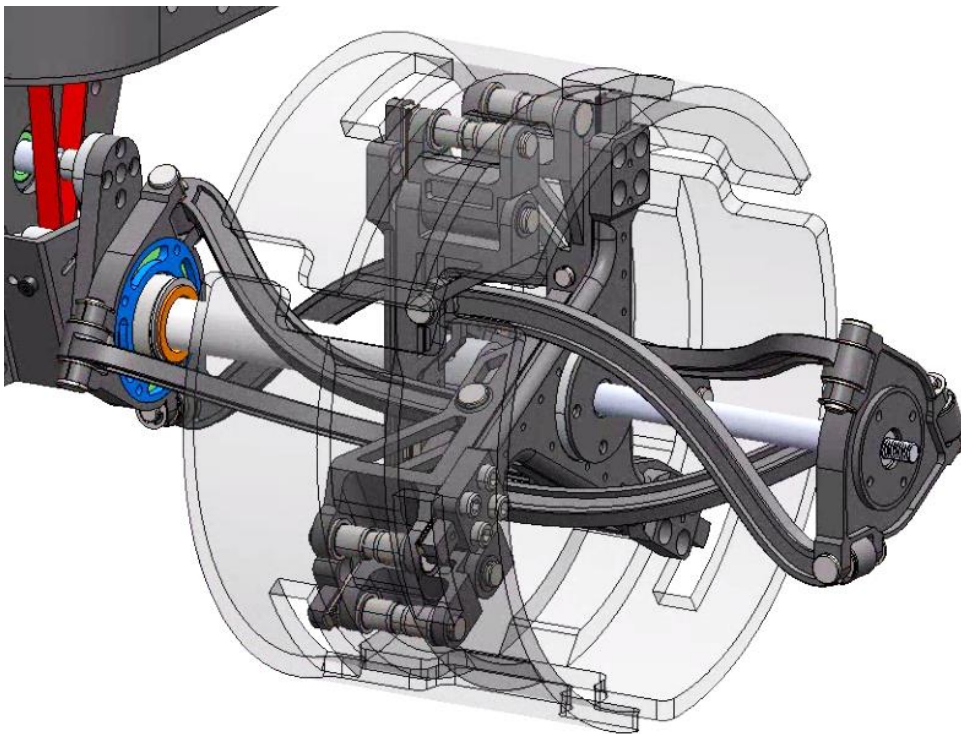


Figure 4.10 Designed Transformable wheel part

The transforming motion of the wheel is as follows. The transmitting link at both ends is connected to the end of each ball screw, and it transfers the linear motion to the mechanism. As can be seen in Figure 4.11, it can be seen that the wheels are transformed into various shapes depending on the movement of the red link and the blue link.

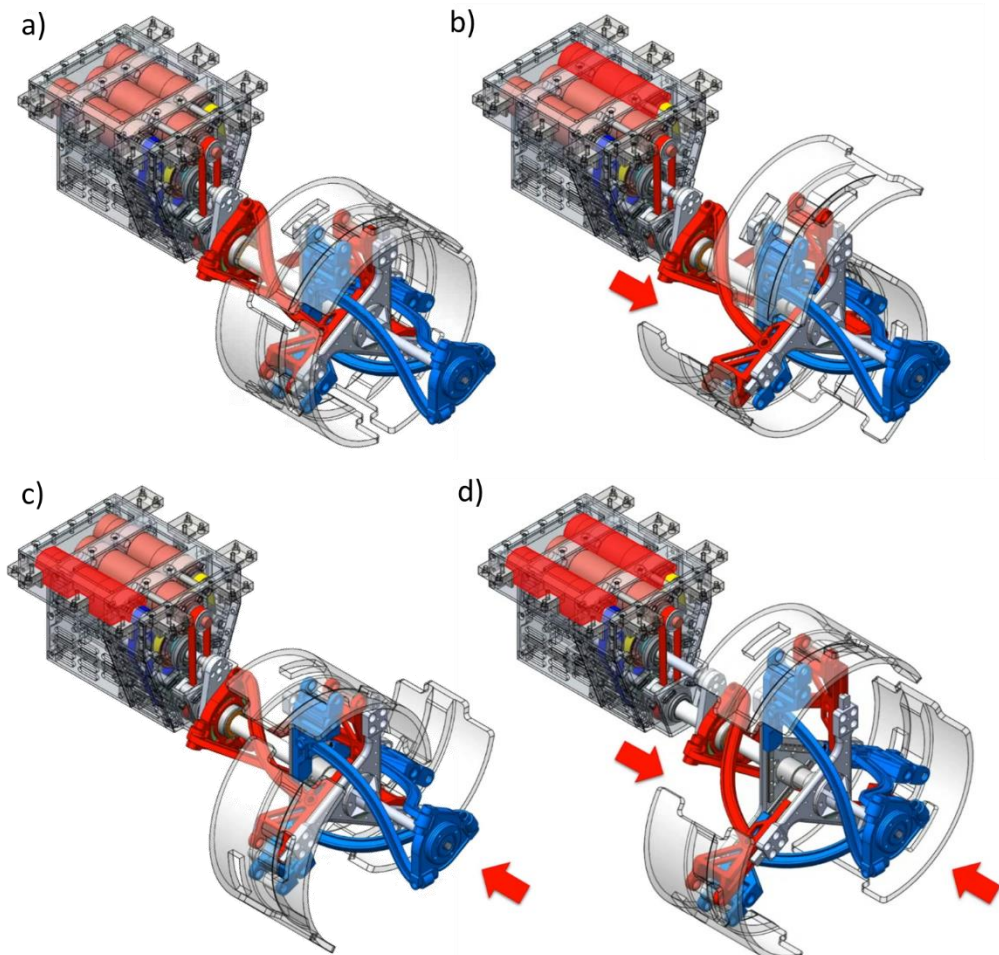


Figure 4.11 The transformed motion of the wheel mechanism (a) Wheel state (b) Transformation DOF-1. Red highlighted motor and red link operation (c) Transformation DOF-2. Red highlighted motor and blue link operation (d) both DOF transformation. blue and red links operate to make r_1 large.

4.2.2. Kinematics based parameter selection

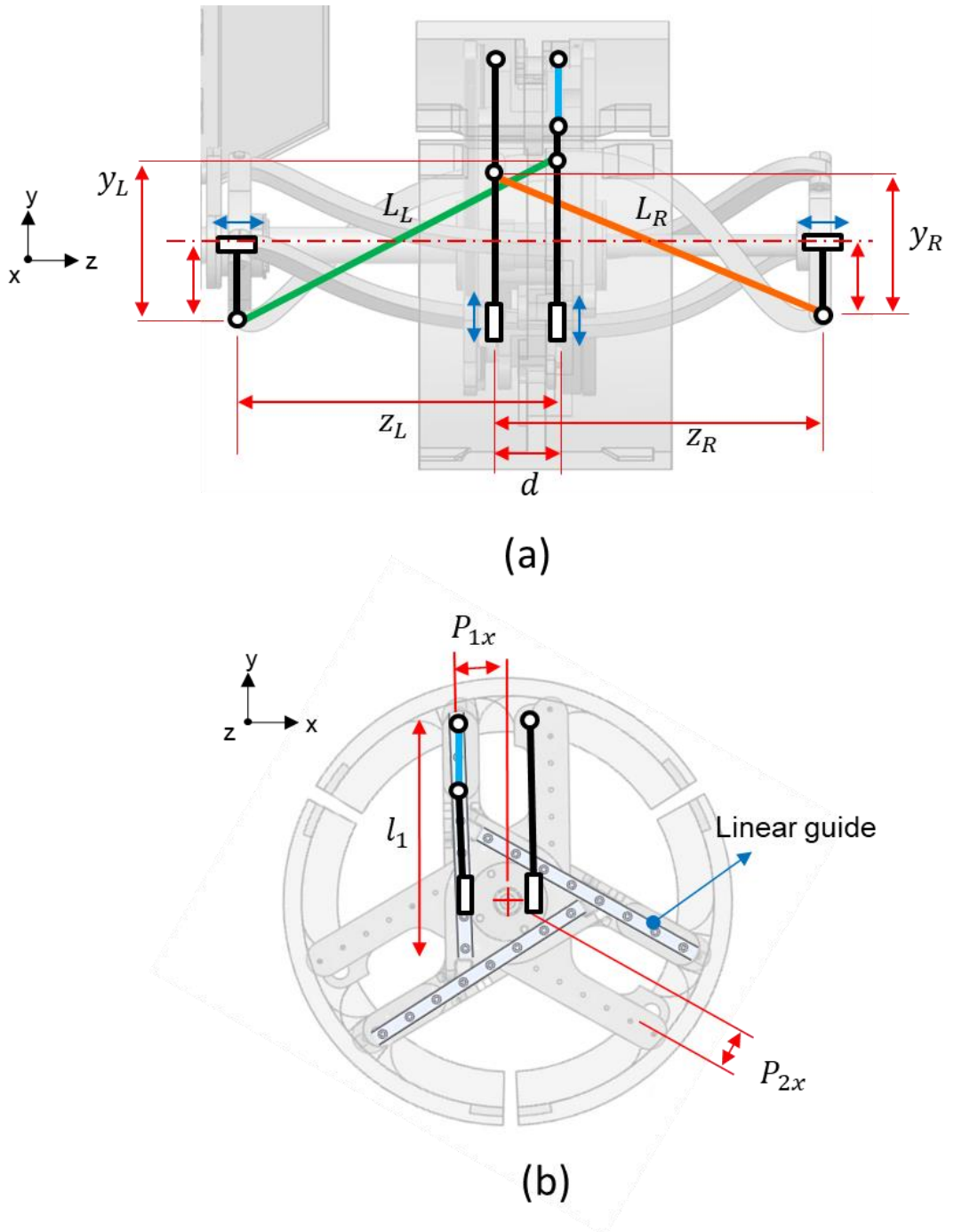


Figure 4.12. Kinematic parameters of the mechanism

The wheel mechanism proposed in this study is basically a thick structure of the wheel. Therefore, it is structurally designed to overlap the wheel-hub by d to minimize the width.

The design parameters of the transformation mechanism to be determined are shown in Figure 4.9. The link lengths of the 5-bar mechanism on the wheel-hub must be determined, and the wheel-hub of the wheel is designed to cross d -lengths as shown in Figure 4.9 (a) to minimize the width of the wheel.

The design parameters of the designed transformer wheels were derived from trial-error processes to satisfy the following kinematic requirements.

1. Wheel radius is 125 mm
2. Mechanism satisfies required transform range
3. Avoid interferences

The selected design variables are as follows.

$$P_{1x} = 15 \text{ mm}$$

$$P_{2x} = 25 \text{ mm}$$

$$R_{2y} = 105 \text{ mm}$$

$$R_{4y} = 80 \text{ mm}$$

$$R_{3y} = 105 \text{ mm}$$

$$y_R = 80 \text{ mm}$$

$$y_L = 80 \text{ mm}$$

$$Z_L = 180 \text{ mm}$$

$$Z_R = 180 \text{ mm}$$

The simulation results of the step overcome with selected design variables are shown in Fig. 4.13 a) to h), and it is confirmed that interference, singularity do not occur while overcoming step obstacle. In addition, selected design parameter based design is performed.

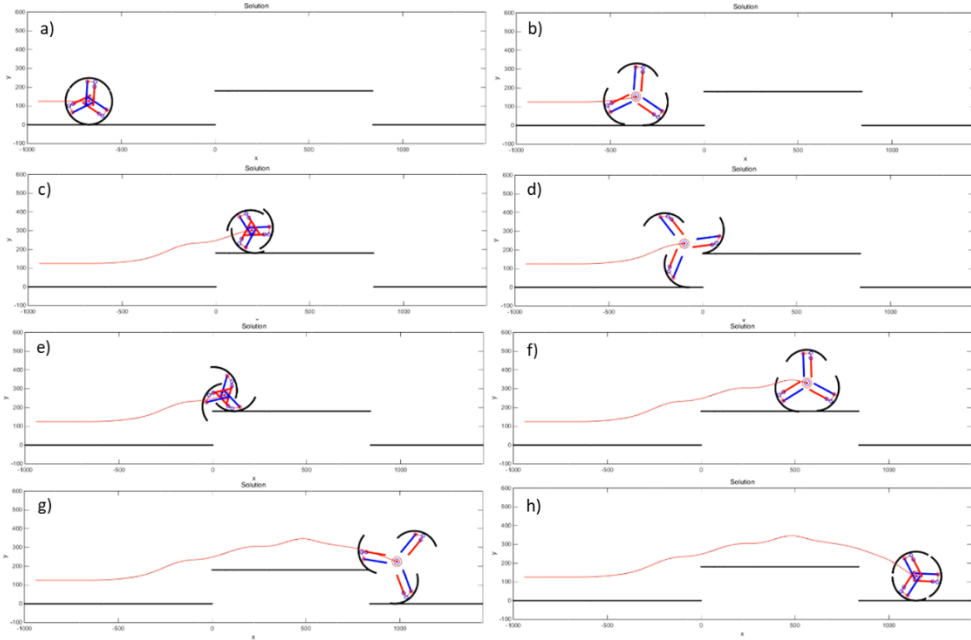


Figure 4.13. Step overcoming simulation of selected design parameters

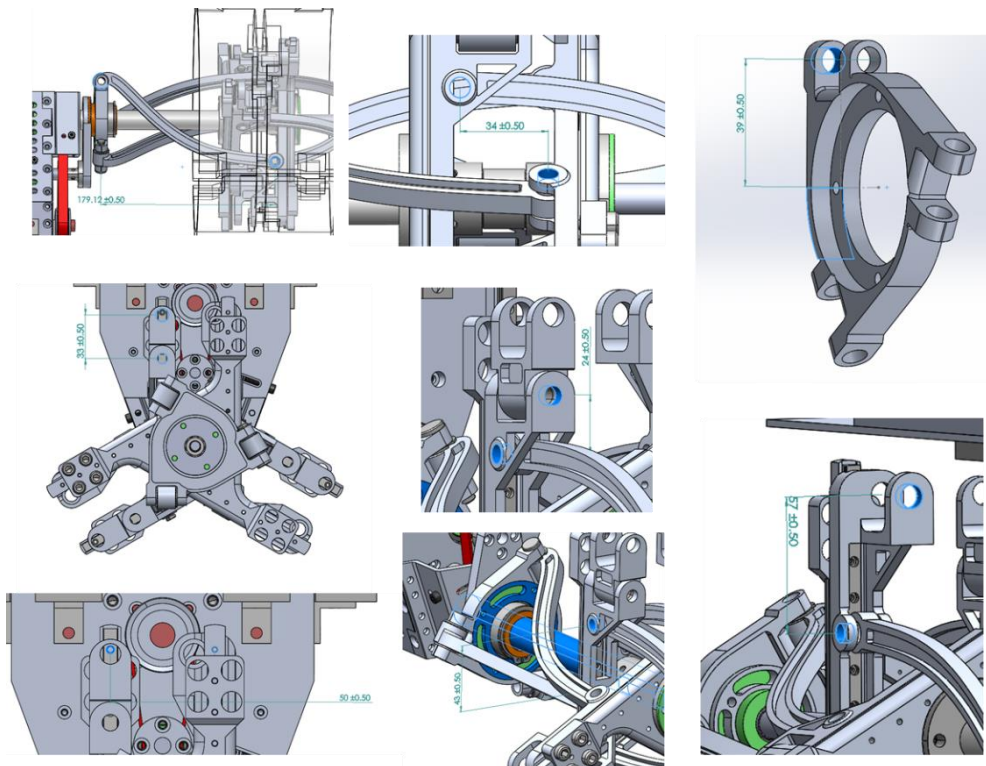


Figure 4.14. Selected design parameter based 3d cad design

4.2.3. Static analysis

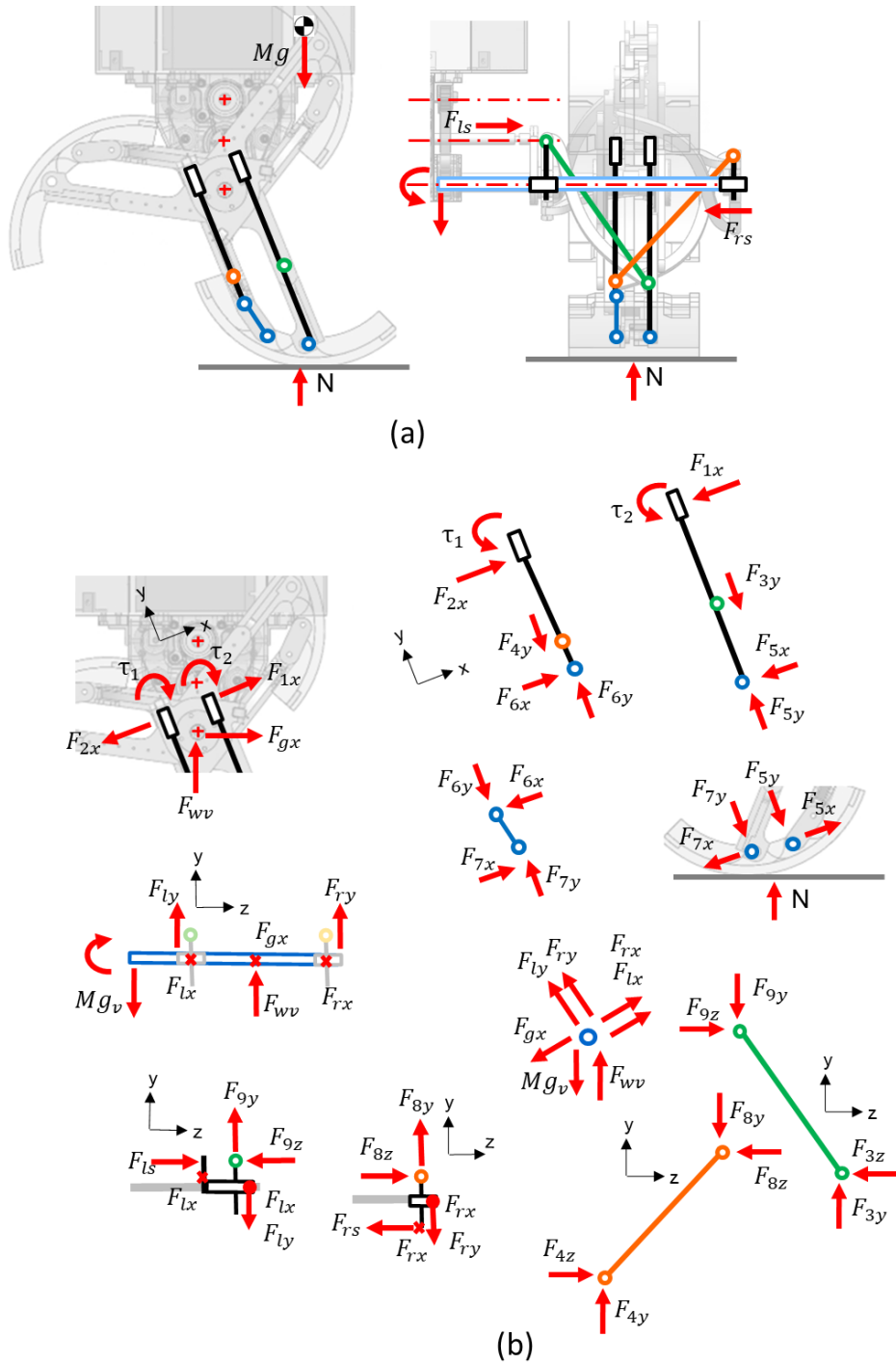


Figure 4.15. Static modeling of STEP wheel mechanism

The required torque was analyzed in the process of the transformable wheel based robot overcoming the step obstacles. The trajectory in the process of overcoming the target step obstacles are described in section 3.4.

The free body diagram of the STEP platform is shown in Fig. 4.15.

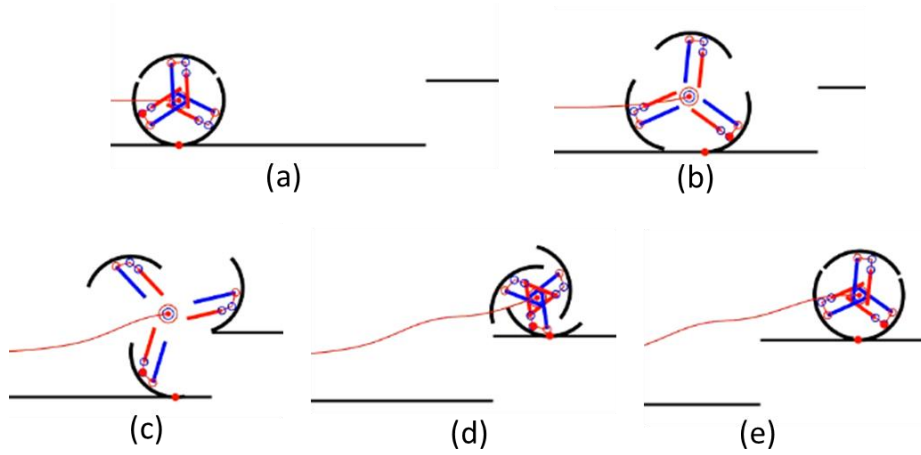


Figure 4.16 Step obstacle overcoming simulation

A quasi-static analysis assuming a very slow speed was carried out assuming that the weight of the robot is 30 kg. We also assumed a harsh condition where the two wheels support all loads. The force needed to overcome the step obstacles was calculated and equations are shown below.

$$F_{1x} = -F_{5x} \quad (4.1)$$

$$F_{3y} = F_{5y} \quad (4.2)$$

$$\tau_2 = l_1 * F_{5x} \quad (4.3)$$

$$F_{2x} = -F_{6x} \quad (4.4)$$

$$F_{4y} = F_{6y} \quad (4.5)$$

$$\tau_1 = -l_2 * F_{6x} \quad (4.6)$$

$$F_{4y} = F_{6y} \quad (4.7)$$

$$\tau_2 = l_1 * F_{5x} \quad (4.8)$$

$$\tau_2 = l_1 * F_{5x} \quad (4.9)$$

$$F_{wv} * \sin\varphi + F_{2x} - F_{gx} * \cos\varphi = F_{1x} \quad (4.10)$$

$$F_{wv} * \cos\varphi + F_{gx} * \sin\varphi = 0 \quad (4.11)$$

$$F_{gx} = F_{rx} + F_{lx} - Mg_v \sin\varphi + F_{wv} \sin\varphi \quad (4.12)$$

$$F_{ly} = F_{ry} - Mg_v \cos\varphi + F_{wv} \cos\varphi \quad (4.13)$$

$$F_{6y} = F_{7y} \quad (4.13)$$

$$F_{6x} = F_{7x} \quad (4.14)$$

$$\overline{P2R3}_x * F_{6y} + \overline{P2R3}_y * F_{6x} = 0 \quad (4.15)$$

$$-F_{7x} + F_{5x} + Mgsin\varphi = 0 \quad (4.16)$$

$$F_{7y} + F_{5y} - Mgc\cos\varphi = 0 \quad (4.17)$$

$$d * F_{5y} = (-P_{R3x} + CT_x) * Mg \quad (4.18)$$

$$F_{3z} = F_{9z} \quad (4.19)$$

$$F_{3y} = F_{9y} \quad (4.20)$$

$$\overline{Q1W1}_y * F_{3z} = \overline{Q1W1}_z * F_{3y} \quad (4.21)$$

$$F_{4z} = F_{8z} \quad (4.22)$$

$$F_{4y} = F_{8y} \quad (4.23)$$

$$\overline{Q2W2}_y * F_{4z} = \overline{Q2W2}_z * F_{4y} \quad (4.24)$$

$$F_{9y} = F_{ly} \quad (4.25)$$

$$F_{ls} = F_{9z} \quad (4.26)$$

$$F_{8y} = F_{ry} \quad (4.27)$$

$$F_{8z} = F_{rs} \quad (4.28)$$

The result of static analysis of step climbing simulation by solving the equations above is shown in Figure 4.17. Required forces L and R represent the required force of the body side and outer side of ball screw respectively, with respect to the wheel mechanism. In addition, the required torque graph shows the torque required for the ball screw axis, and power is the product of RPM and torque, representing instantaneous required output power.

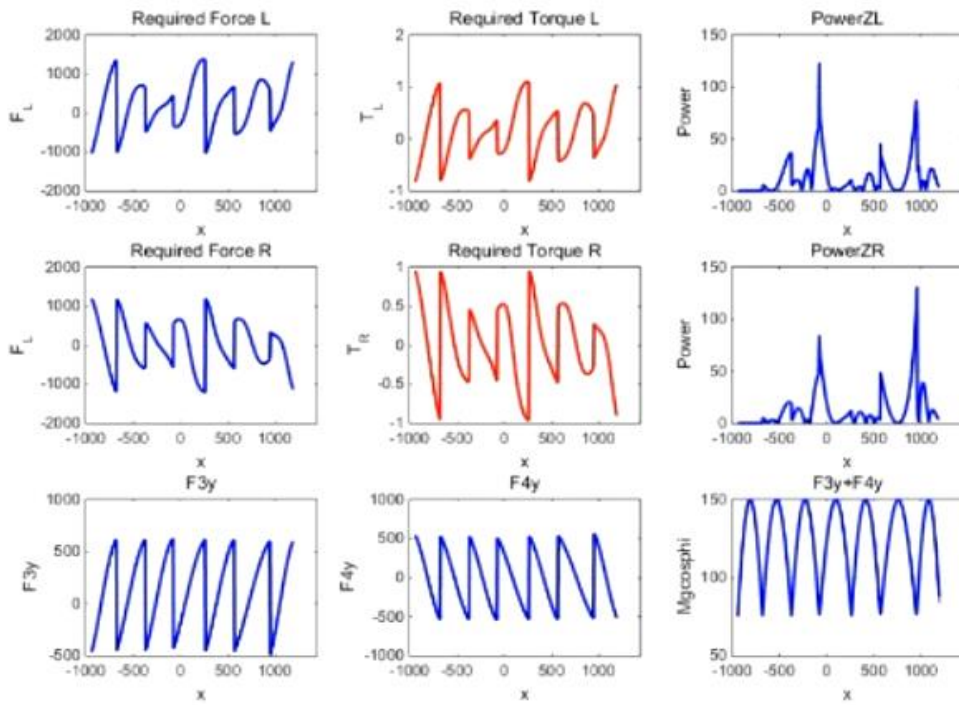


Figure 4.17 Static analysis results

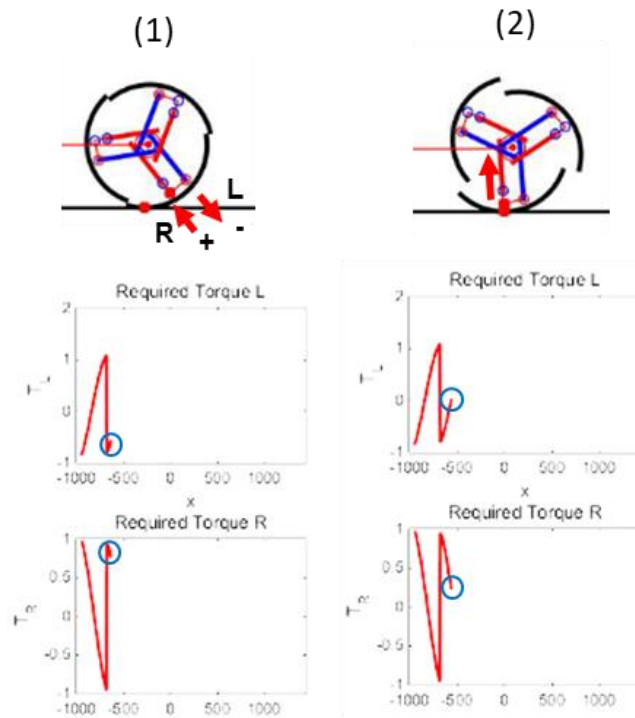


Figure 4.18 Analysis of the results of static analysis 1

In order to verify the validity of the simulation results, we examined the tendency of the torque graph results. In the torque graph of Figure 4.18 (1), each torque has a $-$ sign and a $+$ sign because the $+$ and $-$ loads are applied to R and L due to the moment acting on the spokes. The reason why the sign changes instantaneously is that the direction of the moment is reversed when the spokes that are in contact are switched.

In Figure 4.18 (2), the value of τ_L is close to 0 because the load of the robot exists at the vertical position of the point, and the moment does not act statically.

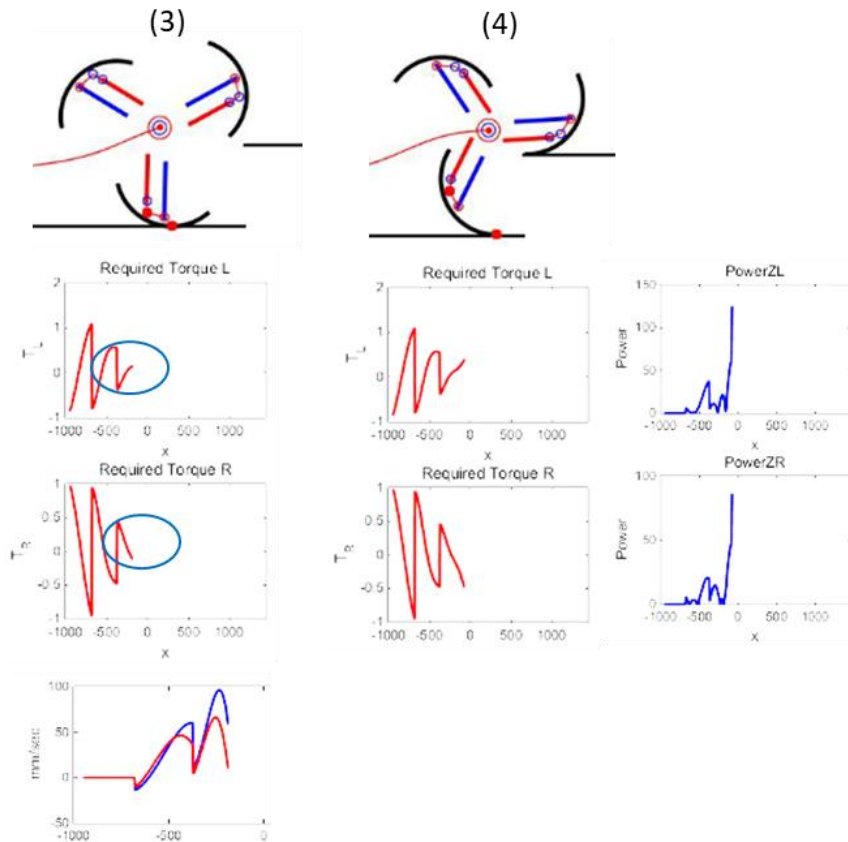


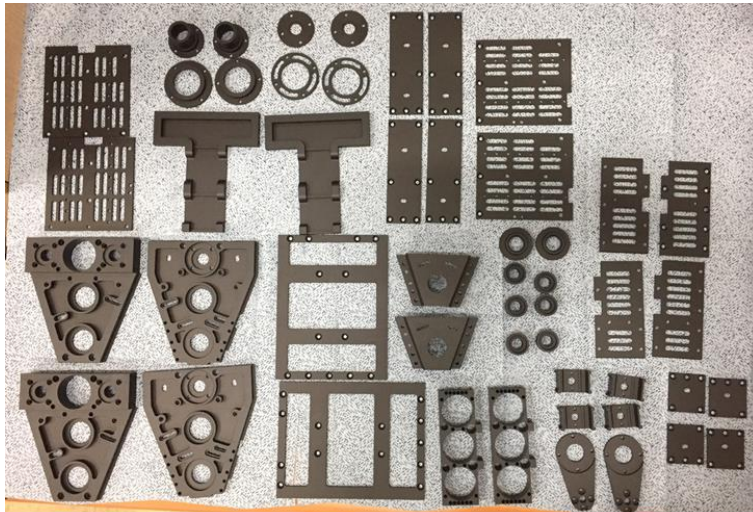
Figure 4.19 Analysis of the results of static analysis 2

Figure 4.19 (3), which shows that the required torque is reduced and the required slide speed is increased in the course of going over the step. This is due to the feature of the RRPP 4-link mechanism in which the required torque becomes smaller as the radius of the wheel becomes larger. In particular, the required output increases sharply in Fig. 4.19 (4) because it is closer to the singular point and the required RPM rise ratio is higher than the torque reduction amount.

The maximum torque required for the ball screw shaft having the transformation is $1 \text{ N} \cdot \text{m}$. Based on the static analysis, the actuator and actuator parts satisfying the target payload of 30 kg are selected. The gear ratio of the maxon RE40 is 3.5: 1. The reduction ratio of the pulley system to the ball screw shaft is 1.71: 1 (teeth ratio, 24:14) and the lead of the ball screw is 5 mm. As a result, the torque of the screw shaft is $1 \text{ N} \cdot \text{m}$ and the velocity of the ball screw shaft is 96 mm / sec, which is a result of satisfying both the target payload and the RPM.

4.3. Fabricated STEP Platform

Most parts of the platform are made of aluminum. Due to space constraints, long and thin link parts are made of high rigidity steel. Wheel segments which are made of PET are 3D printed. The wheels are equipped with a wheel made of hyper rubber so that high friction can be obtained.



(a)



(b)

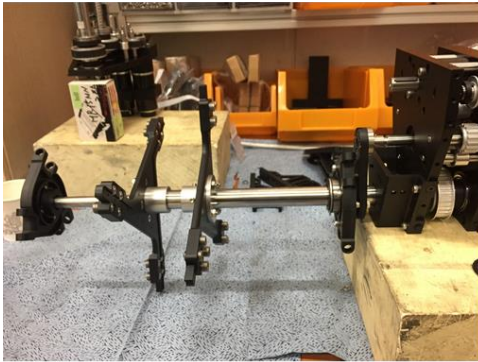
Figure 4.20 Fabricated parts of the STEP platform (a) Motor-box parts (b) Wheel mechanism parts



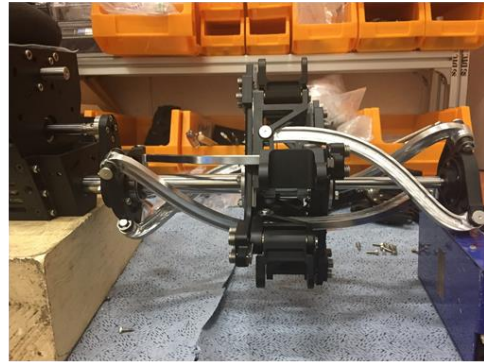
(a)



(b)

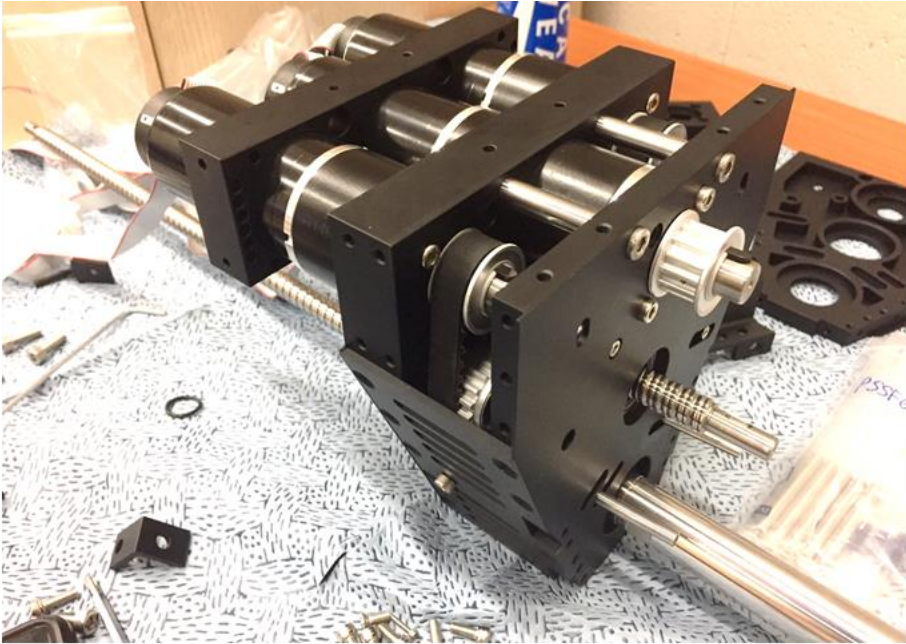


(c)



(d)

Figure 4.21 Fabricated wheel parts assembly of the STEP platform



(a)



(b)



(c)

Figure 4.22 Fabricated motor-box parts assembly of the STEP platform

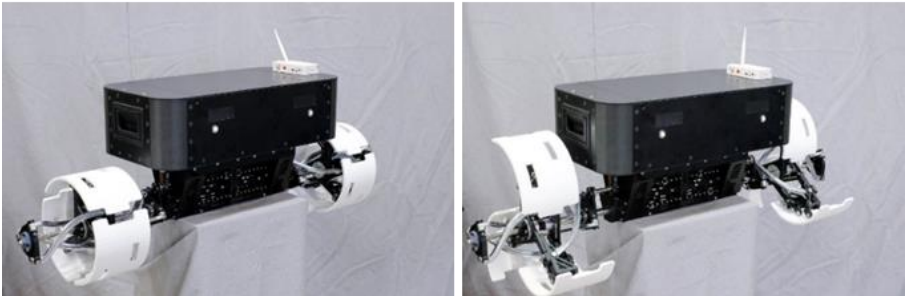
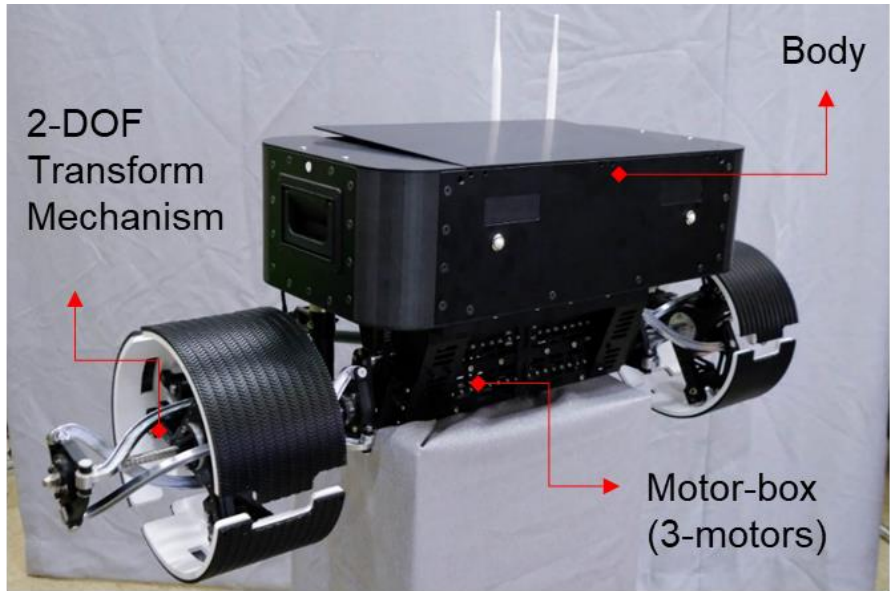


Figure 4.23. the STEP platform



NI cRIO-9024



RE40 3.5:1 (Wheel motor x 2)
RE40 43:1 (Transform motor x 4)



CAN module



Analog input module



Epos2 50/5 * 8EA



MSENS-IN360-MV



Figure 4.24. Electric parts of the STEP platform

Table 4.1. Specifications of the STEP platform

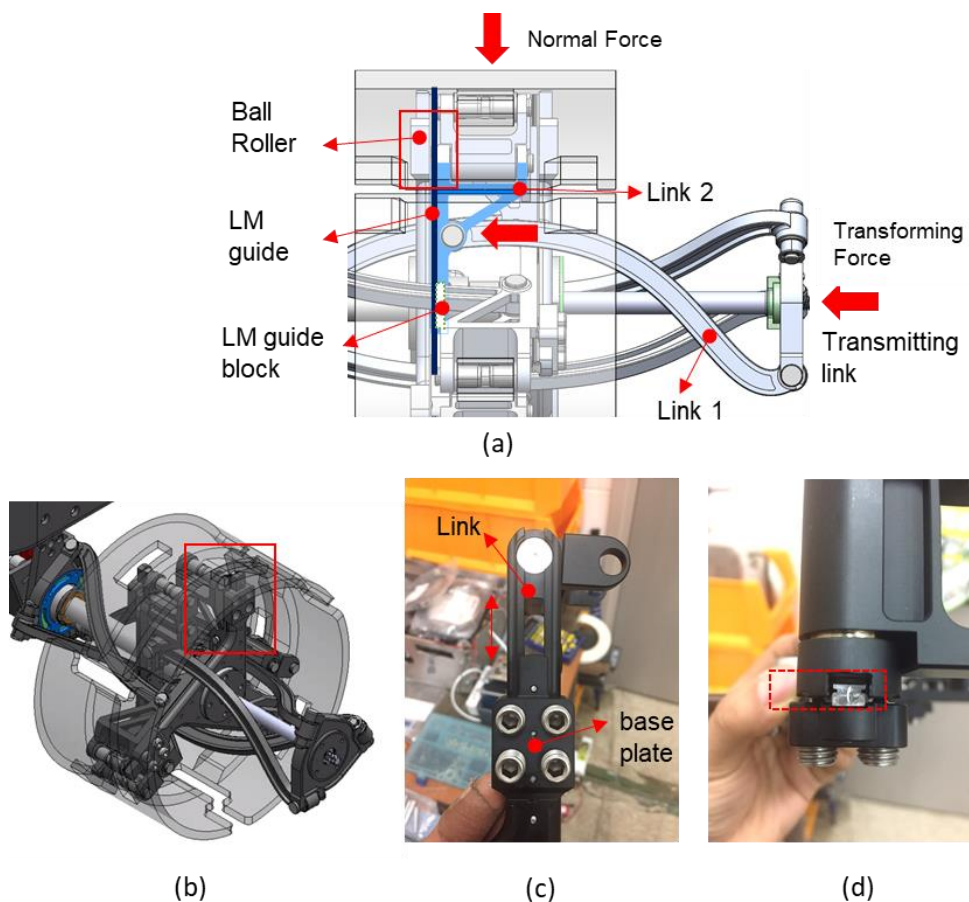
Dimension	1150 mm x 350 mm x 420 mm
Weight	18 kg
Motor driver	EPOS 2 50/5 * 4, EPOS 2 70/10 * 2
Motors	<p>Main wheel drive motor Maxon RE40 (150W), Reduction ratio 230:1 * 2EA</p> <p>Transform motor Maxon RE40 (150W), Reduction ratio 3.5:1 * 4EA</p>
Main controller	<p>NI CompactRio 9024</p> <ul style="list-style-type: none"> - High speed CAN module (9853), - Analog input module (9215) - Digital input module (9411)
Power supply	<ol style="list-style-type: none"> 1. SMPS 1000 W 2. Batteries PT-B12000 – FX30 (22.2V, 6S1P, 30C)
Mechanical parts	<p>Ball screw – $\Phi 12$, lead 5mm</p> <p>Pulley teeth ratio (wheel axis) – 32:30</p> <p>Pulley teeth ratio (transform axis) – 14:26</p> <p>Wheel – PET white</p>
Sensor	IMU – MSENS-IN360-MV

4.4. Design Modifications

For the initial prototype of a new mechanism-based robot, there are various failure modes. Followings are some of the major design modifications from initial design to production.

4.4.1. Link supporting ball roller

The mechanism proposed in this study transmits force through the transmitting link at the end of the ball screw, as shown in Fig.4.23. Transmitting force is transmitted to Link2 through long Link1 of Fig 4.23(a). At this time, since Link2 is fastened to the LM guide block on the wheel base plate, it is pressed by a large force of the transmitting force, so that the frictional force with the floor can be increased.

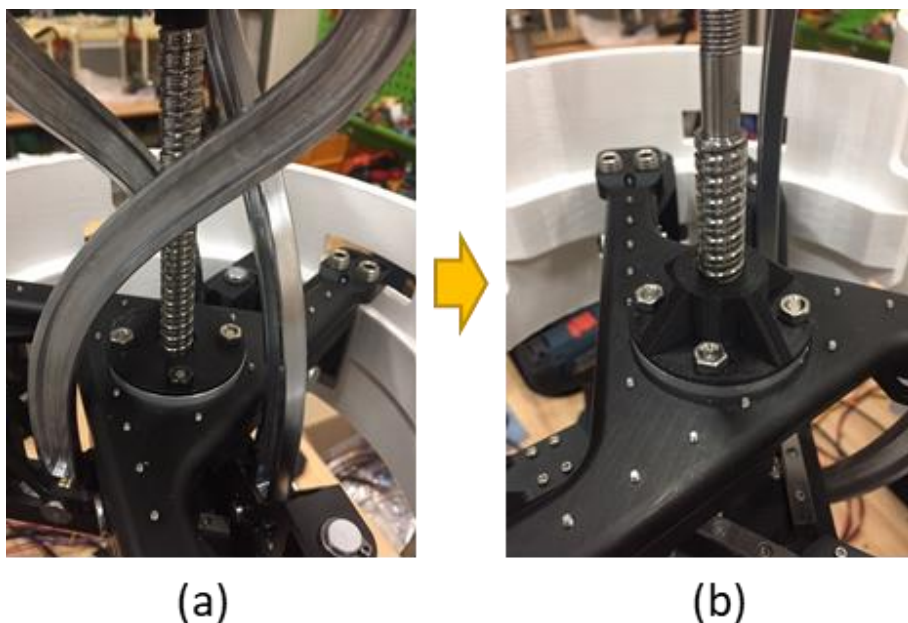


4.25. Link supporting parts description

Therefore, a ball roller was designed so that Link2 can move with minimum friction on the wheel base plate. The ball roller has a ball at the end of the screw, minimizing friction during relative motion with the contacting surface.

4.4.2. Clearance of a screw axis

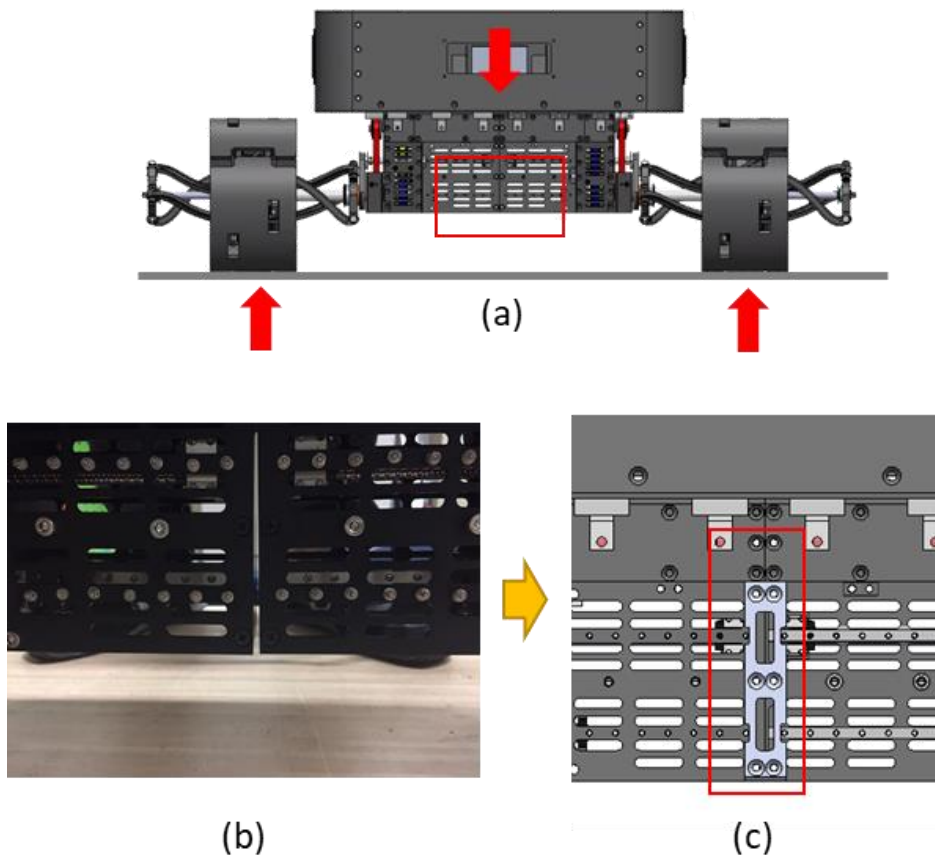
While the transformation mechanism is in operation, the screw shaft makes a relative movement with respect to the center of the wheel base plate. In this case, the gap between the screw shaft and the base plate was generated in the conventional design, which caused an error of transformation. Therefore, as shown in Figure 4.24 (b), the part is modified to minimize the gap between the wheel base plate and the screw.



4.26. Modification on screw axis contacting parts

4.4.3. A Gap between Motor-boxes

As shown in Fig.4.25 (a), the gap between the motor boxes occurred due to the load of the robot itself. Especially, due to the characteristics of the STEP platform with a long width, the center of the robot is deflected by the load of the robot. (Fig.4.25 (b)) Therefore, the part shown in Fig. 4.25 (c) is output as 3D printing to prevent widening between the motor boxes.

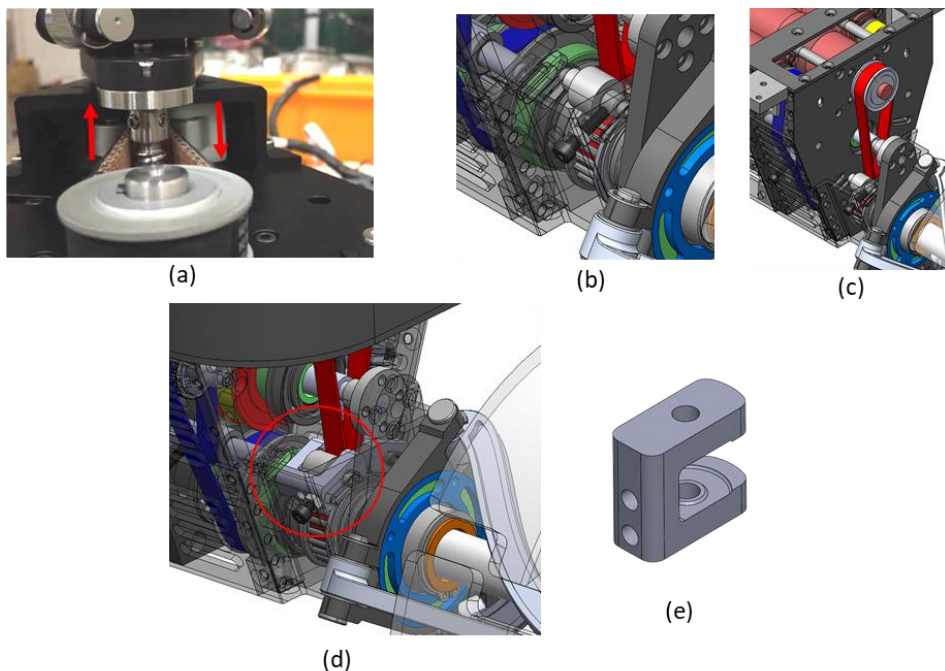


4.27. Modification on motor-box parts

4.4.4. Timing belt deviation

The most important and difficult part of the design of the deformation mechanism was the design of the timing belt. It is also important to ensure that the timing belt is well aligned with the pulleys, and at the same time it is important to properly maintain the tension of the belt through the tensioner.

If neither of these two things is done properly, the power may not be transmitted properly, and the belt may deviate from the idler, as shown in Figure 4.26(a). In particular, the problem that has arisen in this study is that the tensioner idler, which makes the tension, does not win the tension and the shaft is twisted so that the belt is pulled out. To solve the problem, blocks as shown in Fig. 4.26(d) – (e) was designed to secure the parallelism of the idler and to restrict the belt from escaping.



4.28. Timing belt deviation (a) Tensioner block escaping phenomenon (b) previous tensioner design (c) Motor box (d) Modified tensioner block (e) Additional tensioner block

Chapter 5 Experiments

5.1. Experimental setup

A set-up for the verification of the 2-DOF transformable wheel based platform STEP was performed. Experimental stairs were designed and fabricated, active supporter for stability of main body was installed, and setting of initial state for consistent experiment was performed.

5.1.1. Test bench: various sizes of stairs and steps

Size variable test bench is fabricated through aluminum profile of 40 mm x 40 mm with tapped holes. The stair is without risers. The bottom of the stairs is made of MDF plywood thickness 12t. By reassembling, staircases can be changed to various sizes ranging from 260–340 (20 mm interval) and 100–200 (20 mm interval) in height. The target size of the target staircase was 300 x 100, 320 x 140, and 300 x 160. However, all spaces in a staircase that are present in reality are not ideally the same size, and the stair that you have made may be a staircase that changes in size through reassembly. In addition, it can be configured as a test bench for jaw climb and descent experiments.

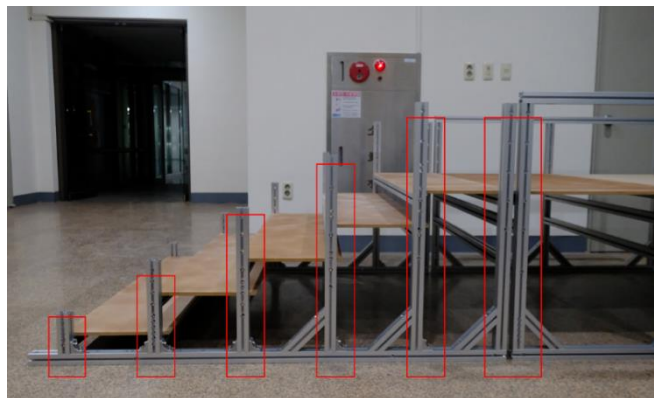
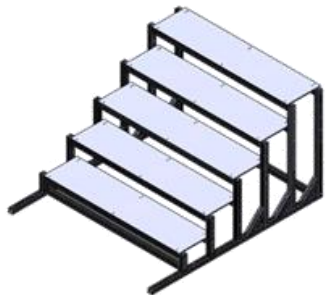
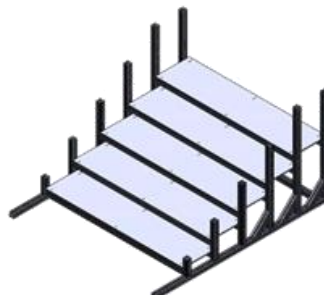


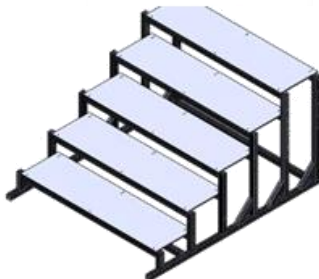
Figure 5.1 Tap hole position in testbench



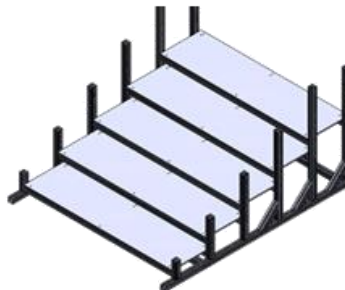
260 x 180



280 x 120



300 x 160



300 x 100

Figure 5.2. Various stair sizes for experiments

5.1.2. Active supporter

In order to verify the function of the transformable wheel, it is necessary to ensure the platform stable by make at least three point supporting point. Rear tail supporting structure is designed. If a fixed angle support is used, the steady slope of the main body cannot be expected from flat, various size stairs. So the active supporter was designed so that the main body is kept close to the horizontal when climbing the stairs. Con35 linear actuators were selected for the actuator. The specifications are 50 mm stroke and 400 N maximum load. An aluminum pipe of pi28 was used for the support. Through a kinematic simulation, a link length of 600 mm, which allows the body to maintain a horizontal angle on the ground and various target stairs, was selected. The angle of the tail was also controlled by a simple P control via the IMU value.

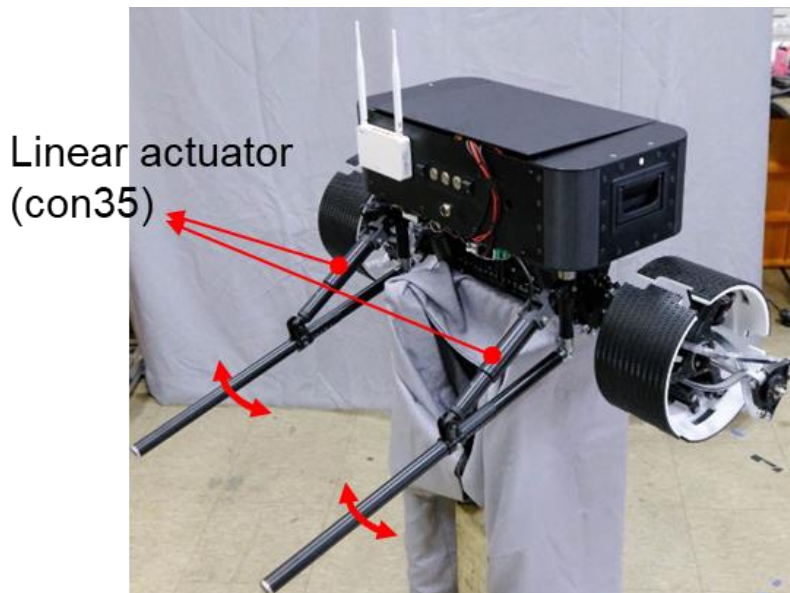


Figure 5.3. Active supporter

5.1.3. Initial condition

Since there is no absolute encoder in the motor of the robot, a method was required to consistently guarantee the initial angle of the wheel and the initial transformation state for each experiment. Therefore, in this study, the fixture was designed and manufactured to secure the initial state. In addition, the start position of the obstacle is made the same, so that the traveling test can always be performed under the same condition.

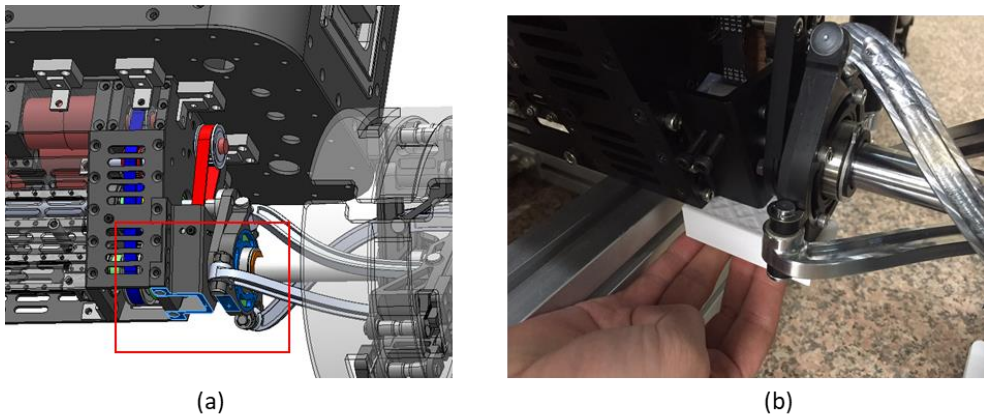


Figure 5.4 Block for Initial condition setting

5.1.4. Guide to constrain pitch motion & trajectory

To measure the trajectory of the robot, a LM guide was installed on the step and a linear encoder to sense the movement was attached. A 4000 mm long LM guide was installed and a magnetic linear encoder was attached, which is counted through CompatRio's 9411 module and quadrature encoder counting method from using labview. The effect of restricting the pitch angle of the robot due to the guide can also be obtained.

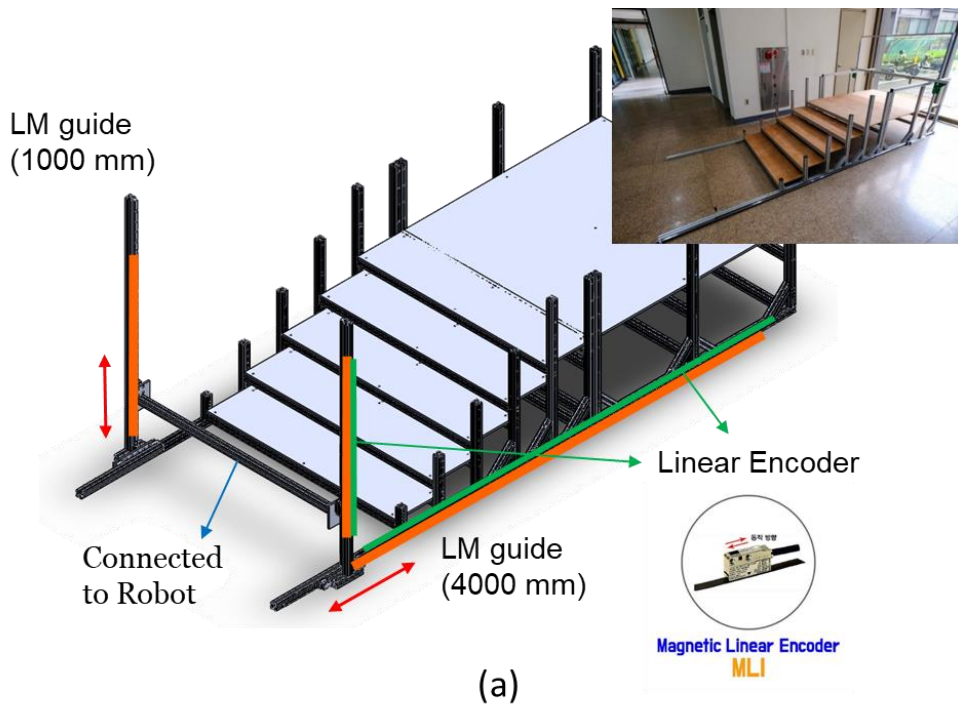


Figure 5.5. Guide structure to constrain pitch motion & trajectory

5.2. Transformation tests

In order to check whether the transforming function works well, we carried out an experiment that transforms without supporting the load. On Fig.5.6 left side of (a) – (d) shows the transformed shape in the CAD modeling, and the pictures on the right show the transformed shape in the experiment. The target sizes of obstacle sizes are 300 mm x 100 mm, 300 mm x -100 mm, 340 mm x 180 mm, 340 mm x -180 mm respectively.

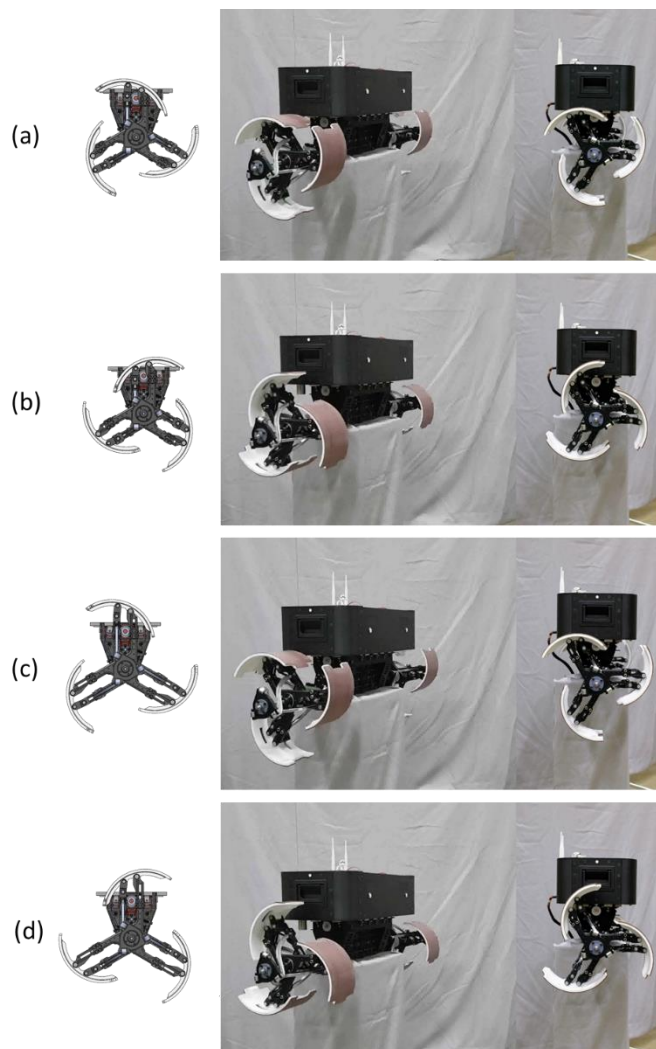


Figure 5.6 Transformation test results

5.3. Tests on flat surfaces

Forward driving on flat ground was performed as shown in Fig.5.7 (a) – (b). It can travel up to 20 m / min on flat ground. It is also possible to steer in place. That is, the radius of rotation is zero.

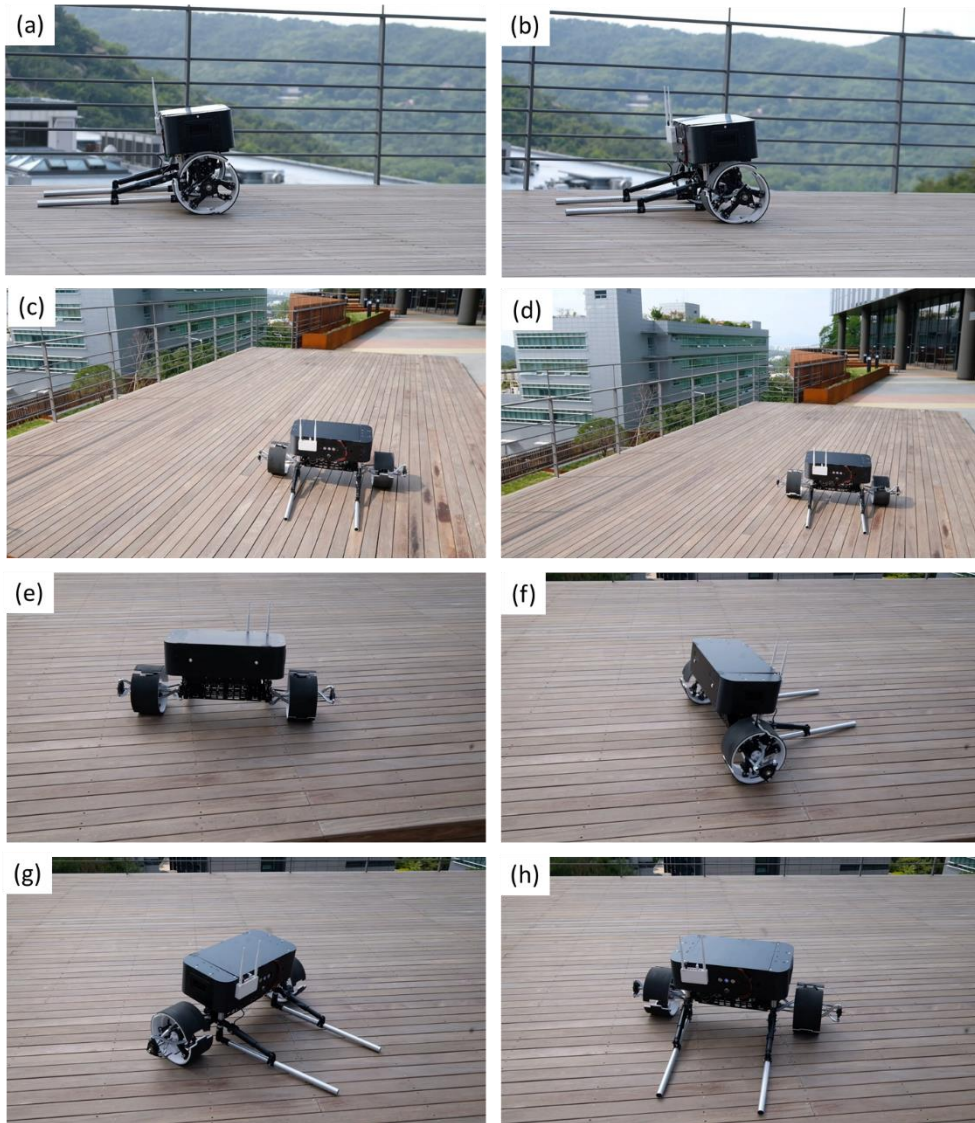


Figure 5.7 Tests on flat surfaces

5.4. Stair overcoming experiments

Various size of stair climbing test was performed. The performance of the 2 DOF wheel based mobile platform was verified by experiments on step obstacles of various heights (70 mm, 110 mm) and stair obstacles of various sizes (300 mm x 100 mm, 320 mm x 140 mm, 300 mm x 160 mm).

First, the performance test of the stair obstacle was performed by two methods. First experiments were performed to climb the stairs with the active rear supporter without the LM guide. At second experiments, by attaching the LM guide, the pitch angle of the robot was fixed and the position was measured by the linear encoders.

The wheel was driven at constant RPM through speed control, and the position control of transformation motors was performed based on the rotation angle of the wheel. by transforming based on the angle of wheel rotation, the transformation at the position of the desired wheel is achieved. Experiments have also been carried out assuming that the information about obstacles is known. The transformations were performed through the position control of each actuator through the lookup table of transformation target sizes. The table is as follows.

Table 5.1. Lookup table of transformation for various stair climbing

Stair sizes	zL (mm)	zR (mm)
260 x 100	9.99	0.96
260 x 120	13.39	2.65
260 x 140	17.13	4.72
260 x 160	21.19	7.13
260 x 180	25.59	9.89
300 x 100	21.83	12.09
300 x 120	25.34	13.85
300 x 140	29.36	19.08
300 x 160	33.83	18.72
300 x 180	38.79	21.83
320 x 100	29.57	19.29
320 x 120	33.25	21.13
320 x 140	37.45	23.46
320 x 160	42.21	26.29
320 x 180	47.55	29.62
340 x 100	38.74	27.74
340 x 120	42.64	29.70
340 x 140	47.13	32.19
340 x 160	52.27	35.24
340 x 180	58.13	38.85

Table 5.2. Lookup table of transformation for various stair descending

Stair sizes	zL (mm)	zR (mm)
260 x -100	2.42	11.91
260 x -120	4.39	15.71
260 x -140	6.74	19.82
260 x -160	9.44	24.21
260 x -180	12.45	28.88
300 x -100	14.45	22.54
300 x -120	16.53	26.34
300 x -140	19.08	30.57
300 x -160	22.09	35.25
300 x -180	25.57	40.38
320 x -100	22.16	29.66
320 x -120	24.35	33.56
320 x -140	27.05	37.96
320 x -160	30.27	42.88
320 x -180	34.02	48.35
340 x -100	31.21	38.17
340 x -120	33.55	42.24
340 x -140	36.45	46.89
340 x -160	39.94	52.14
340 x -180	44.03	58.06

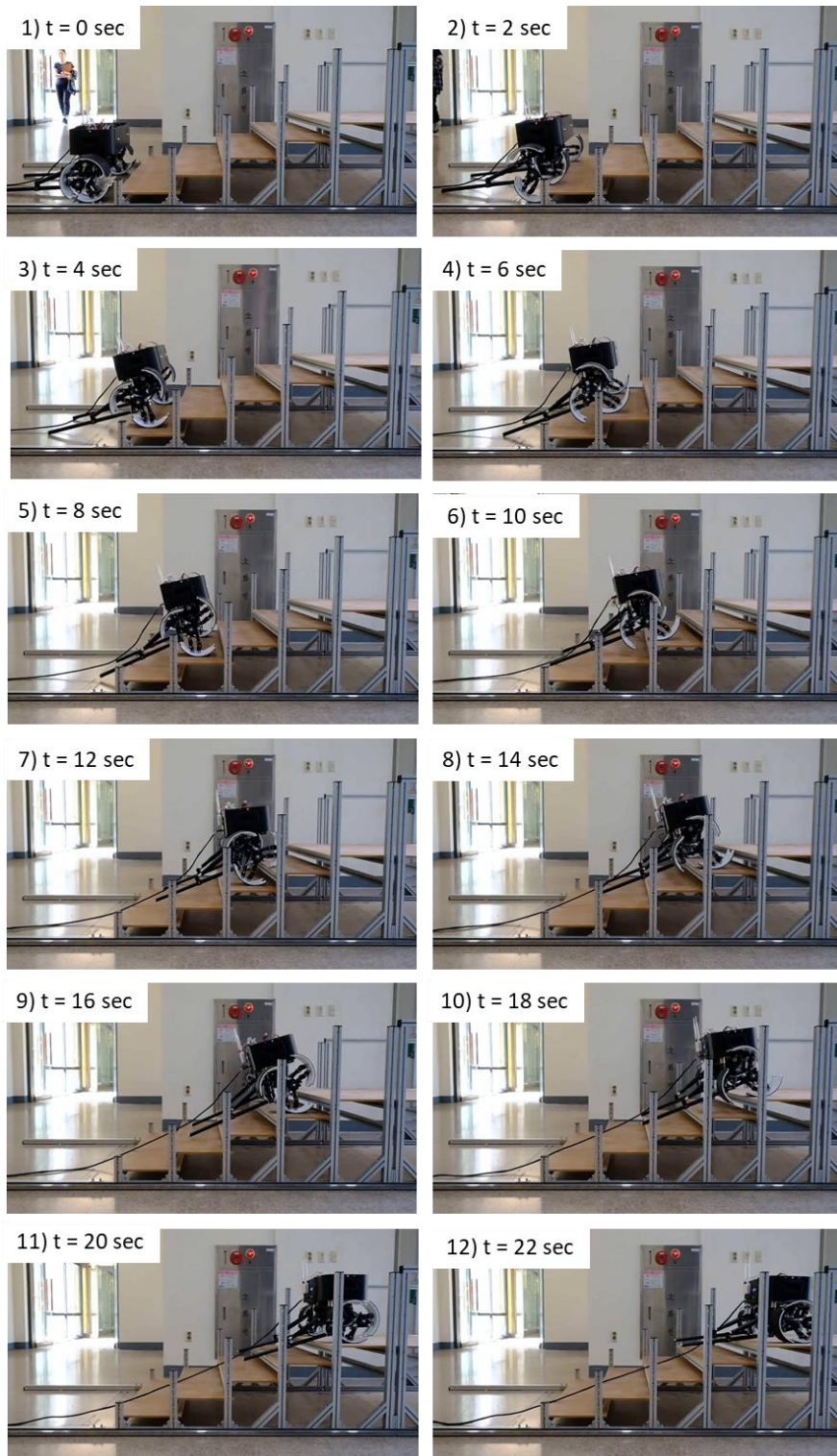


Figure 5.8. Experiments on stairs 300 x 100, 5 m/min

Figures 5.8 to 5.11 show the stair overcoming experiment results. The platform climbed various size of stairs at a speed of up to 20 m / min (1 step / sec).

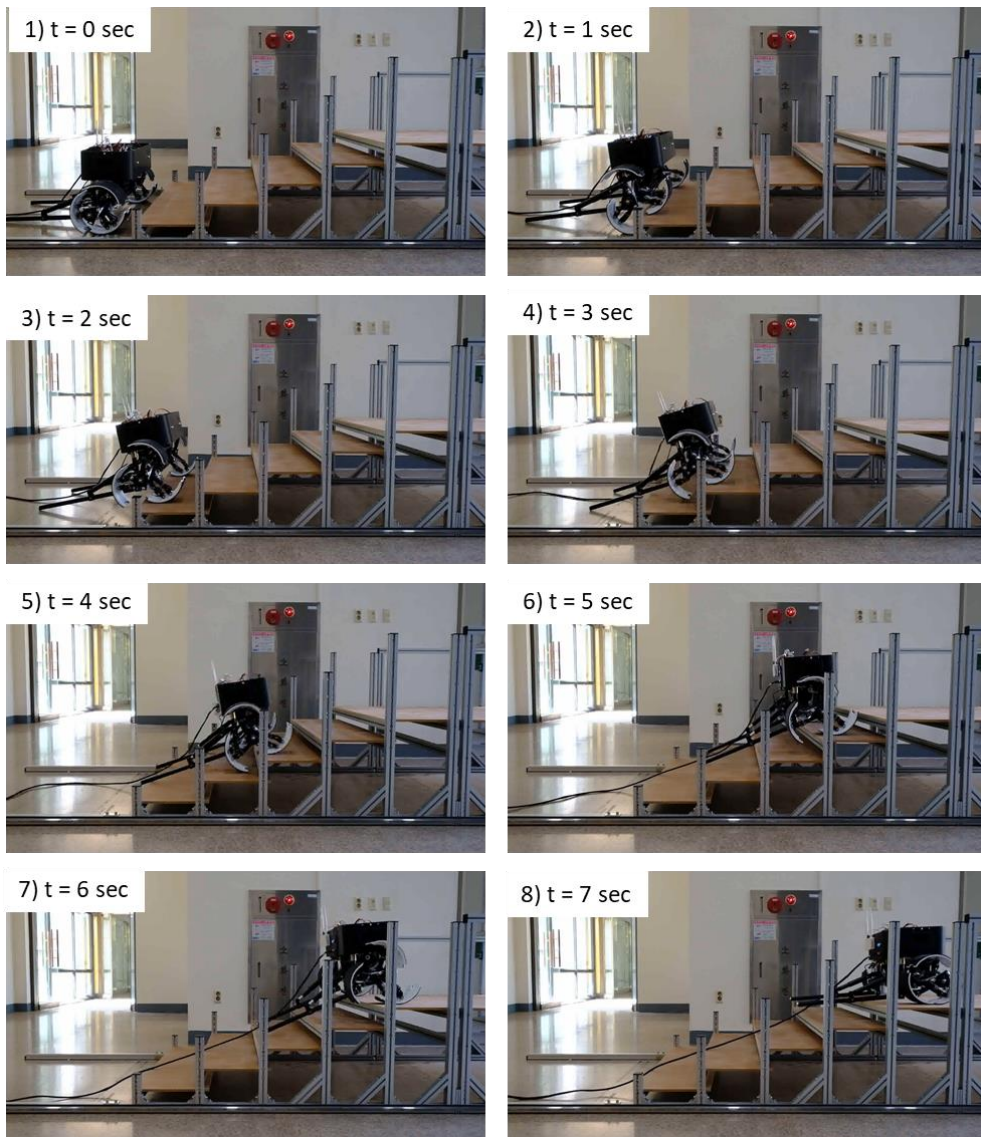


Figure 5.9. Experiments on stairs 300 x 100, 20m/min

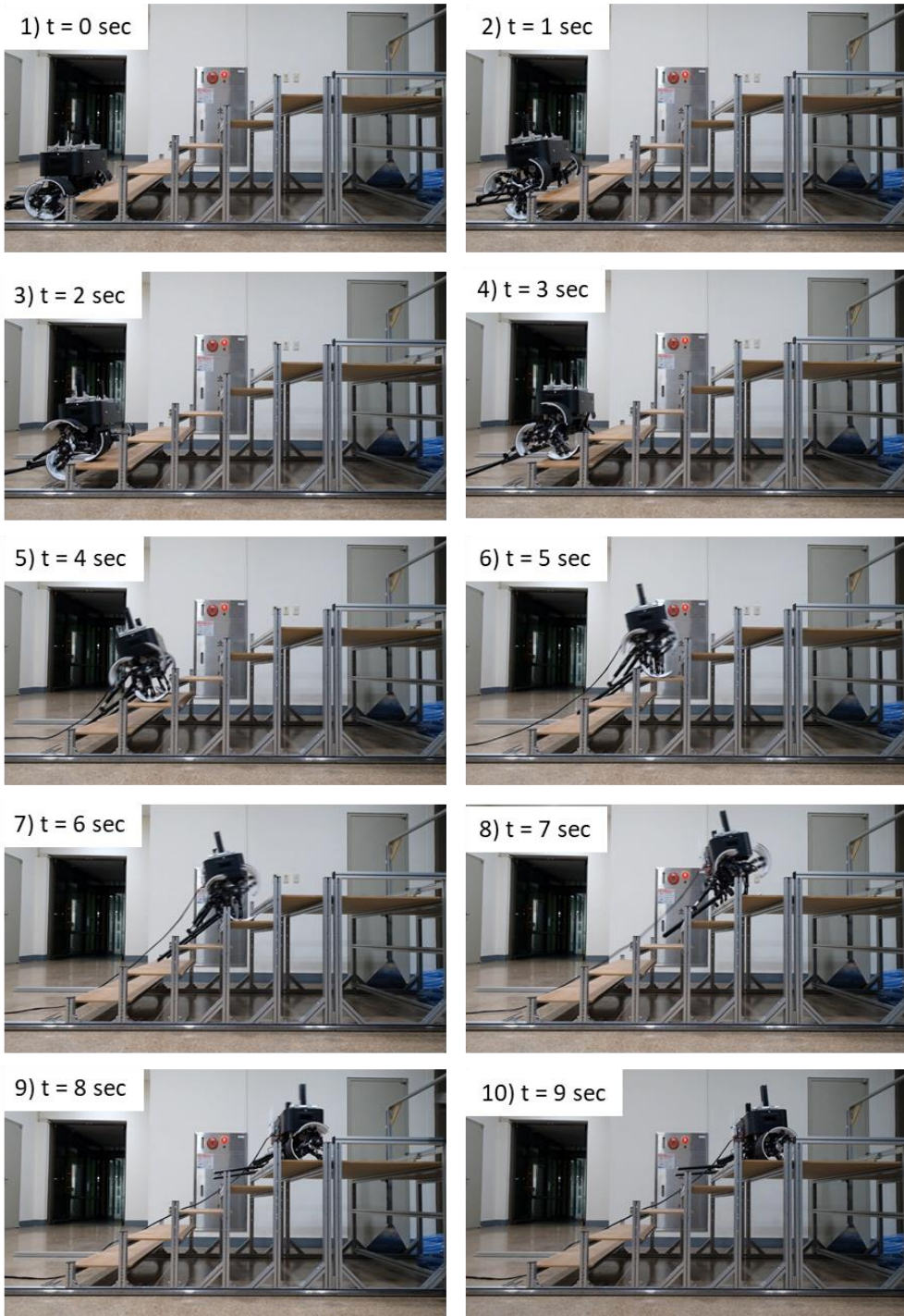


Figure 5.10. Experiments on stairs 300 x 160 20m/min

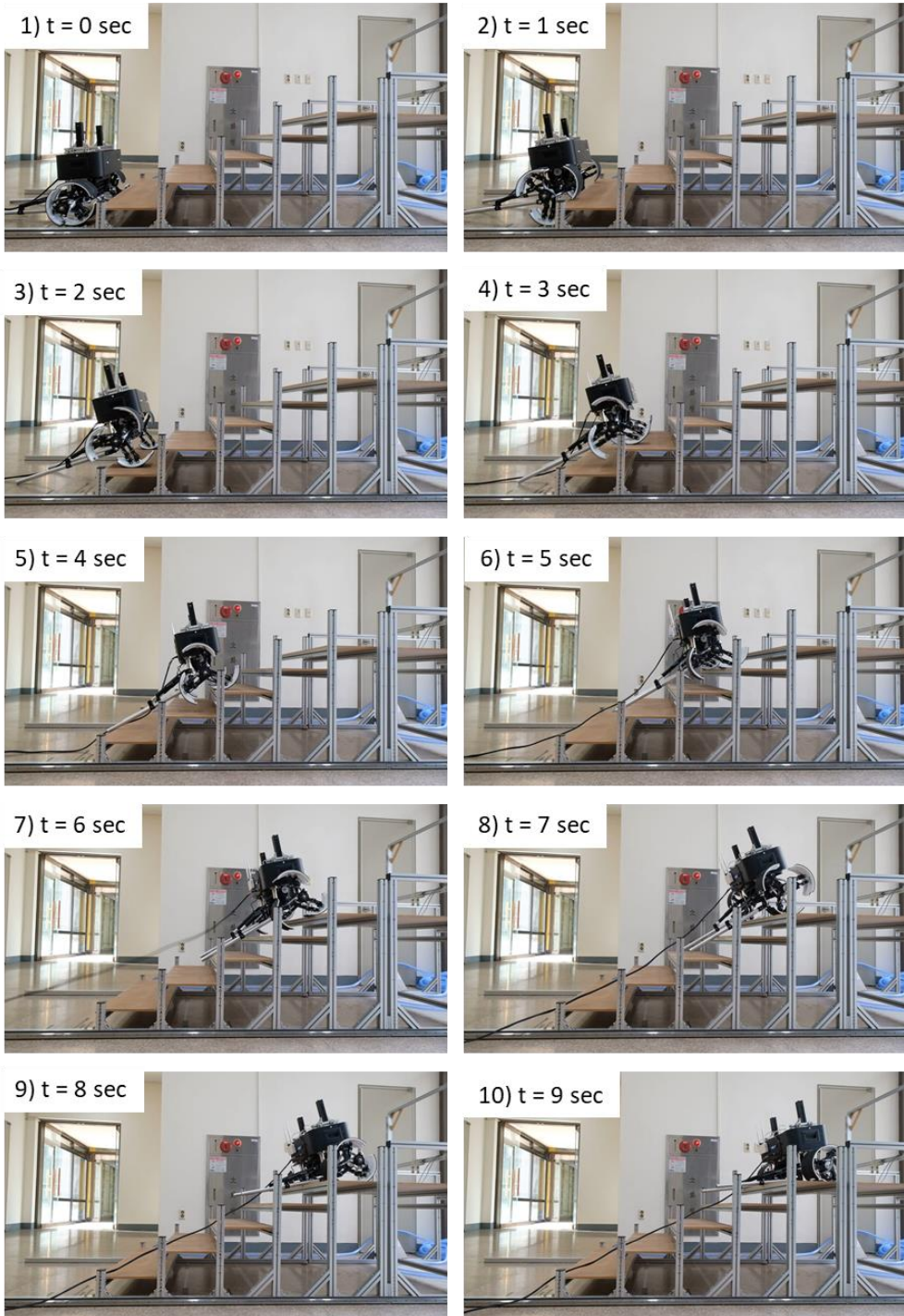


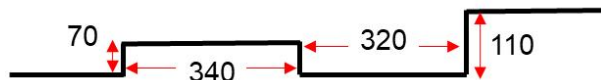
Figure 5.11 Experiments on stairs 320 x 140, 20m/min

5.5. Step overcoming experiments

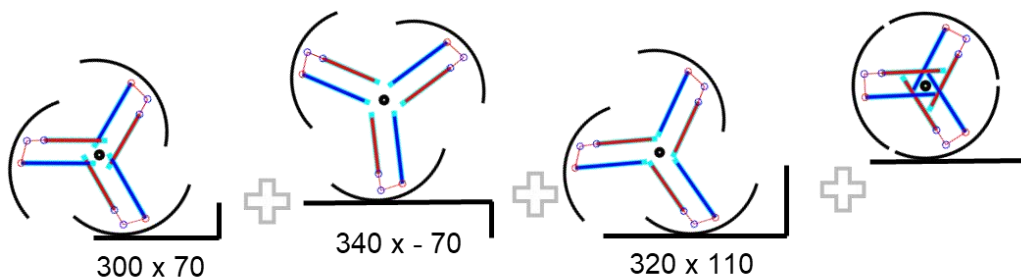
In addition to single-step obstacles, it is possible to overcome various step obstacles in a combination of horizontal and vertical surfaces. This can be represented by a combination of a number of step obstacles. In this research, as shown in Fig.5.12 (a), arbitrary obstacles combining step obstacles were constructed. The height



(a)



(b)



(c)

Figure 5.12. Objective step obstacle and concept of overcoming the obstacle

was 70 mm, -70 mm, and 110 mm, respectively, and the width was 340 mm and 320 mm. The obstacle can be represented as shown in Fig. 5.12 (b), which can be regarded as a continuous step obstacle of 300 mm x 70 mm, 340 mm x -70 mm, and 320 mm x 110 mm as shown in Fig. 5.12 (c). As a result, it is possible to overcome obstacles by transforming to shapes that fit each step. (Fig.5.12)

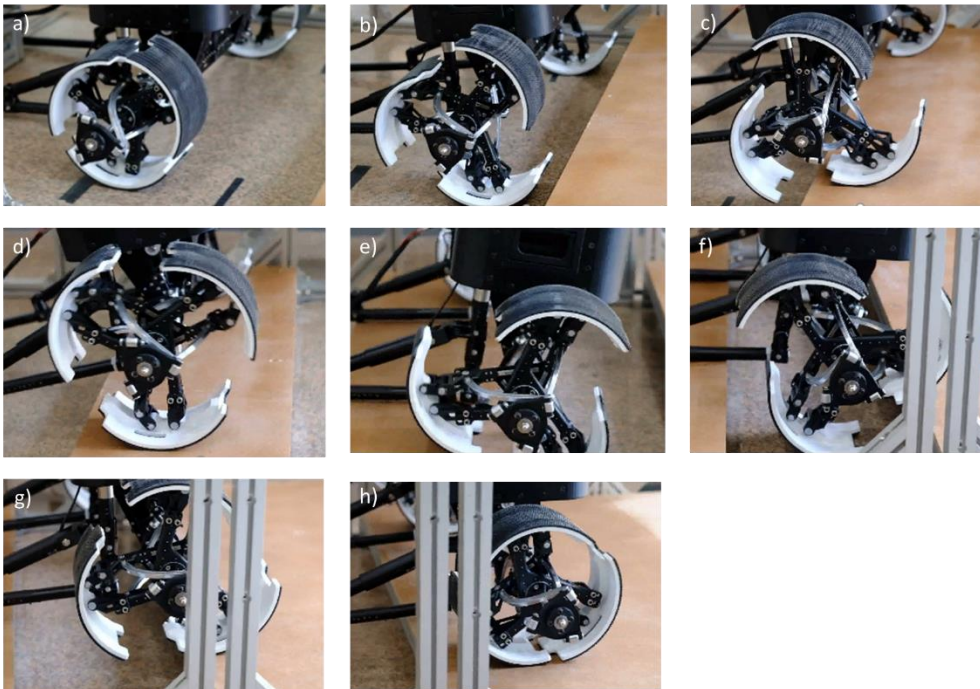


Figure 5.13. Step overcoming test

5.6. Size varying stairs overcoming experiments

Stairs that exist in reality are not ideally identical in size. The transformable wheel platform STEP that is proposed in this study can also actively climb stairs with height deviation. Therefore, we constructed different stairway obstacles and performed tests on the obstacle.

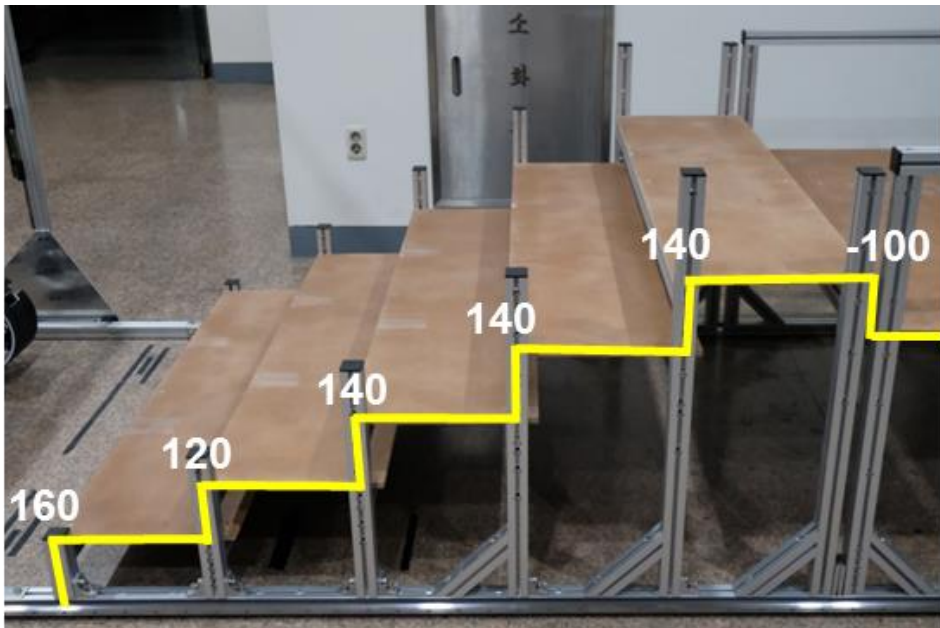


Figure 5.14 Size varying stairs

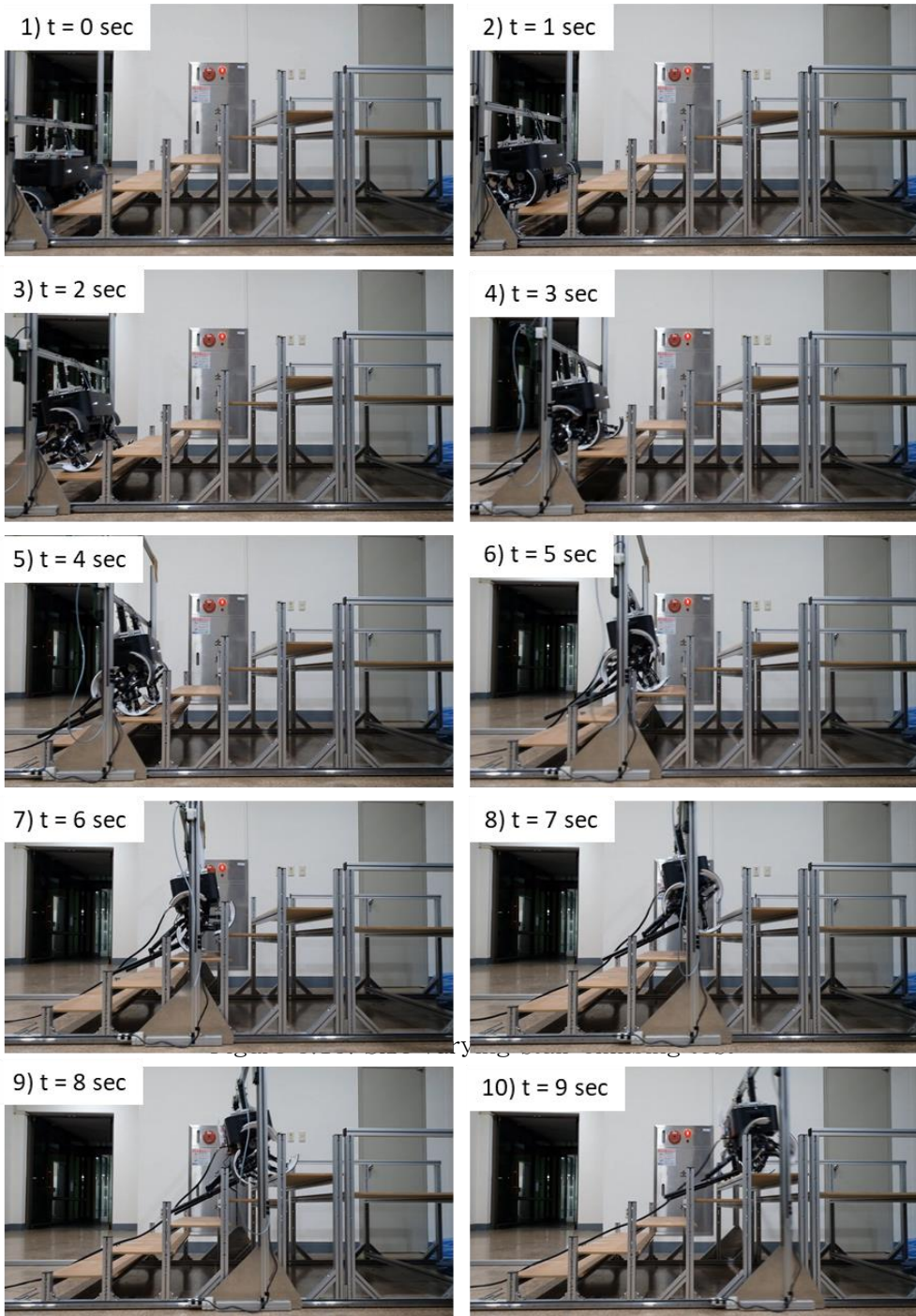


Figure 5.15 Experiments on size varying stairs

5.7. Field Tests

The Field Test was conducted on step and stair obstacles in daily life.

Experiments were also carried out to climb actual stairs in everyday life. It was able to climb a 120 mm step obstacle in front of building 300 in Seoul National University.

Climbing 300 mm x 160 mm stairs between building 300 and 301 were performed.

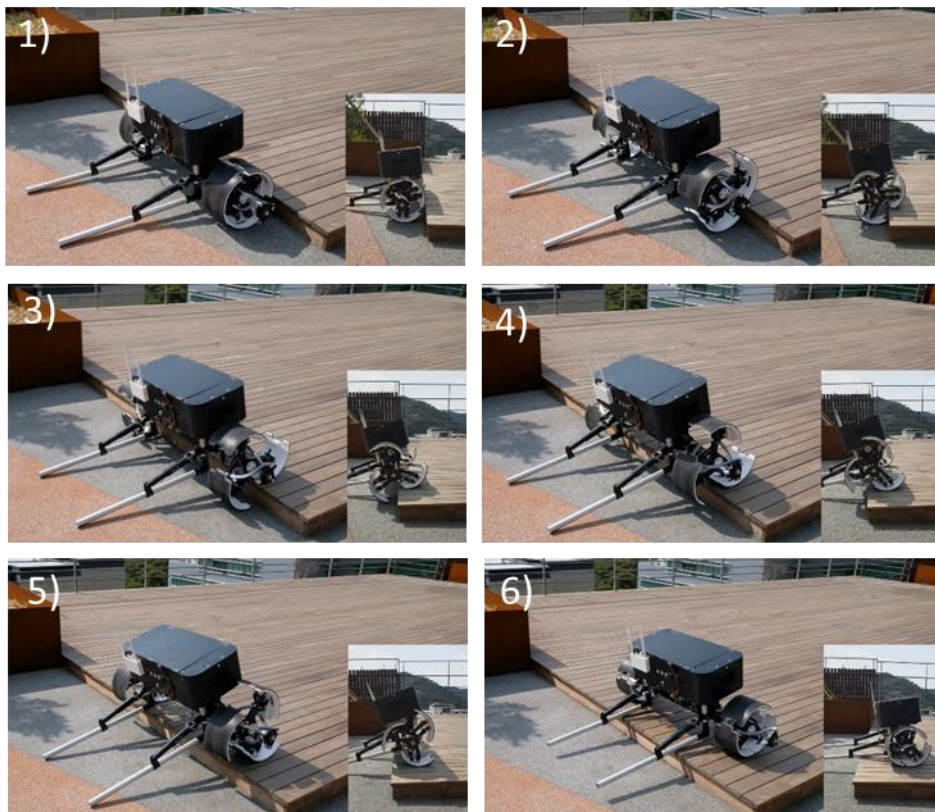
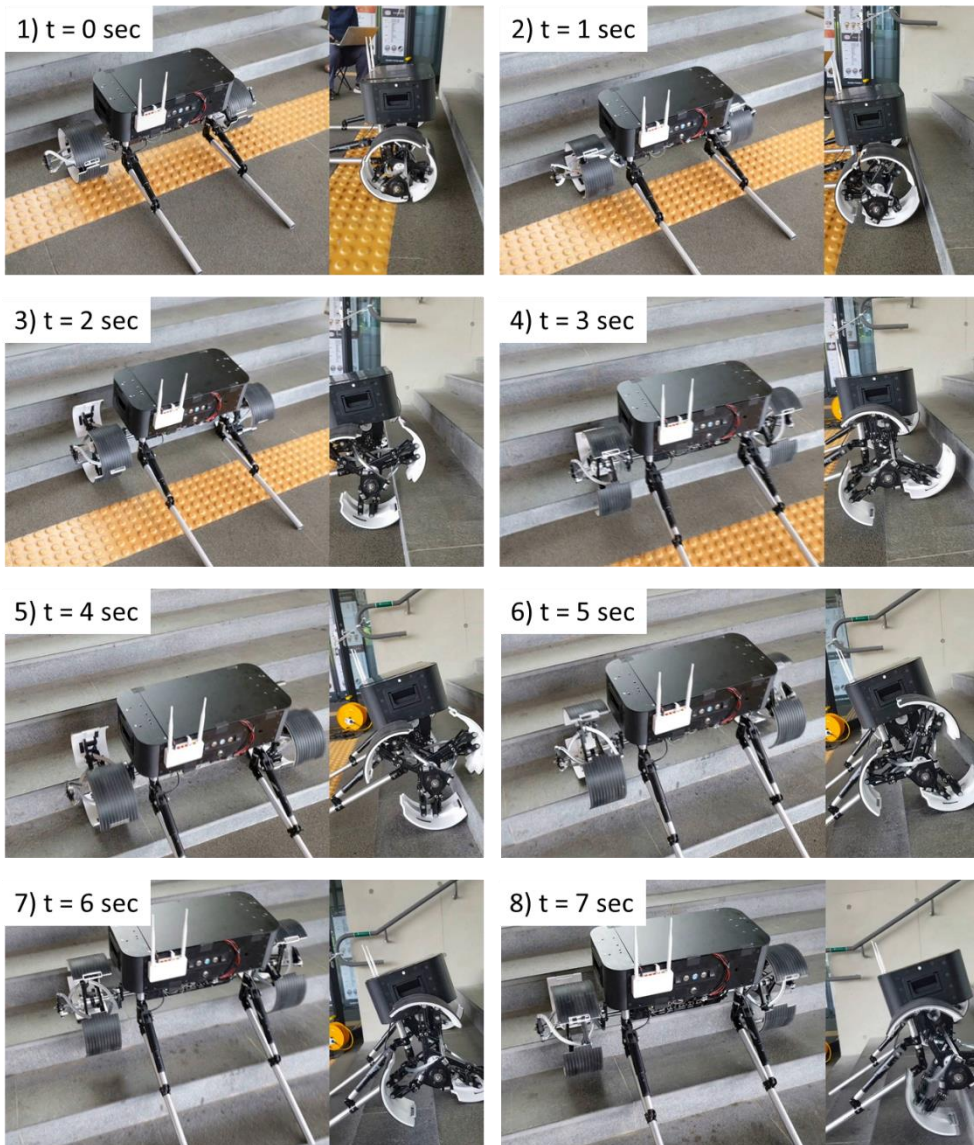


Figure 5.16 Field test on step obstacle:120 mm



5.17. Field test on stair obstacle

Chapter 6 Conclusion

In this thesis, the concept of 2-DOF transformable wheel is defined and a preliminary experiment is performed to verify performance of wheel shape. We explore and analyze 2-DOF transformable wheel mechanisms that satisfies kinematic requirements of 2-DOF transformable wheel concept. 36 Types of 2-DOF transformable mechanism is explored by type synthesis of 2-bar and 5-bar mechanisms. Five types of design alternative mechanism are created by combining synchronizing mechanisms. Kinematic characteristics of design alternatives in terms of range of variation, interference, and singularity is performed. The analysis of the pros and cons of each mechanism has been performed through the step overcoming simulation. The criterion for selecting the final mechanism is that it meets the required transformation range, interference occurs, and does not pass the singular point. The selected mechanism based mobile robot is designed and fabricated to verify the performances. It is designed to allow independent transformation of the wheel's rotational freedom. The design variables are selected to satisfy the required transform range through kinematic analysis, and motor selection and reinforcement design were performed through static analysis. The driving performance of the 2 DOF wheel based mobile platform is verified by experiments on step obstacles and stair obstacles of various sizes.

The transformable wheel based mobile platform that is proposed in this study can be used as a traveling platform of a service robot which can replace the conventional wheel mechanism.

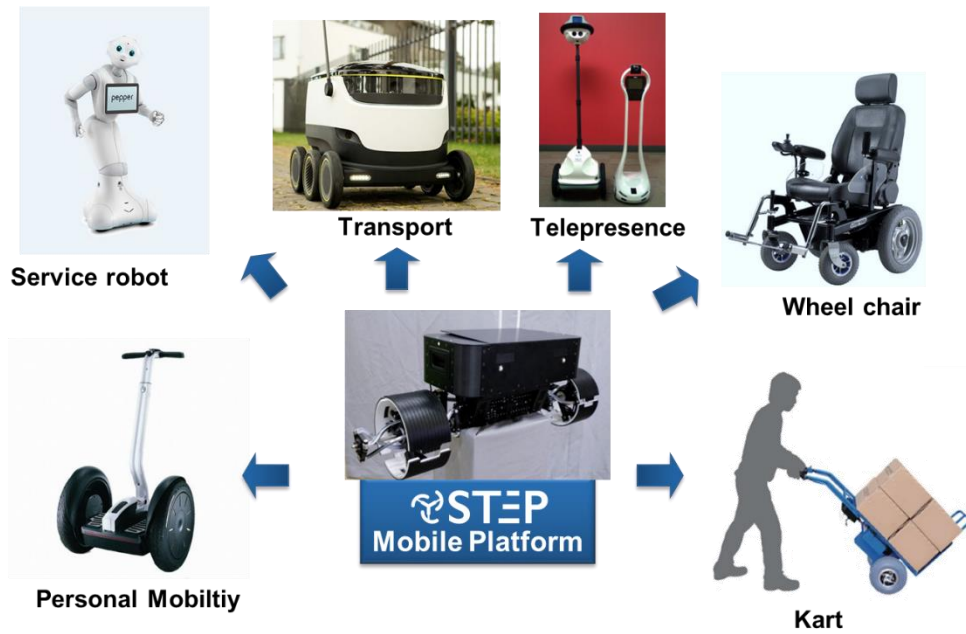


Figure 6.1. Application of STEP mobile platform

Bibliography

- [1] R. A. Lindemann and C. J. Voorhees, "Mars exploration rover mobility assembly design, test and performance" in *IEEE international conference on systems, man and cybernetics*, Waikoloa, USA, 2005, pp. 450–455.
- [2] Kubota, T., Kuroda, Y., Kunii, Y., & Nakatani, I. "Small, light-weight rover " Micro5 " for lunar exploration." *Acta Astronautica* 52.2 (2003): 447–453.
- [3] Iagnemma, K. D., Rzepniewski, A., Dubowsky, S., Pirjanian, P., Huntsberger, T. L., & Schenker, P. S. "Mobile robot kinematic reconfigurability for rough terrain." *Intelligent Systems and Smart Manufacturing*. International Society for Optics and Photonics, 2000.
- [4] T. Thueer, A. Kerbs and R. Siegwart, "Comprehensive Locomotion Performance Evaluation of All-Terrain Robots", *IEEE/RSJ International Conference on Intelligent Robots and Systems*, 2006
- [5] T. Estier, Y. Crausaz, B. Merminod, M. Lauria, R. Piguët, R. Siegwart, "An Innovative Space Rover with Extended Climbing Abilities" *Fourth International Conference and Exposition on Robotics for Challenging Situations and Environments*, 2000
- [6] B. Chen, R. Wang, Y. Jia, L. Guo and Lu Yang, "Design of a High Performance suspension for lunar rover based on evolution" *Acta Astronautica*, February 27–March 2, 2000, Volume 64 Issues 9–10, pp.925–934
- [7] Y.S. Kim, G.P. Jung, H. Kim and K.J. Cho, "Wheel Transformer: A Miniaturized terrain adaptive robot with passively transformed

wheels”, 2013 IEEE International Conference on Robotics and Automation (ICRA), pp.5605–5610

- [8] Youtube, <https://www.youtube.com/watch?v=HrQrJ57J9eE> , DARPA Morphing wheel system Morphing wheel, 2019.05.15.
- [9] Wen zeng, Feng gao, Hui Jiang, Chuan Huang, Jianxing Liu, Hanfei Li, School of Transfortation Science and Engineering, Beijing Univ. , “Design and analysis of a compliant variable–diameter mechanism used in variable–diameter wheels for lunar rover”, Mechanism and Machine Theory, 2018
- [10] Youtube, <https://www.youtube.com/watch?v=pyCgcX9fKlc>, 계단을 성큼성큼! 1 인용 모빌리티 나무(NAMU), 2018.12.03.
- [11] T. Thueer, A. Kerbs and R. Siegwart, “Comprehensive Locomotion Performance Evaluation of All–Terrain Robots”, *IEEE/RSJ International Conference on Intelligent Robots and Systems*, 2006
- [12] International Residential Code, (2006, The Stairway Manufacturing Code Association)
- [13] D.K. Choi, J.R. Kim, S.M. Cho, S.M. Jung and J.W.Kim, “Rocker–Pillar : Design of the Rough Terrain Mobile Robot Platform with Caterpillar Tracks and Rocker Bogie Mechanism”, *IEEE/RSJ International Conference on Intelligent Robots and Systems*, October 7–12, 2012. Vilamoura, Algarve
- [14] D.K. Choi, Y.S. Kim, S.M. Jung, J.W. Kim and H.S. Kim, “A New Mobile Platform(RHyMo) for smooth movement on Rugged Terrain”, *Transactions on Mechatronics*, 2016.

- [15] D.M. Kim, H.S. Hong, H.S. Kim and J.W. Kim. “Optimal design and kinetic analysis of a stair-climbing mobile robot with rocker-bogie mechanism”, *Mechanism and Machine Theory*, 2011
- [16] J.J. Cervantes-Sánchez, J.G. Rendon-Sánchez, University of Guanajuato, Faculty of Mechanical, Electrical and Electronic Engineering, Mexico, “A simplified approach for obtaining the workspace of a class of 2-dof planar parallel manipulators”, *Mechanism and Machine Theory*, 1999

Abstract in Korean

본 논문은 새로운 2-자유도 변형 바퀴 기반의 주행 플랫폼(STEP)에 관한 연구이다. 기존의 원형 바퀴는 구조가 단순하고 구동이 간단하여 평지 주행에 효과적인 대안이지만 인간 생활 환경에 존재하는 다양한 장애물을 극복하기엔 마찰력에 대한 의존도가 높으며 흔들림이 크다는 한계가 존재한다. 본 논문에서는 2-자유도의 변형 메커니즘을 제안하여, 변형된 바퀴가 바닥 면과의 접촉만을 유지하게 함으로써 장애물 극복 시 마찰력에 대한 의존도를 효과적으로 감소시킨다. 또한 변형된 곡선형상의 바퀴를 통해 본체의 흔들림도 감소시켜, 결과적으로는 사람이 걷는 속도인 40 m/min 의 주행 속도에서도 안정적으로 다양한 크기의 장애물 극복이 가능하다.

본 연구에서는 기구학을 기반으로 2-자유도 변형 바퀴의 개념 및 기구학적 요구조건을 정의하였다. 변형된 바퀴 형상을 3D 프린팅을 통해 제작하였으며, 예비 실험 및 해석을 통해 계단 장애물 극복 성능을 검증하였다. 2-자유도의 변형 기능을 수행할 수 있는 직렬 2절 링크 및 병렬 5절 링크 메커니즘이 총 36가지 탐색 되었다. 요구조건을 만족하지 못하는 메커니즘을 제외하고, 동기화 메커니즘을 결합하여 최종적으로 다섯 가지 유형의 설계 대안 메커니즘을 도출하였다. 설계대안들은 장애물 극복 과정의 기구학 시뮬레이션 및 변형 범위, 간섭 및 특이점 회피 여부를 통해 평가가 수행되었으며, 최종적으로 3R2P 5절 링크 메커니즘이 선정되었다. 설계를 단순화하면서 바퀴의 회전에 대해 바퀴의 변형 자유도를 독립시키기 위해, 한 쌍의 4절 RRPP 메커니즘을 합성하였다. 최종 변형 메커니즘의 기능 및 주행 플랫폼의 성능을 검증하기 위해, 모바일 플랫폼 “STEP” 이 설계되고 제작되었다. 설계 변수는 기구학 해석을 통해 필요한 변형 범위를 충족하도록 선정되었으며, 모터 선택 및 보강 설계는 정적 해석을 통해 수행되었다. 제작된 플랫폼의 크기는 1150 mm x 250 mm x 420 mm 이며 무게는 18 kg 이다. 주 제어기로 CompactRio 가 사용되었으며, PC 의 labview 로 무선으로 구동되었다. 2-자유도 변형 바퀴 기반 모바일 플랫폼 “STEP” 의 주행 성능은 다양한 크기의 계단 장애물 (300 mm x 100 mm, 320 mm x 140 mm, 300 mm x 160 mm)과 턱 장애물에 대한 실험을 통해 검증되었다.



